



UNIVERSITY OF LEEDS

This is a repository copy of *Oceanic response to Pliensbachian and Toarcian magmatic events: Implications from an organic-rich basinal succession in the NW Tethys*.

White Rose Research Online URL for this paper:  
<http://eprints.whiterose.ac.uk/85238/>

Version: Accepted Version

---

**Article:**

Neumeister, S, Gratzner, R, Algeo, TJ et al. (4 more authors) (2015) Oceanic response to Pliensbachian and Toarcian magmatic events: Implications from an organic-rich basinal succession in the NW Tethys. *Global and Planetary Change*, 126. 62 - 83. ISSN 0921-8181

<https://doi.org/10.1016/j.gloplacha.2015.01.007>

---

© 2015. This manuscript version is made available under the CC-BY-NC-ND 4.0 license  
<http://creativecommons.org/licenses/by-nc-nd/4.0/>

**Reuse**

Unless indicated otherwise, fulltext items are protected by copyright with all rights reserved. The copyright exception in section 29 of the Copyright, Designs and Patents Act 1988 allows the making of a single copy solely for the purpose of non-commercial research or private study within the limits of fair dealing. The publisher or other rights-holder may allow further reproduction and re-use of this version - refer to the White Rose Research Online record for this item. Where records identify the publisher as the copyright holder, users can verify any specific terms of use on the publisher's website.

**Takedown**

If you consider content in White Rose Research Online to be in breach of UK law, please notify us by emailing [eprints@whiterose.ac.uk](mailto:eprints@whiterose.ac.uk) including the URL of the record and the reason for the withdrawal request.



[eprints@whiterose.ac.uk](mailto:eprints@whiterose.ac.uk)  
<https://eprints.whiterose.ac.uk/>



35 excursion in the study section questions its unrestricted use as a global chemostratigraphic  
36 marker. Stratigraphic correlation of the thermally immature Bächental bituminous marls with  
37 the Posidonia Shale of SW Germany on the basis of C<sub>27</sub>/C<sub>29</sub> sterane ratio profiles and  
38 ammonite data suggests that deposition of organic matter-rich sediments in isolated basins in  
39 the Alpine realm commenced earlier (late Pliensbachian *margaritatus* Zone) than in  
40 regionally proximal epicontinental seas (early Toarcian *tenuicostatum* Zone). The late  
41 Pliensbachian onset of reducing conditions in the Bächental basin coincided with an influx of  
42 volcanoclastic detritus that was possibly connected to complex rifting processes of the Alpine  
43 Tethys and with a globally observed eruption-induced extinction event. The level of  
44 maximum organic matter accumulation in the Bächental basin corresponds to the main  
45 eruptive phase of the Karoo-Ferrar large igneous province (LIP), confirming its massive  
46 impact on global climate and oceanic conditions during the Early Jurassic. The Bächental  
47 marl succession is thus a record of the complex interaction of global (i.e., LIP) and local (e.g.,  
48 redox and salinity variations, basin morphology) factors that caused reducing conditions and  
49 organic matter enrichment in the Bächental basin. These developments resulted in highly  
50 inhomogeneous environmental conditions in semi-restricted basins of the NW Tethyan  
51 domain during late Pliensbachian and early Toarcian time.

52

53 **Keywords:** Bächental marl; Sachrang Member; Allgäu Formation; oceanic anoxic event;  
54 anoxia; sea level; carbon isotopes; Northern Calcareous Alps; Karoo-Ferrar; Alpine Tethys

55

## 56 **1. Introduction**

57

58 The early Toarcian was characterized by the deposition of organic-rich sediments in  
59 marine systems globally (e.g., Jenkyns, 1985, 1988; Jenkyns et al., 2002; Pearce et al., 2008),  
60 although the main controls on organic matter (OM) production and preservation at that time  
61 remain controversial. Widespread anoxia in epicontinental areas of the western Tethyan  
62 region (i.e., depositional area of the Posidonia Shale) has been attributed to a surface-water  
63 layer with reduced salinity that caused intensified water-column stratification (Praus and  
64 Riegel, 1989; Littke et al., 1991; Sælen et al., 1996). Other possible influences include minor  
65 sea-level fluctuations that controlled watermass exchange and, hence, dissolved oxygen levels  
66 in semi-restricted basins within the western European epicontinental sea (Röhl et al., 2001;  
67 Schmid-Röhl et al., 2002; Frimmel et al., 2004). In contrast, Jenkyns (1985, 1988; a summary  
68 is given by Jenkyns, 2010) postulated upwelling connected with the T-OAE of global scale

69 for causing the high rates of organic carbon accumulation in lower Toarcian strata. Tsikos et  
70 al. (2004a) found that the definition of Toarcian organic-rich sediments on the basis of their  
71 stratigraphic distribution is problematic as preservation and dilution of OM was affected by  
72 local variations in depositional and diagenetic conditions.

73 Changes in global climate during the Early Jurassic created oceanic conditions that  
74 were generally conducive to development of anoxia. Significant climatic warming had begun  
75 with release of large quantities of greenhouse gases during the CAMP eruptions at ~201 Ma  
76 (Marzoli et al., 1999; Whiteside et al., 2007). An interval of relative global cooling during the  
77 late Pliensbachian (Price, 1999; Morard et al., 2003; Dera et al., 2010) was followed by  
78 eruption of two large igneous provinces in the Early Jurassic: (1) the Karoo LIP at ~183 Ma  
79 (Svensen et al., 2007, 2012; Sell et al., 2014), and (2) the Ferrar LIP at ~184-183 Ma  
80 (Encarnación et al., 1996; Minor and Mukasa, 1997). These eruptions served to induce further  
81 climatic warming from the Pliensbachian/Toarcian boundary onwards, leading to “greenhouse  
82 Earth” conditions (Palfy and Smith, 2000; Weissert, 2000; Jenkyns, 2003). The prevailing  
83 subtropical climate was accompanied by an accelerated hydrological cycle with heavy  
84 monsoonal rainfalls and intense continental weathering that triggered an extensive supply of  
85 nutrients for ocean-surface waters, enhancing primary productivity (Parrish and Curtis, 1982;  
86 Parrish, 1993; Cohen et al., 2004). In addition, rifting of the Alpine Tethys was associated  
87 with several regional magmatic pulses during late Triassic to middle Jurassic time (Mohn et  
88 al., 2010; Decarlis et al., 2013). Oceanic break-up in the Penninic realm occurred in the  
89 Pliensbachian-Toarcian (Ratschbacher et al., 2004). These environmental changes operated in  
90 concert to produce conditions favourable to marine anoxia and black shale accumulation  
91 variably at global to local scales during the Early Jurassic.

92 Several studies have documented significant variation in total organic carbon (TOC)  
93 levels within lower Toarcian deposits of northern and southern Europe (see Jenkyns, 2010, for  
94 references). Whereas black shales deposited in epicontinental settings in Britain, France, and  
95 Germany reach peak TOC contents of up to 20% (e.g., Küspert, 1982; Jenkyns and Clayton,  
96 1997; Röhl et al., 2001), coeval sediments of the pelagic Tethyan realm generally contain  
97 smaller amounts of OM (<5 %; e.g., Jenkyns, 1985; 1988; Sabatino et al., 2009, 2013).  
98 Bituminous marls of Early Jurassic age (Bächentaler Bitumenmergel) are found in the  
99 Bächental valley of the Northern Calcareous Alps (Fig. 1.A). The Bächental basin was located  
100 in the NW part of the Tethys Ocean during the Toarcian (Figs. 1.B-C). A detailed  
101 investigation of the depositional environment of the Bächental bituminous marls as well as  
102 exact data regarding the onset and duration of its accumulation are lacking. However,

103 exceptionally high TOC contents (13 %) and an onset of OM accumulation during the  
104 Pliensbachian were reported by Kodina et al. (1988).

105 A multidisciplinary approach with high sample resolution was applied to the  
106 investigation of the Bächental bituminous marls. The use of a variety of proxies yielded  
107 information on source and thermal maturity of OM, redox conditions, salinity, water-column  
108 stratification, sea-level fluctuations, diagenetic processes, and volcanic influences. A  
109 comprehensive interpretation of these data permits the establishment of an overall model for  
110 the deposition of the Bächental bituminous marls. In addition, new findings regarding the age  
111 of marl accumulation facilitate stratigraphic correlation of lower Toarcian deposits from  
112 Alpine and epicontinental settings. The present study provides insights concerning the role of  
113 global events (e.g., Karoo and Ferrar LIP magmatism, opening of the Atlantic Ocean) as well  
114 as the influence of local basinal factors (e.g., redox and salinity variations) on OM  
115 accumulation in semi-restricted basins (e.g., Bächental basin) of the northwestern Tethyan  
116 domain during the late Pliensbachian and early Toarcian.

117

## 118 **2. Geological setting and samples**

119

120 The investigated section is situated in the Bächental valley, which is part of the  
121 Karwendel Mountains of northern Tyrol (Fig. 1.A; GPS: 47°30'31.38"N; 11°37'46.00"E). In  
122 this area, lithostratigraphic units of Triassic to Jurassic age belonging to the Lechtal nappe of  
123 the Bavaric Unit, a tectonic domain of the Northern Calcareous Alps, are exposed.

124 The paleogeography of the depositional area of the Bächental bituminous marls (Figs.  
125 1.B-C) was controlled by extensional tectonics, related to late Hettangian rifting and Toarcian  
126 oceanic break-up in the Penninic realm (e.g., Ratschbacher et al., 2004). During late  
127 Hettangian to Sinemurian time (Schlager and Schöllnberger, 1973) the final configuration of  
128 the roughly north-south trending Bächental basin with half-graben geometry, a depocenter  
129 located in the northern part of the basin, tilt block tectonics and antithetic step faults were  
130 established (Spieler and Brandner, 1989; Fig. 1.D). The distribution of bituminous marls (Fig.  
131 1.E) deposited during the early Toarcian was limited to the poorly ventilated deepest part of  
132 the Bächental basin (Spieler and Brandner, 1989).

133 The study section has an overall thickness of 35.54 m (Fig. 2) and is well exposed in  
134 large parts due to its position in an open-pit mine. At its base, limestone beds with a total  
135 thickness of 4.00 m occur. These strata are assigned to the *Scheibelberg Formation*  
136 (Sinemurian to Pliensbachian) and were deposited in water depths of several hundred meters

137 at the transition of distal slope to basin (Spieler and Brandner, 1989). Directly above a 0.25-  
138 m-thick weathered mudstone, the Bächental bituminous marls of the upper Pliensbachian to  
139 lower Toarcian *Sachrang Member* of the *Middle Allgäu Formation* (Tollmann, 1976a; Ebli,  
140 1991; Ebli et al., 1998; Gawlick et al., 2009; this study) are exposed with a total thickness of  
141 23.70 m. The alternating sequence of limestone and marl with a thickness of 4.69 m forming  
142 the top of the succession belongs to the *Upper Allgäu Formation* (upper Toarcian to early  
143 Middle Jurassic; Spieler and Brandner, 1989). The dating of the Bächental bituminous marls  
144 to the Toarcian was originally based on the occurrence of *Harpoceras* sp. (Klebelsberg,  
145 1935). Kodina et al. (1988) inferred that bituminous marl sedimentation began during the late  
146 Pliensbachian based on the occurrence of *Arietoceras* sp. and *Arietoceras* sp. or *Leptaleoceras*  
147 sp. near the base of the marls. This is consistent with the presence of *Cleviceras exaratum* in  
148 the middle part of the section (13.40 m; Fig. 2), a taxon associated with the early Toarcian  
149 *falciferum* Zone. A late Pliensbachian age (*margaritatus* Zone) for the base of the *Sachrang*  
150 *Member* in the Bächental basin is further supported by correlations based on C<sub>27</sub>/C<sub>29</sub> sterane  
151 ratios (Fig. 2; see Section 5.3.1 for discussion). At its type locality in Bavaria, deposition of  
152 the *Sachrang Member* commenced at the base of the *tenuicostatum* Zone and continued  
153 through the entire early Toarcian (Ebli et al., 1998).

154 Samples were collected from fresh exposures in a trench that was dug up to 4 m deep.  
155 A total of 68 samples was collected for geochemical analyses (Fig. 2). The *Scheibelberg*  
156 *Formation* at the base of the study succession is represented by six samples. The *Sachrang*  
157 *Member*, including a basal mudstone, bituminous marls, and a 1-meter-thick debrite layer  
158 (Fig. 2), is represented by 52 samples resulting in an average sampling interval of ca. 0.50 m.  
159 Ten samples at intervals of 0.10 to 0.90 m were collected from the *Upper Allgäu Formation* at  
160 the top of the section.

161

### 162 **3. Analytical methods**

163

164 A total of 28 thin sections were made for analyses via transmitted light microscopy.  
165 Polished blocks of 12 samples were prepared for maceral analyses that were performed with a  
166 Leica MPV microscope.

167 Total carbon (TC) and sulphur (S) contents were measured with a Leco 300 CSTM  
168 analyser. For the determination of total organic carbon (TOC) sample material was pre-treated  
169 with concentrated hydrochloric acid to remove the carbonate-bound carbon. Total inorganic  
170 carbon (TIC = TC – TOC) was used to calculate calcite equivalent percentages ( $C_{c_{eq}} = TIC \times$

171 8.33). Rock Eval pyrolysis was carried out using a Delsi Rock Eval RE II+ instrument. By  
172 means of this method the amount of free hydrocarbons ( $S_1$ ; mg HC/g rock) released at a  
173 constant temperature as well as the amount of pyrolysate ( $S_2$ ; mg HC/g rock) generated from  
174 non-volatile OM during subsequent gradual heating of the rock powder in a helium stream  
175 can be measured. These values are used to calculate the production index [ $PI = S_1/(S_1 + S_2)$ ]  
176 and the hydrogen index [ $HI = (S_2/TOC) \times 100$ ]. The temperature of maximum hydrocarbon  
177 generation ( $T_{max}$ ) can be used as maturity indicator.

178 X-ray diffraction (XRD) was carried out using Philips X-pert equipment with the  
179 following measuring conditions: [i] bulk samples, 2 to 65° 2 $\theta$ , random powder mount (29  
180 samples); [ii] clay mineral analysis of clay-rich samples, oriented powder mounts (smear on  
181 glass; Vortisch, 1982), 2 to 38° 2 $\theta$ , untreated, ethylene glycol-treated, heat-treated, 350 °C/2  
182 h, 550 °C/2 h (2 samples); [iii] bulk samples, 25 to 35° 2 $\theta$ , random powder mount (21  
183 samples). A rough quantification of the amount of diagenetic carbonate (unit: peak area) was  
184 established using the carbonate peaks between 30.0 and 31.2° 2 $\theta$  in XRD diffractograms.

185 Inorganic carbon ( $\delta^{13}C_{carb}$ ) and oxygen isotope ( $\delta^{18}O_{carb}$ ) measurements were carried  
186 out for all samples. Measurements were performed by adding 100 %  $H_3PO_4$  to samples heated  
187 at 70 °C in an online system (Gasbench II with carbonate option). Analysis was carried out  
188 with a ThermoFisher DELTA V isotope ratio mass spectrometer (Delta V IRMS). The results  
189 are reported relative to the Vienna Pee Dee Belemnite (VPDB) standard. Reproducibility was  
190 better than 0.2‰. All samples were analysed for their organic carbon isotope composition at  
191 the University of Leeds using an Elementar Pyrocube coupled to an Isoprime IRMS. Samples  
192 were weighed into tin capsules in sufficient quantity to produce peaks of between 1 and 10nA  
193 and combusted at 1150 °C in a helium stream (CP grade) enriched with pure oxygen (N5.0).  
194 The resulting gases were passed over tungstic oxide (also at 1150 °C) and excess oxygen and  
195 water removed using copper wires held at 850 °C and Sicapent respectively. All solid  
196 reagents were sourced from Elemental Microanalysis, UK, and all gases were sourced from  
197 BOC, UK.  $CO_2$  was separated from other gases using a temperature controlled  
198 adsorption/desorption column. The  $\delta^{13}C$  of the sample is derived from the integrated mass 44,  
199 45 and 46 signals from the pulse of sample  $CO_2$ , compared to those in an independently  
200 introduced pulse of  $CO_2$  reference gas (CP grade). Samples were run in batches of 12-16  
201 bracketed by in-house C4 sucrose and urea standards. These were assigned values of  $-11.93$   
202  $\pm 0.24$  and  $-46.83 \pm 0.22$ ‰ respectively based on 10 replicate analyses and calibration using  
203 LSVEC lithium carbonate ( $-46.479$ ‰), IAEA-CH7 polyethylene ( $-31.83$ ‰), IAEA-CH6  
204 sucrose ( $-10.45$ ‰) and IAEA-CO1 Carrara marble ( $2.48$ ‰). Samples were batch corrected

205 using a simple linear equation. Analysis of the C-isotopic composition of acyclic isoprenoids  
206 was performed using a Trace GC Ultra attached to a Delta V IRMS via a combustion interface  
207 (GC IsoLink) and an autodilution unit (ConFlow IV), all from Thermo-Fisher. For calibration,  
208 a CO<sub>2</sub> standard was injected at the beginning and end of each analysis. The GC coupled to the  
209 IRMS was equipped with the column described above and the temperature program was the  
210 same as for conventional GC-MS analysis. Isotopic compositions are reported in the  $\delta$   
211 notation relative to the VPDB standard.

212 Major- and trace-element concentrations were determined on whole-rock samples  
213 using a wavelength-dispersive Rigaku 3040 X-ray fluorescence (XRF) spectrometer at the  
214 University of Cincinnati. Raw intensities were calibrated using a set of 65 standards from the  
215 USGS, the National Bureau of Standards, and internal lab standards that were analyzed by  
216 XRAL Incorporated using XRF and INAA. Analytical precision based on replicate analyses  
217 was better than  $\pm 2\%$  for major and minor elements and  $\pm 5\%$  for trace elements, and  
218 detection limits were 1 to 2 ppm for most trace elements.

219 For organic geochemical analyses, samples were extracted using dichloromethane in a  
220 Dionex ASE 200 accelerated solvent extractor (temperature: 75 °C; pressure: 50 bar). After  
221 separation of asphaltenes, the hexane soluble fractions were separated into NSO compounds,  
222 saturated hydrocarbons and aromatic hydrocarbons using medium pressure liquid  
223 chromatography with a Köhnen-Willsch instrument (Radke et al., 1980). The saturated and  
224 aromatic hydrocarbon fractions were analysed with a GC equipped with a 30 m DB-1 fused-  
225 silica capillary column (i.d. 0.25 mm; 0.25  $\mu$ m film thickness) coupled to a Finnigan MAT  
226 GCQ ion trap mass spectrometer. The oven temperature was programmed from 70 to 300 °C  
227 at 4 °C/min, followed by an isothermal period of 15 min. Helium was used as carrier gas. The  
228 spectrometer was operated in the electron ionization mode over a scan range from m/z 50 to  
229 650. Relative percentages and absolute concentrations of different compound groups in the  
230 saturated and aromatic hydrocarbon fractions were calculated using peak areas in the total ion  
231 current chromatograms in relation to those of internal standards (deuterated n-tetracosane and  
232 1,1'-binaphthyl, resp.), or by integration of peak areas in appropriate mass chromatograms  
233 using response factors to correct for the intensities of the fragment ion used for quantification  
234 of the total ion abundance. The concentrations were normalized to TOC.

235

## 236 **4. Results**

237

### 238 ***4.1 Lithology, microfacies, and mineralogy***



239 At the base of the studied section, massive and thick-bedded grey limestones of the  
240 *Scheibelberg Fm.* (0.50-4.50 m; Fig. 2) are exposed. These rocks are hemipelagic to pelagic,  
241 bioturbated wackestones containing radiolarians, echinoderms, foraminifera, and ostracods.  
242 The top is formed by a breccia horizon containing carbonate lithoclasts.

243 The *Sachrang Member* (4.50-29.45 m; Fig. 2) comprises a 25-cm-thick basal  
244 mudstone (4.50-4.75 m), the Bächental bituminous marls (4.75-21.55 m and 22.55-29.45 m)  
245 and a debrite (21.55-22.55 m). The carbonate-free basal mudstone consists of black OM-  
246 enriched layers that are frequently interrupted by continental-derived OM-free lithoclasts.  
247 Quartz and smectite are the main minerals, whereas illite, chlorite, and plagioclase occur in  
248 minor amounts. The Bächental bituminous marls can be subdivided based on differing colour  
249 reflecting variations in OM richness. The lower part of the section (subsequently Unit 1: 4.75-  
250 11.00 m) and its upper part (Unit 3: 22.55-29.45 m) consist of greyish marls, whereas the  
251 OM-rich middle part is black-coloured (Unit 2: 11.00-21.55 m). Rocks of Units 1 and 3 are  
252 laminated to bioturbated wackestones containing mainly radiolarians and subordinated  
253 filaments (*Bositra*), ostracods, sponge spicules, and some foraminifera (Figs. 2.A, 2.E).  
254 Samples from Unit 2 show varying microfacies. In the lower part (Subunit 2a: 11.00-19.35 m)  
255 finely laminated mudstones with mainly radiolarians and additionally *Bositra*, sponge  
256 spicules, ostracods, and foraminifera occur (Fig. 2.B). Small channels, onlap structures as  
257 well as low energetic, fine-grained turbidites with carbonate detritus are present. The  
258 occasional occurrence of radiolarian wackestones in the middle and upper parts of Subunit 2a  
259 indicate episodic blooms of radiolarians as well as a significant contribution of these  
260 organisms to the planktonic biomass of the sediment (Fig. 2.C; cf. Sabatino et al., 2009). The  
261 most striking characteristic in Subunit 2b (19.35-21.55 m) is the presence of re-deposited  
262 carbonate detritus layers containing abundant pyrite (Fig. 2.D). These layers become thicker  
263 and more frequent towards the top of Unit 2, which is formed by a 1-m-thick bioturbated  
264 wackestone with reworked carbonate intraclasts, interpreted as debris flow deposit.  
265 Bioturbation is generally weak, except for samples at the base of Unit 3.

266 Apart from OM, the Bächental bituminous marls consist mainly of quartz and  
267 carbonate minerals. The latter appear as [i] detrital calcite, [ii] secondary calcite, and [iii]  
268 typically Mn-rich diagenetic carbonate phases (subsequently referred to as diagenetic Mn-rich  
269 carbonates) featuring varying incorporation of Mn, Ca, Mg, and Fe. Pyrite is abundant in all  
270 samples. The rock matrix consists of clay and carbonate minerals; muscovite and feldspar  
271 occur in subordinate amounts. Diagenetic Mn-rich carbonates are the most abundant  
272 carbonate minerals in the majority of samples from Units 1 and 3 showing significant vertical

273 variations in peak area from 2200 to 21300 (Fig. 3.A; Table 1 in the Appendix). In contrast,  
274 diagenetic Mn-rich carbonates are generally rare in Unit 2 (260-7800 in peak area; Fig. 3.A;  
275 Table 1 in the Appendix), which contains larger amounts of secondary calcite instead.  
276 Diagenetic Mn-rich carbonates appear with broad, irregular peaks in the diffractograms,  
277 suggesting a low degree of crystallinity.

278 The *Upper Allgäu Fm.* (30.85-35.54 m) at the top of the section is formed by an  
279 alternating sequence of bioturbated light grey limestones and dark grey marls. Both contain  
280 radiolarians, *Bositra*, and some ostracods. The contact of the *Sachrang Member* and the  
281 overlying *Upper Allgäu Fm.* is not exposed (29.45-30.85 m).

282

#### 283 **4.2 Bulk geochemical parameters**

284 The vertical variation of bulk geochemical parameters is shown in Figs. 3.B-E and  
285 4.A. The full dataset is presented in the Appendix (Table 1).  $T_{\max}$  (416-427 °C) and PI values  
286 (<0.1) indicate that the bituminous marls are thermally immature. Higher  $T_{\max}$  values (~ 444  
287 °C) are restricted to the basal mudstone. Limestones and marls from the *Scheibelberg Fm.* and  
288 the *Upper Allgäu Fm.* show very low TOC contents (<0.2 and 0.4%, resp.).

289 The basal mudstone of the *Sachrang Member* contains very low S contents (ca. 0.1%),  
290 but significant amounts of OM (TOC: 1.8%). Low HI values (74 and 37 mg HC/g TOC)  
291 indicate a high proportion of inert OM. Unit 1 of the Bächental bituminous marls is  
292 characterized by moderate TOC (1.1-3.3%) and high S contents (2.2-5.7%).  $C_{c_{eq}}$  range  
293 between 24.4 and 43.6%. HI varies between 306 and 612 mg HC/g TOC. Fe contents are  
294 rather uniform (3.3-5.2%), but reach 9.2% in a sample at 6.65 m. Samples from Subunit 2a  
295 show a wide variety of TOC contents (2.9-12.9%). Two positive TOC excursions are visible  
296 from 11.00 to 15.65 m and from 18.05 to 19.55 m. Despite strong TOC variations, HI values  
297 are quite uniform (588-687 mg HC/g TOC). The S curve does not mirror the TOC trend but  
298 stays constant at relatively low levels (2.1-3.2%). Between 15.15 and 18.05 m S contents  
299 show strong fluctuations (1.3-7.1%) and an inverse correlation with both TOC and  $C_{c_{eq}}$  (17.4-  
300 58.8%). Marls in Subunit 2b (18.6-38.8%  $C_{c_{eq}}$ ) exhibit TOC contents from 2.9 to 6.3% and  
301 high HI values (572-683 mg HC/g TOC) and S contents (3.5-5.9%). Fe concentrations in Unit  
302 2 vary strongly from 0.1 to 6.1%. The carbonate debrite, poor in OM and S, marks a  
303 significant change in bulk source-rock parameters. TOC contents in Unit 3 are rather uniform  
304 (~1.5-2.0%) and are slightly higher (up to 3.0%) only near its top.  $C_{c_{eq}}$  (22.8-64.8%) and S  
305 contents (1.3-5.8%) show significant vertical variations. In general,  $C_{c_{eq}}$  is decreasing towards  
306 the top, whereas S contents are higher in the upper half of Unit 3. HI values in the lower part

307 of Unit 3 are significantly lower (300-400 mg HC/g TOC) than in the underlying Unit 2 (>600  
308 mg HC/g TOC), but show an upward increase (up to 550 mg HC/g TOC). Fe contents are  
309 rather uniform (3.2-6.1%). A single sample with only 1.4% Fe occurs at 27.55 m.

310

### 311 **4.3 Organic petrology**

312 The basal mudstone contains mainly amorphous OM. High reflectivity suggests the  
313 presence of charred land-plant material. In addition, inertinite occurs together with traces of  
314 liptinite. The OM of the Bächental bituminous marls is dominated by lamalginite (Figs. 5.A-  
315 D). Telalginite, sporinite and fish remains are present with slightly varying, but always low  
316 amounts (Figs. 5.A-D). The sporinite content is slightly increasing upsection. Terrestrial  
317 inertinite and vitrinite occur rarely with tiny irregularly shaped particles. Consequently  
318 vitrinite reflectance could not be measured. Pyrite is frequent in Units 1 and 3, whereas most  
319 rocks of Unit 2 contain lower pyrite percentages. Pyrite appears disseminated with crystals of  
320 framboidal as well as subhedral to euhedral shape; pyritization of organism fragments  
321 (especially radiolarians) is also common. In Subunit 2b the bulk of pyrite present is bound to  
322 carbonate turbidite layers.

323

### 324 **4.4. Stable isotope composition of carbonate minerals and organic matter**

325 Bulk carbonate and organic carbon isotope values are shown in Figs. 4.B-D. The full  
326 dataset is presented in the Appendix (Table 1). Limestones and marls from the *Scheibelberg*  
327 *Fm.* and the *Upper Allgäu Fm.* show rather constant  $\delta^{13}\text{C}_{\text{carb}}$  isotope values (0.8 to 1.5‰  
328 VPDB and -0.8 to 0.2‰ VPDB). The same is true for  $\delta^{18}\text{O}_{\text{carb}}$  isotope values for limestone  
329 samples from the *Scheibelberg Fm.* (-2.3 to -1.2‰ VPDB) and the *Upper Allgäu Fm.* (-2.1 to  
330 -1.8‰ VPDB). In contrast, marls from the *Upper Allgäu Fm.* show significant lower  $\delta^{18}\text{O}_{\text{carb}}$   
331 isotope values (-5.0 to -3.5‰ VPDB). Isotope data from the *Sachrang Member* are more  
332 inhomogeneous.  $\delta^{13}\text{C}_{\text{carb}}$  isotope values vary strongly in Unit 1 (-10.0 to -1.8‰ VPDB). In  
333 contrast,  $\delta^{13}\text{C}_{\text{carb}}$  isotopes are rather constant in Unit 2 (-4.2 to -1.5‰ VPDB). While bulk  
334 carbonate isotope values of the debrite ( $\delta^{13}\text{C}_{\text{carb}}$ : -0.2 to 0.8‰ VPDB;  $\delta^{18}\text{O}_{\text{carb}}$ : -2.3 to -1.4‰  
335 VPDB) are in the range of the *Scheibelberg Fm.*,  $\delta^{13}\text{C}_{\text{carb}}$  isotopes from Unit 3 demonstrate a  
336 wide range (-12.7 to -2.2‰ VPDB).  $\delta^{18}\text{O}_{\text{carb}}$  isotope values of the bituminous marls vary from  
337 -6.0 to -2.1‰ VPDB.

338 Organic carbon isotope values of the OM-poor *Scheibelberg Fm.* and *Upper Allgäu*  
339 *Fm.* are in a similar range (-28.7 to -23.6‰ VPDB and -29.4 to -25.6‰ VPDB).  $\delta^{13}\text{C}_{\text{org}}$   
340 isotope values oscillate in a narrow range in the bituminous marls (-32.7 to -30.6‰ VPDB)

341 and the debrite (-30.1 to -28.7‰ VPDB), showing the strongest fluctuations in Unit 2. Carbon  
342 isotope compositions of pristane (Pr) and phytane (Ph) are in a similar range (Pr: -34.6 to -  
343 33.0‰ VPDB; Ph: -34.4 to -33.1‰ VPDB) for all samples.

344

#### 345 **4.5 Molecular composition of hydrocarbons**

346 The samples show relative uniform *n*-alkane distributions characterized by high  
347 relative proportions of short- and mid-chain *n*-alkanes ( $n\text{-C}_{15-19}/\Sigma n\text{-alkanes}$ : 0.23-0.56;  $n\text{-C}_{21-}$   
348  $_{25}/\Sigma n\text{-alkanes}$ : 0.26-0.43, resp.; Figs. 6, 7.A). Short-chain *n*-alkanes dominate over mid-chain  
349 *n*-alkanes in all but five samples. Long-chain *n*-alkanes ( $n\text{-C}_{27-31}/\Sigma n\text{-alkanes}$ ) are present with  
350 proportions from 0.05 to 0.32 (Figs. 6, 7.A). The carbon preference index (CPI; after Bray and  
351 Evans, 1961) varies between 0.85 and 3.20 with lowest values in Unit 2. The vertical variation  
352 of the acyclic isoprenoid ratio (Pr/Ph) is shown in Fig. 7.B. The Pr/Ph ratio is moderately high  
353 in Units 1 and 3 (0.88-1.76) and generally lower in Subunits 2a (0.70-1.01) and 2b (0.89-  
354 1.30).

355 Among steroids, the  $\alpha\alpha\alpha$ -steranes are present in the range of  $C_{27}$  to  $C_{29}$  and  
356 predominate over  $\beta\alpha\alpha$ -isomers (Fig. 8). The ratio of  $C_{27}$  vs.  $C_{29}$  steranes (Fig. 7.C) increases  
357 upwards from 0.70 to 1.24 in the lower part of Unit 1 and decreases in the upper part. The  
358 ratio is very low ( $\sim 0.60$ ) in the lowermost 3 m of Subunit 2a and increases upwards to reach a  
359 maximum of 1.10 in Subunit 2b. In Unit 3 the ratio varies from 0.59 to 1.03. The ratio of  
360  $C_{27}/C_{29}$   $\alpha\alpha\alpha R$  steranes displays a similar vertical trend (Fig. 7.C). Diasteranes occur with low  
361 concentrations and are represented by their  $C_{27}$  homologues in all units.  $C_{29}$  diasteranes are  
362 restricted to Unit 1. The ratio of 4-methylsteranes vs.  $\Sigma C_{29}$  steranes is relatively high in the  
363 lower part of the section and decreases sharply from 3.10 to 1.04 at the boundary between  
364 Subunits 2a and 2b (Fig. 7.D). The ratio of 20*S*/(20*S* + 20*R*) isomers calculated from  $\alpha\alpha\alpha$   $C_{29}$   
365 steranes is generally between 0.11 and 0.18 in Units 1, 2b and 3 (Fig. 7.E). Two outliers occur  
366 at 6.15 m (0.27) and 22.60 m (0.32). The ratio in Subunit 2a is higher (0.25-0.33). The vertical  
367 trend of mono- vs. triaromatic steroids is shown in Fig. 7.D. It displays a reversed image to  
368 the sterane isomerization ratio, with low values for Unit 2 (1.25-2.17) and high ratios for the  
369 rest of the succession (up to 3.81).

370 The hopane distribution is characterized by the predominance of  $\alpha\beta$  homologues from  
371  $C_{27}$  to  $C_{35}$ ; additionally  $\beta\alpha$  hopanes and bisnorhopane could be detected (Fig. 9).  
372 Bisnorhopane is enriched in Subunit 2a (25.7-124.7  $\mu\text{g/g}$  TOC) compared to the remaining  
373 units (2.5-56.3  $\mu\text{g/g}$  TOC). The ratio of 22*S*/(22*S* + 22*R*) isomers of the  $\alpha\beta$   $C_{31}$  hopane varies  
374 from 0.39 to 0.64 (Fig 7.F). The vertical trend with high values in Subunit 2a (0.50-0.64; Fig.

375 7.F) is identical to the sterane isomerization. Gammacerane could be detected in all samples.  
376 The gammacerane index [GI = gammacerane/(gammacerane +  $\alpha\beta$  C<sub>30</sub> hopane)] reaches  
377 maximum values (0.80) in Subunit 2a and is lower in the other units (0.05-0.59; Fig. 7.F).

378 Aryl isoprenoids occur in all samples, but their concentrations vary significantly (3.2-  
379 112.1  $\mu\text{g/g}$  TOC). The median values of different units suggest a general upward increase  
380 from ca. 15  $\mu\text{g/g}$  TOC (Units 1, 2a) to values exceeding 50  $\mu\text{g/g}$  TOC (Units 2b, 3).

381 Dibenzothiophene (DBT) and phenantrenes (Phen) are present with variable amounts in all  
382 samples. The DBT/Phen ratio is low in Units 1 and 3 (0.23-0.48) and higher in Subunits 2a  
383 (0.64-0.83) and 2b (0.46-0.60; Fig. 7.E). The full dataset of organic geochemical analyses is  
384 presented in the Appendix (Tables 2, 3).

385

## 386 **5. Discussion**

387

### 388 ***5.1 Organic matter sources and preservation***

#### 389 *5.1.1 Thermal Maturity*

390 The degree of thermal maturity can be estimated using vitrinite reflectance (VR), Rock  
391 Eval parameters ( $T_{\text{max}}$ , PI), and biomarker ratios. However, some biomarker ratios can be  
392 inaccurate as maturity indices when applied to the study units. The measurement of VR was  
393 impossible because of the low amount and small size of vitrinite particles in the study  
394 samples. Low thermal maturity is indicated by low  $T_{\text{max}}$  and PI values. The equation  $\text{VR} =$   
395  $0.018 \times T_{\text{max}} - 7.16$ , proposed for type I and II kerogen (Peters et al., 2005) suggests a  
396 maturity corresponding to a VR of ca. 0.45%  $R_o$ . The occurrence of charred organic material  
397 in the basal mudstone suggest that its elevated  $T_{\text{max}}$  values, corresponding to a VR of ca.  
398 0.80%  $R_o$  (equation after Peters et al., 2005), are due to the change in organic matter type.

399 Isomerization ratios of hopanes and steranes in samples from Units 1, 2b, and 3 as  
400 well as aromatization of steroids are consistent with a maturity in the range of 0.40 to 0.50%  
401  $R_o$  (cf. Mackenzie and Maxwell, 1981; Mackenzie et al., 1982). However, biomarker ratios  
402 suggest a slightly higher thermal maturity ( $\sim 0.60\%$   $R_o$ ) for Subunit 2a, which is located in the  
403 middle part of an undisturbed and continuous succession. A thermal overprint as the reason  
404 for the apparent higher maturity can be excluded. Salinity and/or lithotype variations are  
405 regarded as possible triggers of sterane ratio variations (ten Haven et al., 1986; Peters et al.,  
406 1990). Bitumen from immature source rocks deposited under hypersaline conditions tends to  
407 show more mature hopane patterns owing to unusual diagenetic pathways (ten Haven et al.,  
408 1987). For this reason, isomerization ratios are not reliable as a maturity parameter in Subunit

409 2a (see section 5.2.2), and the Bächental bituminous marls are inferred to have a low maturity  
410 corresponding to a VR of 0.40 to 0.50%  $R_o$ . These results confirm the questionability of  
411 applying isomerization ratios as maturity proxies to sections deposited under hypersaline  
412 conditions or strongly variable salinities.

413

#### 414 5.1.2 Organic matter sources

415 The relative proportions of marine and terrestrial OM determine the kerogen type and  
416 provide information about OM source, productivity, and preservation, as well as basin setting  
417 and water depth. OM of the basal mudstone mainly consists of charred material indicating  
418 terrestrial sources. The occurrence of charred OM is commonly connected to wildfire activity  
419 (e.g., Brown et al., 2012). In contrast, the dominant maceral group in Bächental bituminous  
420 marls is alginite, which suggests a mainly marine algal source of OM (Taylor et al., 1998).  
421 The most abundant maceral is lamalginite, which may derive from thin-walled planktonic and  
422 benthic organisms, including green algae, cyanobacteria, and bacterial mats (Oschmann,  
423 2000). Telalginite originates from algae such as *Botryococcus*, *Tasmanites*, and  
424 *Gloeocapsomorpha* that occur as thick-walled unicellular organisms with some internal  
425 structure (Hutton, 1987). The low frequency of vitrinite and inertinite suggests terrestrial  
426 inputs of OM to be of subordinate importance. The occurrence of radiolarian wackestones in  
427 the middle and upper part of Subunit 2a indicates episodic blooms of radiolarians and, hence,  
428 significant input of OM from planktonic heterotrophs as well as autotrophs.

429 HI values vary considerably within the study section, suggesting a mixture of kerogen  
430 types II and III. However, relatively invariant maceral compositions imply that OM is derived  
431 dominantly from marine algae and bacterioplankton, an inference also supported by the  
432 predominance of low molecular weight *n*-alkanes ( $<n-C_{20}$ ; Cranwell, 1977). Variations in HI  
433 values therefore reflect an early diagenetic overprint rather than multiple OM sources (see  
434 section 5.1.3). Unit 2 has been less affected by this diagenetic overprint than Units 1 and 3,  
435 and its HI of 600 to 700 mg HC/g TOC, which is indicative of type II kerogen, is taken as  
436 representative of primary OM in the entire section. The primary (i.e., pre-diagenetic) HI of  
437 diagenetically altered OM can be estimated from a plot of TOC vs.  $S_2$  (Langford and Blanc-  
438 Valleron, 1990), which yields values of ~770 mg HC/g TOC for Units 1 and 3 of the study  
439 section (correlation coefficient  $r^2 = 0.99$ ). This is consistent with little variation in kerogen  
440 type through the entire profile and a dominantly marine source of OM. The varying HI values  
441 are therefore not reflecting the primary source of OM but are rather caused by the mineral

442 matrix effect (Langford and Blanc-Valleron, 1990). However, an influence of early diagenetic  
443 OM oxidation on reduced HI values is also likely (cf. Röhl et al., 2001).

444 Biomarkers provide additional insights regarding OM sources. Algae are the  
445 predominant producers of C<sub>27</sub> sterols; C<sub>29</sub> sterols are more typically associated with land  
446 plants (Volkman and Maxwell, 1986). However, results from biomarker studies add to the  
447 growing list of microalgae that contain high amounts of 24-ethylcholesterol (Volkman et al.,  
448 1999; Peters et al., 2005). 4-methylsteroids with a C<sub>30</sub> dinosterol structure are considered as  
449 biomarkers of dinoflagellates (Robinson et al., 1984), while others are related to marine and  
450 lacustrine precursors (Mackenzie et al., 1982; Volkman et al., 1990; Peters et al., 2005; Auras  
451 and Püttmann, 2004). Thus, the relative abundance of non-aromatic steroids in the Bächental  
452 bituminous marls indicate the contribution of biomass from marine phytoplankton and a  
453 minor input of terrestrial OM. The 4-methylsteranes most probably originate from  
454 dinoflagellates (see also Köster et al., 1995). The most probable biological precursors of the  
455 hopane derivatives found in the samples are bacteriohopanepolyols (Ourrison et al., 1979;  
456 Rohmer et al., 1992). These compounds have been identified in bacteria as well as in some  
457 cryptogames (e.g., mosses and ferns) and in sulphate-reducing bacteria (Blumenberg et al.,  
458 2006). The predominance of homohopanes up to C<sub>35</sub> and the occurrence of benzohopanes  
459 from C<sub>22</sub> to C<sub>35</sub> in the aromatic hydrocarbon fraction suggest that bacteriohopaneols were a  
460 significant constituent of the biomass. In summary, we infer that algal and bacterial biomass  
461 of marine origin are the predominant OM sources for Bächental bituminous marls whereas  
462 OM input from terrestrial sources is of minor importance. In contrast, the bulk of OM  
463 contained in the basal mudstone, including charred material, was derived from terrestrial  
464 sources.

465

### 466 *5.1.3 Influence on organic matter by diagenetic processes*

467 Varying environmental conditions in the Bächental basin also affected diagenetic  
468 processes. Different degrees of bacterial degradation of OM and concurrent formation of  
469 diagenetic Mn-rich carbonates had a significant impact on bulk source-rock parameters. Early  
470 diagenetic degradation mainly controlled OM preservation in Units 1 and 3. This is supported  
471 by low TOC contents and HI values, which show a correlation with the amount of diagenetic  
472 Mn-rich carbonates. In Units 1 and 3, labile algal OM primarily present in the samples was  
473 degraded to a rather constant residual TOC level of ca. 2% during early diagenesis. The  
474 generated <sup>12</sup>C-enriched carbon was fixed in diagenetic Mn-rich carbonates.

475 The carbonate C-isotope profile of the study section has been strongly influenced by  
476 these diagenetic processes, resulting in a mixed signal derived from primary and secondary  
477 carbonate phases. The vertical trends of  $\delta^{13}\text{C}_{\text{carb}}$  isotope values and diagenetic Mn-rich  
478 carbonate contents show a significant negative correlation (compare Figs. 3.A and 4.B).  
479 Isotope ratios get more negative with increasing amounts of diagenetic Mn-rich carbonates,  
480 especially where high contents are observed in Units 1 and 3. The carbonate C-isotope  
481 compositions of the diagenetic Mn-rich carbonates in those units were determined by the  
482 relative proportions of isotopically light carbon from early diagenetic degradation of OM on  
483 the one hand and isotopically heavy seawater-sourced dissolved inorganic carbon in sediment  
484 pore waters on the other. A minor input of organic-derived carbon into calcite is also possible  
485 but not important compared to the strength of the effect on diagenetic Mn-rich carbonates.  
486 Very low  $\delta^{13}\text{C}_{\text{carb}}$  values (-11‰ VPDB) in limestone beds of the Posidonia Shale are also  
487 attributed to early diagenetic carbonate precipitation and incorporation of  $^{12}\text{C}$ -rich carbon  
488 derived from organic matter degradation via sulphate reduction (Röhl et al., 2001).

489 Unit 2 exhibits anomalously heavy  $\delta^{13}\text{C}_{\text{carb}}$  values (-2 to -3‰ VPDB) compared to  
490 Units 1 and 3, but values that are nonetheless lighter than those of other lower Toarcian  
491 sections (~0‰ VPDB; e.g. Röhl et al., 2001; Hesselbo et al., 2007; Sabatino et al., 2009).  
492 These relatively heavy  $\delta^{13}\text{C}_{\text{carb}}$  values are interpreted to be least altered (i.e., relative to  
493 primary marine carbonate phases). In Unit 2, the bulk of carbonate present is secondary  
494 calcite whereas the quantity of diagenetic Mn-rich carbonates is typically low (Fig. 3.A). The  
495 lack of the latter also implies smaller amounts of organically sourced carbon that were fixed  
496 in secondary carbonates of Unit 2. The precipitation of diagenetic Mn-rich carbonates was  
497 inhibited because anoxic bottom waters existed during deposition of Unit 2 (cf. Calvert and  
498 Pedersen, 1996; see Section 5.2.1). Overall, it is clear that the measured  $\delta^{13}\text{C}_{\text{carb}}$  values reflect  
499 the nature and extent of diagenetic processes rather than the primary isotopic signal.

500 The carbonate O-isotope composition of the study section is also dominated by  
501 diagenetic effects. The heaviest values (~-1.0‰ VPDB) are found in the limestones  
502 underlying the Bächental bituminous marls (Fig. 4.C). These values are consistent with a  
503 primary normal-marine isotopic composition (~-1.0‰ VPDB, ice-free; e.g., Röhl et al.,  
504 2001). All  $\delta^{18}\text{O}_{\text{carb}}$  isotope ratios for the bituminous marls record shifts toward lighter isotopic  
505 compositions that are a function of precipitation of diagenetic carbonate at burial temperatures  
506 exceeding contemporaneous sea-surface temperatures (cf. Algeo et al., 1992). The more  $^{18}\text{O}$ -  
507 depleted values are likely to represent precipitation of secondary phases at later diagenetic  
508 stages and, hence, higher burial temperatures (cf. Algeo et al., 1992). For this reason,



509 diagenetic carbonate in Units 1 and 3 appears to have formed earlier on average than that in  
510 Unit 2. This inference indicates an earlier formation of diagenetic Mn-rich carbonates in Units  
511 1 and 3 compared to the secondary calcite of Unit 2.  $\delta^{18}\text{O}_{\text{carb}}$  isotope ratios for the  
512 epicontinental Posidonia Shale of Dotternhausen plot within a narrower range ( $\sim -5.0$  to  $-7.0\%$   
513 VPDB) compared to those of the Alpine Bächental bituminous marls ( $\sim -2.0$  to  $-6.0\%$  VPDB).  
514 However, whereas the former represents a primary depositional signal derived from carbonate  
515 of well-preserved coccoliths and schizosphaerelles (Röhl et al., 2001), the  $\delta^{18}\text{O}_{\text{carb}}$  signal of  
516 the latter was controlled by diagenetic processes.

517

## 518 ***5.2 Depositional environmental conditions***

### 519 *5.2.1 Redox conditions and iron availability*

520 The Latest Triassic and the Early Jurassic were characterized by global perturbations  
521 caused by the activity of LIPs (CAMP, Karoo-Ferrar; Marzoli et al., 1999; Svensen et al.,  
522 2007, 2013; Jourdan et al., 2008; Caruthers et al., 2013; Sell et al., 2014) and the rifting of the  
523 Alpine Tethys in the Penninic realm with oceanic break-up in the Pliensbachian/Toarcian  
524 (Ratschbacher et al., 2004; Mohn et al., 2010; Decarlis et al., 2013) that induced major  
525 environmental changes and climate warming (“greenhouse Earth” conditions; Palfy and  
526 Smith, 2000; Weissert, 2000; Jenkyns, 2003) resulting in oceanic conditions generally  
527 conducive to development of anoxia. The prevailing redox conditions in a depositional basin  
528 commonly vary with time and are sensitive to changes in environmental conditions as  
529 reflected in the stratigraphic trends of various proxies (e.g., Pr/Ph ratio, arylisoprenoids,  
530 bioturbation, and Fe-TOC-S) in the sedimentological record.

531 In the study section, extensive bioturbation and relatively low TOC contents are  
532 indicative of normal-marine conditions without major perturbations of the carbon cycle during  
533 deposition of the *Scheibelberg Fm.* and the *Upper Allgäu Fm.* In contrast, redox conditions  
534 varied significantly during deposition of the Bächental bituminous marls, as shown by the  
535 multiple redox proxies discussed below.

536 The Pr/Ph ratio is commonly used as a redox indicator during early diagenesis.  
537 According to Didyk et al. (1978), Pr/Ph ratios  $<1.0$  indicate anaerobic conditions whereas  
538 values  $>1.0$  speak for suboxic to oxic environments. However, Pr/Ph ratios are also known to  
539 be affected by maturation (Tissot and Welte, 1984) and different precursors for isoprenoids  
540 (Goosens et al., 1984; Volkman and Maxwell, 1986; ten Haven et al., 1987). Both influences  
541 can be ruled out in the case of the Bächental section, because of its limited thickness and the  
542 similar isotopic compositions of Pr and Ph, which indicates a common precursor. Hence,

543 Pr/Ph ratios suggest generally suboxic conditions for Units 1 and 3; however, short-term  
544 anoxia cannot be completely excluded. In contrast, an environment with strictly anoxic  
545 bottom waters is suggested for Subunit 2a. Subunit 2b features a shift to less reducing (i.e.  
546 suboxic to anoxic) conditions. The postulated paleoredox trend is also visible in a plot of  
547 Pr/Ph vs. DBT/Phen (Fig. 10). The vertical redox trend suggested by Pr/Ph ratios is confirmed  
548 by bioturbation patterns. Small-scale bioturbation is visible in sections from Units 1 and 3, but  
549 totally missing in Unit 2. In addition, the occurrence of larger amounts of bisnorhopane  
550 argues for an elevated input of anaerobic bacteria typical of predominantly anoxic conditions  
551 in Unit 2 (Grantham et al., 1983; Rullkötter and Wendisch, 1982; Watson et al., 2009). Aryl  
552 isoprenoids derive from special green sulphur bacteria (Chlorobiaceae) that perform  
553 anoxygenic photosynthesis which requires light penetration into H<sub>2</sub>S saturated waters  
554 (Schwark and Frimmel, 2004). Therefore, aryl isoprenoids can be used to estimate whether  
555 the anoxic water column extended into the photic zone (Summons and Powell, 1986; Grice et  
556 al., 1996a; Koopmans et al., 1996). Aryl isoprenoids occur in all samples, although in variable  
557 amounts, suggesting frequent but transient episodes of photic-zone anoxia.

558         Several authors used TOC/S ratios for determining paleoredox conditions (e.g. Berner,  
559 1970, 1984; Leventhal, 1983; Berner and Raiswell, 1983). However, this approach is  
560 problematic when Fe is limiting, as is often observed in carbonate environments (cf. Berner  
561 and Raiswell, 1983; Raiswell and Berner, 1985). The ternary plot of Dean and Arthur (1989)  
562 additionally includes Fe contents and consequently all phases relevant for pyrite formation.  
563 Therefore, this approach is used for the Bächental section. Most samples of Units 1 and 3 plot  
564 either along the pyrite line or in the field of excess Fe availability (Fig. 11). The former  
565 indicates anoxic conditions and a sulfidization of all the available Fe; the latter suggests the  
566 presence of non-pyritized Fe and suboxic conditions during deposition (Dean and Arthur,  
567 1989; Hofmann et al., 2000; Rimmer et al., 2004). Hence, varying suboxic and anoxic  
568 conditions with intense sulphate reduction rates are reflected by the Fe-TOC-S diagram for  
569 Unit 1 and the upper part of Unit 3, whereas less reducing conditions prevailed during  
570 deposition of the lower part of Unit 3. The large amounts of available Fe in Units 1 and 3  
571 triggered enhanced pyritization during diagenesis. In contrast, the Fe-TOC-S diagram  
572 confirms Fe limitation in TOC-rich samples of Unit 2 (Fig. 11) consistent with a postulated  
573 anoxic to euxinic environment. The presence of excess S in Subunit 2a is reflected by  
574 elevated DBT/Phen ratios due to the incorporation of S in the aromatic fraction of OM during  
575 early diagenesis (“natural sulphurization”; Kohnen et al., 1991).

576 The negative correlation of S contents with both TOC and  $C_{c_{eq}}$  in the interval from  
577 15.15 to 18.05 m (Subunit 2a; Figs. 3.B-D) suggests changing Fe availability and alkalinity.  
578 The large amounts of  $H_2S$  produced in the OM-rich layers by sulphate reduction could not be  
579 fixed as pyrite because of an insufficient amount of reactive Fe, resulting in significant  
580 amounts of free  $H_2S$ . Only a small portion of this  $H_2S$  was incorporated in OM, producing  
581 elevated DBT/Phen ratios in the high-TOC/low-S layers, whereas the excess free  $H_2S$  diffused  
582 upward until it was fixed as pyrite in layers with relatively low TOC contents but large  
583 amounts of reactive Fe, resulting in low-TOC/high-S intervals (cf. Jaminski et al., 1998). The  
584 high alkalinity generated by sulphate reduction (e.g., Thomas et al., 2008) triggered the  
585 enhanced precipitation of secondary calcite in the high-TOC/low-S intervals. Iron-limiting  
586 conditions are directly connected to the available pool of Fe oxides (Raiswell et al., 1994).  
587 Several studies confirm a direct relationship between bulk sedimentation rates and variable  
588 organic input and clastic flux, respectively (cf. Mangini and Dominik, 1979; Kuehl et al.,  
589 1993; Arthur et al., 1994; Jaminski et al., 1998). The mudstone samples of Subunit 2a were  
590 deposited in a low-energy environment characterized by the rareness of detrital carbonate  
591 layers. We interpret the absence of turbiditic input to have caused Fe limitation in those  
592 samples. In contrast, infrequent carbonate turbidites within Subunit 2b provided sufficient  
593 reactive Fe to fix  $H_2S$  as pyrite in an otherwise Fe-limited environment (e.g., Fig. 2.D).  
594 Consequently, the bulk of pyrite present in Subunit 2b is bound to fine-grained carbonate  
595 turbidites. Therefore, detrital influx controlled Fe availability and the degree of pyritization in  
596 Unit 2.

597 Summing up, several redox changes affected the depositional environment of the  
598 Bächental bituminous marls. Suboxic to possibly short-term anoxic conditions prevailed  
599 during deposition of Units 1 and 3. Intense sulphate reduction and oxidation of OM in the  
600 sediment during diagenesis generated  $H_2S$  that reacted with available Fe in the basin to  
601 produce large amounts of pyrite in Units 1 and 3. In contrast, all redox parameters suggest  
602 anoxia for Unit 2. Strongly reducing Subunit 2a is Fe-limited in large part, whereas carbonate  
603 turbidites triggered pyritization and, in addition, induced a shift to less reducing (i.e. suboxic  
604 to anoxic) conditions during deposition of Subunit 2b.

605

### 606 *5.2.2 Salinity and water-column stratification*

607 Several authors suggested salinity stratification caused by basin restriction resulting  
608 from minor sea-level fluctuations to be the trigger of black shale deposition in the European  
609 Toarcian (e.g. Röhl et al., 2001; Frimmel et al., 2004; van de Schootbrugge et al., 2005).

610 Salinity stratification may have resulted from an accelerated hydrological cycle due to a  
611 monsoonal climate reducing the salinity of ocean-surface waters (e.g., Sælen et al., 1996). The  
612 reconstruction of salinity changes during deposition of the Bächental bituminous marls is  
613 based on GI and a plot of GI vs. 4-methylsteranes/ $\Sigma C_{29}$  steranes (Fig. 12). High values for GI  
614 indicate a stratified water column in marine and non-marine source-rock depositional  
615 environments, commonly resulting from a deep hypersaline water body (Fu et al., 1986).  
616 Alternatively, gammacerane may also originate from bacterivorous ciliates floating at the  
617 chemocline within the water column (Sinninghe Damsté et al., 1996; Schwark et al., 1998).  
618 According to these studies, elevated amounts of gammacerane might reflect a well-stratified  
619 water column, even in the absence of high-salinity bottom waters. However, the occurrence of  
620 bottom waters with elevated salinity in the Bächental basin is also confirmed by increased  
621 hopane isomerization ratios, which result from diagenetic processes specific for hypersaline  
622 conditions (ten Haven et al., 1987; see also section 5.1.1), as well as by large amounts of 4-  
623 methylsteranes, which are frequently related to halophilic microorganisms (e.g., ten Haven et  
624 al., 1985). A well-defined positive correlation exists between GI and 4-methylsteranes (Fig.  
625 12). The profiles of both GI and 4-methylsteranes indicate normal-marine salinity conditions  
626 during deposition of Units 1, 2b and 3. In contrast, generally enhanced salinity of bottom  
627 waters and a stratified water column is suggested for samples from Subunit 2a.

628         During deposition of Unit 1, frequent mixing and ventilation of the water column of  
629 the Bächental basin prevented the establishment of a stratified water mass and permanent  
630 anoxic conditions. The transition to OM-rich Subunit 2a was associated with a distinct  
631 increase of bottom water salinity and a concomitant flourishing of halophilic microorganisms.  
632 This interval is assigned to the lower *falciferum* Zone on the basis of occurrences of  
633 *Cleviceras exaratum*. Samples of Subunit 2a are also characterized by Pr/Ph ratios <1.0.  
634 Hence anoxic conditions in Subunit 2a were typically connected to a stratified water column.  
635 Elevated inputs of freshwater due to an accelerated hydrological cycle resulted in a surface-  
636 water layer with reduced salinity that caused intensified water-column stratification (Praus  
637 and Riegel, 1989; Littke et al., 1991; Sælen et al., 1996) and also may have contributed to  
638 salinity variation within the Bächental basin. Transient small-scale mixing of the watermass  
639 caused by turbidites triggered an episodic decrease of bottom water salinity reflected by lower  
640 GI values for a few samples from the middle and upper parts of Subunit 2a (e.g., 15.65 and  
641 16.55 m; Figs. 7.F, 12). Those samples are additionally characterized by comparatively low  
642 TOC and peak S contents (Figs. 3.B, D). Whereas a stagnant basin setting prevailed during  
643 deposition of Subunit 2a, the episodic occurrence of fine-grained carbonate turbidites caused

644 salinity stratification to break down, resulting in less intensely reducing conditions in Subunit  
645 2b (see Section 5.2.1). During deposition of Unit 3 a water column with uniform normal  
646 salinity went along with suboxic conditions. The observed salinity variations suggest that  
647 global climate processes as described for instance by Sælen et al. (1996) were overprinted by  
648 local factors within the Bächental basin, e.g., mixing of water bodies by turbidites, which also  
649 influenced the intensity of water-column anoxia.

650

### 651 5.2.3 Influence of sea-level variation

652 Variation in sea-level elevations exerted a pronounced influence on deposition of both  
653 the Alpine Bächental bituminous marls and the epicontinental Posidonia Shale (e.g., Röhl et  
654 al., 2001; Frimmel et al., 2004). The long-term eustatic record shows a sea-level fall from the  
655 Pliensbachian into the early Toarcian, a subsequent sea-level rise culminating in a middle  
656 Toarcian highstand, and another fall extending into the Aalenian (Haq et al., 1988; Hallam,  
657 1992). However, the short-term trend exhibits several additional sea-level fluctuations in  
658 Pliensbachian and Toarcian time (Fig. 13). Frimmel et al. (2004) found a remarkable  
659 correlation between the trend of C<sub>27</sub>/C<sub>29</sub> sterane ratios and the proposed sea-level trend of Haq  
660 et al. (1988) for the Posidonia Shale of Dotternhausen. Although sea-level estimations based  
661 on biomarker ratios are a rather untested technique, the sterane data for the Alpine Bächental  
662 bituminous marls also show a strong correlation with the 3<sup>rd</sup> order sea-level curve for the  
663 upper Pliensbachian-lower Toarcian interval (Haq et al., 1988; Fig. 13). These similar  
664 relationships thus provide a basis for correlation of the Bächental bituminous marls with the  
665 Dotternhausen section (Fig. 13; Frimmel et al., 2004; see Section 5.3.1). According to sterane  
666 ratios of the study section, the sea-level rise from the base of Unit 1 reached a highstand  
667 around 9 m, followed by an abrupt sea-level fall. The deposition of Subunit 2a, recording the  
668 highest TOC contents, coincided with a sea-level lowstand dated to the lower *falciferum* Zone  
669 based on the occurrence of *Cleviceras exaratum*, and a subsequent minor sea-level rise.  
670 Another highstand was reached close to the debrite overlying Subunit 2b, followed by minor  
671 sea-level fluctuations during deposition of Unit 3.

672 Sea-level fluctuations strongly influenced watermass exchange and hence ventilation  
673 of the Bächental basin (Fig. 14). Agreement between the sea-level curve and inferred  
674 variations in redox conditions and salinity demonstrate this influence. During the sea-level  
675 lowstand (Subunit 2a), watermass exchange and consequently oxygenation of basinal bottom  
676 waters were sharply reduced. Consequently, strongly anoxic conditions were established  
677 within the stratified watermass. High surface-water productivity and subsequent degradation

678 of OM additionally poisoned the depositional environment. Hence, Subunit 2a is generally  
679 characterized by strongly anoxic conditions and high OM preservation reflected by high TOC  
680 and HI values. The same correlation between stagnant basin conditions, strongest anoxia and  
681 best OM preservation during a sea-level lowstand and a subsequent sea-level rise has been  
682 postulated for the epicontinental Posidonia Shale of SW Germany (e.g. Röhl et al., 2001;  
683 Schmid-Röhl et al., 2002; Frimmel et al., 2004; see Section 5.3.1). In addition, a flourishing  
684 of surface-water productivity during the uppermost *tenuicostatum* to lower *falciferum* zones  
685 (e.g., Ikeda and Hori, 2014) contributed to elevated OM accumulation in Subunit 2a (see  
686 Section 5.2.4). During intervals of higher sea level (e.g., Units 1 and 3), better watermass  
687 exchange with surrounding epicontinental seas and, possibly, the open Tethys Ocean resulted  
688 in improved ventilation of the Bächental basin and in mainly suboxic conditions, reflected by  
689 sediments with lower TOC concentrations. Therefore, we suggest that minor sea-level  
690 fluctuations in combination with the complex bathymetry of the Bächental basin were among  
691 the controlling factors on deposition of the Bächental bituminous marls (Fig. 14).  
692 Consequently, the local basin setting had a strong influence on the establishment of salinity  
693 stratification and anoxic conditions.

694

#### 695 *5.2.4 Marine primary productivity*

696 Marine primary productivity is likely to have been influenced by major changes in  
697 global climate, atmospheric composition, and oceanographic conditions during the Early  
698 Jurassic. Eruption of the Karoo and Ferrar large igneous provinces (Encarnación et al., 1996;  
699 Svensen et al., 2007; Sell et al., 2014) triggered massive perturbations of the global carbon  
700 cycle, leading to strong global warming through volcanic CO<sub>2</sub> emissions (McElwain et al.,  
701 2005), possible methane release from gas hydrates (Hesselbo et al., 2000), and metamorphism  
702 of Paleozoic OM-rich shales (Svensen et al., 2007; Suan et al., 2008). The prevailing  
703 subtropical climate during the early Toarcian induced an acceleration of the hydrological  
704 cycle, modulated by astronomical forcing (Kemp et al., 2005), and an intensification of  
705 continental weathering (Palfy and Smith, 2000; Weissert, 2000; Cohen et al., 2004). These  
706 processes resulted in an elevated supply of nutrients to ocean-surface waters, stimulating  
707 marine primary productivity (Parrish and Curtis, 1982; Parrish, 1993; Cohen et al., 2004).  
708 Jenkyns (2010) hypothesized that there was a globally synchronous increase in organic  
709 productivity in the early Toarcian (upper *tenuicostatum*-lower *falciferum* zones) triggered by  
710 high levels of nutrient availability in surface waters. Orbital-scale productivity cycles are  
711 suggested to have triggered onset and termination of the T-OAE (Ikeda and Hori, 2014).

712 A detailed interpretation of stratigraphic variations of primary productivity is not  
713 possible for the Bächental section owing to intense bacterial degradation of OM in Units 1  
714 and 3 (see Section 5.1.3). However, the remarkable amounts of S in those units suggest a high  
715 amount of OM originally present in rocks. Therefore, it is suggested that, on average, high  
716 primary production of OM in surface waters prevailed throughout the interval of deposition of  
717 the Bächental bituminous marls. Relatively high and uniform HI values suggest a lesser  
718 degree of OM degradation in Unit 2. For this reason, TOC variations in Unit 2 are inferred to  
719 reflect changes in surface-water primary productivity. This interval is also characterized by a  
720 significant TOC increase in the study section (Fig. 3.A) and in several age-equivalent sections  
721 in the European and Mediterranean domains (Jenkyns et al., 1988; Hesselbo et al., 2000; Röhl  
722 et al., 2001; Kemp et al., 2005; Pearce et al., 2008; Sabatino et al., 2009; Kafousia et al.,  
723 2014). The two samples that exhibit peak TOC contents after steady increases (at 13.39 m and  
724 19.15 m) are also significantly enriched in short-chained *n*-alkanes (Fig 7.A). Hence, a  
725 flourishing of marine algae and bacterioplankton in surface waters contributed to elevated  
726 OM accumulation at least in parts of Subunit 2a.

727 There is an ongoing discussion whether enhanced organic productivity or increased  
728 preservation was the main controlling factor behind the accumulation of OM-rich deposits in  
729 the lower Toarcian (e.g., Demaison and Moore, 1980; Pedersen and Calvert, 1990; Ikeda and  
730 Hori, 2014). Increased bioproductivity results in larger amounts of OM in bottom sediments  
731 that subsequently can accelerate the establishment of reducing conditions due to oxygen  
732 depletion by enhanced OM degradation (e.g., Röhl et al., 2001; Ikeda and Hori, 2014). The  
733 intervals exhibiting productivity maxima in Subunit 2a are also characterized by a salinity-  
734 stratified watermass and intense anoxia during a period of relative sea-level lowstand (see  
735 Sections 5.3.1-3). Hence, it cannot be fully resolved whether increased productivity or  
736 enhanced preservation controlled OM accumulation in those units. However, as strictly  
737 reducing conditions and high-salinity bottom waters typically dominated during deposition of  
738 Subunit 2a, we suggest that the TOC cycles culminating at 13.39 m and 19.15 m reflect  
739 primary productivity cycles during periods of rather constant depositional conditions.

740

### 741 ***5.3 Broader implications***

#### 742 *5.3.1 Correlation and dating of Bächental bituminous marls*

743 C-isotope chemostratigraphy has been widely used to correlate and date sections with  
744 poor biostratigraphic control (see Weissert, 2013 for summary). The early Toarcian is  
745 characterized by a distinct negative carbon isotope excursion (CIE) that is commonly

746 recorded by both marine carbonates and marine and terrestrial OM, and that has been used as  
747 a global chemostratigraphic marker (e.g., Sabatino et al., 2009; Al-Suwaidi et al., 2010;  
748 Mazzini et al., 2010; Gröcke et al., 2011; Caruthers et al., 2011; Sell et al., 2014). As  
749 discussed in Section 5.1.3, the carbonate C-isotope profile of the Bächental bituminous marls  
750 records a mixed signal derived from primary and secondary carbonate phases. The diagenetic  
751 overprint especially in Units 1 and 3 is sufficiently strong that it is not possible to extract the  
752 primary isotopic signal, and, hence, correlation with age-equivalent sections on the basis of  
753  $\delta^{13}\text{C}_{\text{carb}}$  chemostratigraphy is not possible.

754 An alternative for correlation of the poorly dated Bächental bituminous marls with the  
755 biostratigraphically well-dated epicontinental German Posidonia Shale is provided by sterane  
756 ratio profiles. The Posidonia Shale includes three ammonite biozones (from base to top):  
757 *tenuicostatum*, *falciferum*, and *bifrons* (Riegraf et al., 1984, 1985; see also Röhl et al., 2001;  
758 Frimmel et al., 2004). Frimmel et al. (2004) documented systematic stratigraphic variation in  
759 sterane ratios ( $\text{C}_{27}/\text{C}_{29}$ ;  $\text{C}_{27}/\text{C}_{29}$   $\alpha\alpha\alpha\text{R}$ ) at Dotternhausen in SW Germany. The onset of  
760 Posidonia Shale deposition is characterized by a shift to lower ratios, from 1.0 in the  
761 underlying strata to 0.6 to 0.8 in the lower *tenuicostatum* Zone (Fig. 13). Sterane ratios  
762 increase progressively through the *falciferum* Zone and peak at ~1.4 in the lowermost *bifrons*  
763 Zone before declining abruptly to constant values of 0.7-0.9 upsection. It has to be mentioned  
764 that stratigraphic correlation based on biomarker data is a rather untested and unconventional  
765 technique. Nevertheless, the Bächental bituminous marls exhibit an almost identical pattern of  
766 stratigraphic variation in sterane ratios, although absolute values are about 20% lower relative  
767 to the Dotternhausen section (Fig. 13). According to this correlation, accumulation of the  
768 Bächental bituminous marls in the Alpine realm commenced during Pliensbachian time  
769 (*margaritatus* Zone), which is consistent with reports of the presence of *Arietoceras* sp. and  
770 *Arietoceras* sp. or *Leptaleoceras* sp. from Unit 1 (Kodina et al., 1988). This correlation  
771 demonstrates that the base of the Bächental bituminous marls is distinctly older than the base  
772 of the Posidonia Shale deposited in epicontinental areas of SW Germany (*tenuicostatum*  
773 Zone; Riegraf et al., 1984, 1985; Frimmel, 2004). Units 2 and 3 at Bächental are correlative  
774 with the Posidonia Shale, with Subunit 2a dating to the mid-*tenuicostatum* to upper *falciferum*  
775 zones, Subunit 2b to the uppermost *falciferum* and lowermost *bifrons* zones, and Unit 3 to the  
776 *bifrons* Zone. This correlation is supported by the occurrence of *Cleviceras exaratum*, which  
777 suggests a stratigraphic age for the base of Subunit 2a (13.40 m) equivalent to the lower  
778 *falciferum* Zone, as well as by common patterns of sea-level variation in the Bächental and  
779 Dotternhausen sections (Fig. 13; see Section 5.2.3). On the basis of these considerations, we



780 infer that the onset of black marl deposition in the Alpine and epicontinental realm was not  
781 coeval (Fig. 13). Global forces were overprinted by local factors regarding timing of initiation  
782 of OM-accumulation in different basin settings in Pliensbachian and Toarcian times.

783

### 784 5.3.2 Applicability of the lower Toarcian CIE as stratigraphic marker

785 A pronounced negative CIE is widely regarded as a defining characteristic of the T-  
786 OAE and a global chemostratigraphic marker for the uppermost *tenuicostatum* and lower  
787 *falciferum* zones. This negative CIE has been reported from sections in NW Europe and the  
788 Mediterranean (e.g., Röhl et al., 2001; Jenkyns et al., 2001; Kemp et al., 2005; Hesselbo et al.,  
789 2007; Sabatino et al., 2009; Kafousia et al., 2014), the NE paleo-Pacific ocean (Caruthers et  
790 al., 2011), South America (Al-Suwaidi et al., 2010; Mazzini et al., 2010; Sell et al., 2014), and  
791 northwestern Panthalassa (Izumi et al., 2012). The negative CIE has been related to a rapid  
792 release of biogenic methane by dissociation of methane hydrates (e.g., Hesselbo et al., 2000,  
793 2007; Jenkyns et al., 2002; Kemp et al., 2005), release of large volumes of CO<sub>2</sub> due to the  
794 emplacement of the Karoo-Ferrar LIP (e.g., Palfy and Smith, 2000; Mazzini et al., 2010),  
795 thermogenic methane resulting from the intrusion of igneous rocks into Gondwanan coals  
796 (McElwain et al., 2005; Svensen et al., 2007), recycling of OM (“recycling model”; Küspert,  
797 1982, 1983; Röhl et al., 2001), and to the contribution of OM deriving either from calcareous  
798 or organic-walled plankton (Jenkyns and Clayton, 1986). Caruthers et al. (2011) inferred that  
799 the early Toarcian negative CIE was a global signal that had been imprinted on all active  
800 global reservoirs of the exchangeable carbon cycle. However, both the organic and inorganic  
801 carbon isotope profiles of the Bächental section do not show the typical early Toarcian  
802 negative CIE (Figs. 4.B, D).

803 Whereas carbonate C-isotope values of Units 1 and 3 reflect a strong diagenetic  
804 overprint,  $\delta^{13}\text{C}_{\text{carb}}$  values of Unit 2 are interpreted to be less altered (see Section 5.1.3). Age  
805 correlation based on sterane data (see Section 5.3.1) as well as the occurrence of *Cleviceras*  
806 *exaratum* suggests an upper *tenuicostatum* to lower *falciferum* Zone assignment for the lower  
807 half of Subunit 2a, i.e., equivalent in time to the early Toarcian negative CIE. However,  
808 neither the organic  $\delta^{13}\text{C}$  nor the carbonate  $\delta^{13}\text{C}$  profile of the study section exhibits the early  
809 Toarcian negative CIE for reasons that remains unclear.

810  $\delta^{13}\text{C}_{\text{org}}$  compositions for the Bächental bituminous marls are considerably lighter (-  
811 32.7 to -30.6‰ VPDB) than typical values for modern marine plankton (-24 to -18‰ VPDB;  
812 e.g., Lewan, 1986; Tyson, 1995). They are also significantly lighter than average values of  
813 other lower Toarcian profiles as the  $\delta^{13}\text{C}_{\text{org}}$  values of the entire Bächental bituminous marls

814 succession are in the range of the lower Toarcian negative organic CIE (Hesselbo et al., 2000;  
815 Kemp et al., 2005; Röhl et al., 2001; Sabatino et al., 2009; Al-Suwaidi et al., 2010; Caruthers  
816 et al., 2011; Gröcke et al., 2011). The origin of the generally light  $\delta^{13}\text{C}_{\text{org}}$  values in the  
817 Bächental bituminous marls is not yet clear, and several mechanisms are possible. [i]  $^{13}\text{C}$ -  
818 depleted OM produced by means of carbon recycling processes mediated by  
819 chemoautotrophic and methanotrophic microbes within an anoxic, stratified water column  
820 (e.g., Küspert, 1982, 1983; Hollander and Smith, 2001). Biogenic methane oxidation at the  
821 oxic/anoxic interface during periods of highest nutrient concentrations in the water column  
822 may have reinforced this signal; hence, the level of eutrophication controls the  
823 biogeochemical processes that influence  $\delta^{13}\text{C}_{\text{org}}$  compositions (Hollander and Smith, 2001).  
824 [ii] Varying contributions of OM from eukaryotic algae, anaerobic chemoautotrophs, and  
825 other microbial plankton (e.g., Luo et al., 2014). In that study, chemoautotrophic bacteria  
826 were suggested to be the source of strongly  $^{13}\text{C}$ -depleted OM in deepwater environments. [iii]  
827 Expandable smectite possibly derived from alteration of volcanic ash is abundant in all  
828 samples; hence a contribution of isotopically light  $\text{CO}_2$  from volcanic emissions is possible.

829 On the other hand, OM-poor rocks of *Scheibelberg Fm.* and *Upper Allgäu Fm.* show  
830 heavier  $\delta^{13}\text{C}_{\text{org}}$  isotope values (-29.4 to -23.6‰ VPDB) that are similar to correlative strata in  
831 other Toarcian sections (see above for references) and, hence, were not affected by processes  
832 described above. In the case of the lower Toarcian Bächental bituminous marls, the  $\delta^{13}\text{C}_{\text{carb}}$ ,  
833  $\delta^{18}\text{O}_{\text{carb}}$ , and  $\delta^{13}\text{C}_{\text{org}}$  isotopes do not show any correlation. Furthermore, the pronounced  
834 negative CIE ( $\delta^{13}\text{C}_{\text{carb}}$  and  $\delta^{13}\text{C}_{\text{org}}$ ) that characterizes the lower Toarcian globally is missing,  
835 questioning its unrestricted applicability as a ubiquitous chemostratigraphic marker for this  
836 time interval. The reason for its absence is not yet clear but may be due to overprinting of the  
837 global signal by local controls.

838

### 839 5.3.3 OM accumulation in Pliensbachian-Toarcian: Oceanic response to magmatic events

840 Significant relationships exist between emplacement of LIPs, long-term environmental  
841 changes, global climate warming, and extinction events reflected by major geochemical  
842 perturbations and increased OM accumulation (“volcanic greenhouse scenario”; Wignall et  
843 al., 2005; Caruthers et al., 2013). The end-Triassic release of large quantities of greenhouse  
844 gases during the CAMP eruptions (~201 Ma) initiated a significant global warming process  
845 during Early Jurassic times (McElwain et al., 1999; McHone, 2003; Cohen and Coe, 2007).  
846 Global warming intensified further as a consequence of volcanic activity associated with the  
847 rift-related Karoo and Ferrar LIPs (Caruthers et al., 2013) during the Early Jurassic

848 (Encarnación et al., 1996; Minor and Mukasa, 1997; Svensen et al., 2007, 2012; Sell et al.,  
849 2014), resulting in peak “greenhouse Earth” conditions in the Toarcian (Jenkyns and Clayton,  
850 1997; Pálffy and Smith, 2000; Weissert, 2000; Jenkyns, 2003). In addition, several volcanic  
851 pulses were associated with complex rifting of the Alpine Tethys ranging from the Late  
852 Triassic to the Middle Jurassic (Decarlis et al., 2013). The establishment and intensification of  
853 greenhouse climate at that time was possibly supported by the release of methane hydrates  
854 (Jenkyns and Clayton, 1997; Hesselbo et al., 2000). In addition, the Karoo-Ferrar volcanism  
855 intensified continental weathering and the hydrological cycle (Cohen et al., 2004). The marine  
856 ecosystem was affected by alterations of seawater chemistry (Martin and Macdougall, 1995)  
857 and development of oceanic anoxia (Harnik et al., 2012). The late Pliensbachian and early  
858 Toarcian were characterized by several marine extinction events that were probably triggered  
859 by eruptions of the Karoo and Ferrar LIPs (Dera et al., 2010; Caruthers et al., 2013). Although  
860 the main phase of extinction occurred within an interval ranging from the Pliensbachian-  
861 Toarcian boundary to the lowermost *falciferum* Zone, a significant global extinction pulse is  
862 also reported for the late Pliensbachian *margaritatus* Zone, indicating a rapid biotic response  
863 to LIP activity (Dera et al., 2010; Caruthers et al., 2013). The combination of these global  
864 changes provided conditions favourable to OM accumulation during upper Pliensbachian and  
865 lower Toarcian in oceanic settings.

866         The apparent onset of OM accumulation in the tectonically complex Bächental basin  
867 during the late Pliensbachian *margaritatus* Zone (Fig. 13) is consistent with data from other  
868 age-equivalent sections in semi-restricted depositional settings, e.g., Cleveland Basin in NW  
869 Europe (McArthur et al., 2008) and the Neuquén Basin in Argentina (Al-Suwaidi et al., 2010).  
870 This suggests a rapid oceanic response of semi-restricted basins to greenhouse gas emissions,  
871 elevated atmospheric CO<sub>2</sub> levels, and global climate warming triggered by the Karoo and  
872 Ferrar LIPs (cf. Mazzini et al., 2010). Whereas high precision U-Pb data suggest a  
873 stratigraphic age of ~183 Ma (equivalent to early Toarcian) for the onset of Karoo volcanism  
874 (Svensen et al., 2007, 2012; Sell et al., 2014), the Ferrar LIP was active already at ~184 Ma  
875 (equivalent to late Pliensbachian; Encarnación et al., 1996; Minor and Mukasa, 1997). Thus,  
876 the early stages of Early Jurassic LIP magmatism may have coincided with the onset of OM  
877 accumulation for the above-mentioned sections. In the Alpine Tethyan domain, the  
878 establishment of anoxia in Pliensbachian to Toarcian times was linked to local basin  
879 geometry, with reducing conditions commencing earlier than the Toarcian in basins that were  
880 prone to restriction and water-column stratification (Fig. 14).

881 The carbonate-free mudstone at the base of the Bächental bituminous marls contains  
882 charred organic material typically connected to wildfires (e.g., Brown et al., 2012) and large  
883 amounts of expandable smectite possibly derived from alteration of volcanic ash. In contrast,  
884 the underlying *Scheibelberg Formation* contains only illite in its clay fraction. This suggests  
885 that onset of OM accumulation and establishment of reducing conditions in the Bächental  
886 basin were associated with a volcanic event of possibly regional scale in the NW Tethyan  
887 domain. Significant amounts of smectite present in all marl samples indicate a pronounced  
888 contribution of volcanic-derived detritus during deposition of the Bächental bituminous marls.  
889 This is consistent with the occurrence of volcanic ashes and lava flows in the Pliensbachian  
890 and Toarcian of the Tethyan domain (Decarlis et al., 2013), the complex rift history of the  
891 Valais, Briançonnais and Piemonte-Liguria domains at the proximal European and Adriatic  
892 margins between late Sinemurian and Callovian time (Mohn et al., 2010), and the  
893 contemporaneous break-up of the Ligurian-Penninic oceanic realm (Ratschbacher et al.,  
894 2004).

895 The main pulses of Karoo and Ferrar LIP magmatism during the upper *tenuicostatum*-  
896 lower *falciferum* zones are thought to have triggered the T-OAE on a global scale (e.g.,  
897 Svensen et al., 2007; Dera et al., 2010; Mazzini et al., 2010; Ikeda and Hori, 2014). The main  
898 eruption stage of these LIPs correlates approximately with the base of Subunit 2a (Figs. 2,  
899 13). Subunit 2a accumulated in a restricted basinal setting characterized by strictly anoxic  
900 conditions, a salinity-stratified watermass, and a concurrent flourishing of surface-water  
901 productivity during a period of relative sea-level lowstand. Hence, local factors (i.e., basin  
902 restriction due to eustatic controls) can sufficiently explain environmental conditions  
903 controlling bituminous marl sedimentation in the Bächental basin. However, LIP-related  
904 perturbations of the carbon cycle triggered global conditions favoring widespread  
905 development of marine anoxia that potentially reinforced the local controlling factors in the  
906 Bächental basin and triggered rapid OM accumulation in Subunit 2a of the study section.

907

## 908 **6. Conclusions**

909

910 The Bächental bituminous marls provide insights into global and local factors  
911 controlling the onset and duration of OM accumulation in semi-restricted basins during late  
912 Pliensbachian and early Toarcian times.

- 913 • A stagnant basin setting during a period of relative sea-level lowstand in Subunit 2a  
914 corresponding to the upper *tenuicostatum* and lower *falciferum* zones triggered the

915 establishment of strong anoxia, a salinity-stratified watermass, and a flourishing of  
916 surface-water productivity that jointly enhanced OM accumulation. Hence, redox and  
917 salinity changes in the tectonically complex Bächental basin were controlled mainly  
918 by minor sea-level fluctuations that resulted in varying watermass exchange and  
919 bottom water oxygenation.

- 920 • Stratigraphic correlation of the Bächental bituminous marls with the time-equivalent  
921 SW German Posidonia Shale suggests that deposition of OM-rich sediments in the  
922 Alpine realm commenced earlier (late Pliensbachian *margaritatus* Zone) than in  
923 proximal epicontinental areas (early Toarcian *tenuicostatum* Zone) indicating a rapid  
924 oceanic response to the major environmental perturbations caused by the activity of  
925 Karoo and Ferrar LIPs and complex rifting of the Alpine Tethys in local basins that  
926 were prone to the development of water-column stratification and deepwater anoxia  
927 because of their geometry or paleogeographic setting. Charred material at the base of  
928 the study section suggests that a possibly regional volcanic event was the trigger for  
929 onset of OM accumulation. Continued inputs of volcanic detritus during marl  
930 deposition confirms volcanic activity during late Pliensbachian and early Toarcian  
931 times in the NW Tethyan domain. Intervals with peak TOC contents in the study  
932 section probably correspond to the main magmatic stage of the Karoo and Ferrar LIPs,  
933 suggesting a massive effect on coeval marine productivity.
- 934 • The early Toarcian negative CIE that is observed in age-equivalent sections worldwide  
935 is not visible in either the carbonate or organic carbon  $\delta^{13}\text{C}$  profiles of the study  
936 section. Thus, this chemostratigraphic marker cannot be used in correlation of the  
937 Bächental bituminous marls. The global CIE appears to have been overprinted owing  
938 to local factors in the study section. Consequently, the unrestricted applicability of the  
939 early Toarcian negative CIE as a ubiquitous chemostratigraphic marker for the early  
940 Toarcian has to be questioned.

941

## 942 **Acknowledgments**

943

944 We gratefully thank family Albrecht (Tiroler Steinöl ®) who operate the Bächental  
945 open pit for their technical support during sampling and Joachim Blau (Giessen) for  
946 identification of the ammonite *Cleviceras exaratum*. Research by TJA is supported by the  
947 Sedimentary Geology and Paleobiology program of the U.S. National Science Foundation, the

948 NASA Exobiology program, and the State Key Laboratory of Geological Processes and  
949 Mineral Resources, China University of Geosciences, Wuhan (Program GPMR201301).

950

951

952

953

954

955

956

957

958

959

960

961

962

963

964

965

966

967

968

969

970

971

972

973

974

975

976

977

978 **Appendix – Full data set for samples of the investigated Bächental section**

979

980 **Table 1:** Bulk geochemical data for samples of Bächental section.

<b>Sample</b>	<b>Diag. carb.</b> <i>[peak area]</i>	<b>TOC</b> <i>[%]</i>	<b>C<sub>c<sub>eq</sub></sub></b> <i>[%]</i>	<b>S</b> <i>[%]</i>	<b>HI</b> <i>[mg HC/g TOC]</i>	<b>Fe</b> <i>[%]</i>	<b>δ<sup>13</sup>C<sub>carb</sub></b> <i>[‰ VPDB]</i>	<b>δ<sup>18</sup>O<sub>carb</sub></b> <i>[‰ VPDB]</i>	<b>δ<sup>13</sup>C<sub>org</sub></b> <i>[‰ VPDB]</i>
<b>BT 68</b>	-	0.1	81.5	0.1	-	0.2	-0.1	-2.1	-26.7
<b>BT 67</b>	-	0.2	43.6	0.0	-	0.8	0.2	-3.9	-25.6
<b>BT 66</b>	-	0.3	29.9	0.0	-	2.6	0.1	-5.0	-26.3
<b>BT 65</b>	-	0.3	35.8	0.0	-	1.5	-0.7	-4.9	-26.0
<b>BT 64</b>	-	0.1	82.2	0.1	-	0.	-0.1	-1.9	-27.1
<b>BT 63</b>	-	0.4	40.4	0.4	-	0.6	-0.8	-4.2	-29.4
<b>BT 62</b>	-	0.1	71.1	0.2	-	-	-0.8	-1.8	-27.6
<b>BT 61</b>	-	0.3	43.4	0.1	-	0.6	-0.8	-4.0	-25.9
<b>BT 60</b>	-	0.3	49.6	0.2	-	0.4	-0.7	-3.5	-26.1
<b>BT 59</b>	-	0.1	78.4	0.1	-	-	-0.6	-2.0	-
<b>BT 58</b>	4990	2.8	23.2	5.4	544	4.7	-2.6	-4.4	-31.6
<b>BT 57</b>	5080	3.0	22.8	5.8	541	6.1	-2.2	-4.2	-31.6
<b>BT 56</b>	17590	2.1	50.8	3.4	541	3.7	-5.8	-3.6	-30.6
<b>BT 55</b>	6250	1.6	33.3	3.2	503	-	-6.0	-3.8	-
<b>BT 54</b>	17560	1.5	53.3	5.0	375	1.4	-7.2	-3.5	-26.4
<b>BT 53</b>	14040	1.6	47.1	5.7	415	4.	-5.6	-3.2	-31.1
<b>BT 52</b>	18680	1.7	52.0	5.0	419	4.0	-10.8	-3.1	-31.2
<b>BT 51</b>	21260	1.5	55.4	2.1	362	3.4	-12.7	-3.0	-30.9
<b>BT 50</b>	14960	1.6	56.7	1.3	325	4.9	-5.2	-2.1	-31.1
<b>BT 49</b>	16860	1.7	52.9	2.6	292	-	-6.9	-2.8	-
<b>BT 48</b>	16510	2.1	51.0	2.5	379	3.9	-7.3	-3.3	-31.1
<b>BT 47</b>	16900	1.6	60.7	2.0	320	5.3	-8.6	-2.3	-31.1
<b>BT 46</b>	15200	1.5	64.8	1.9	370	3.2	-7.9	-2.4	-
<b>BT 45</b>	14100	1.5	56.9	2.6	400	5.2	-8.3	-2.5	-31.1
<b>BT 44</b>	15990	1.9	48.6	5.3	350	5.4	-8.7	-2.7	-31.0
<b>BT 43</b>	-	0.1	82.6	0.2	-	0.9	0.8	-1.4	-28.7
<b>BT 42</b>	-	0.1	90.8	0.0	-	0.6	-0.2	-1.4	-29.0
<b>BT 41</b>	-	0.1	89.5	0.1	-	0.8	-0.2	-2.3	-30.1
<b>BT 40</b>	7830	3.0	36.9	3.5	604	3.5	-2.5	-3.8	-30.6
<b>BT 39</b>	2630	5.6	38.8	5.1	683	1.1	-1.5	-4.0	-30.9
<b>BT 38</b>	2690	5.6	32.3	5.3	661	1.9	-4.2	-4.7	-32.1
<b>BT 37</b>	3370	6.3	18.6	4.4	622	5.2	-1.8	-5.1	-32.7
<b>BT 36</b>	1170	2.9	35.2	5.9	572	3.9	-2.7	-4.3	-30.9
<b>BT 35</b>	710	9.4	56.0	2.1	666	1.5	-2.1	-3.9	-32.0
<b>BT 34</b>	2040	8.0	43.1	2.6	644	0.3	-2.9	-4.6	-31.1
<b>BT 33</b>	2430	3.6	33.9	2.6	670	3.2	-2.4	-4.4	-30.6
<b>BT 32</b>	2400	4.0	27.1	7.0	602	6.1	-2.4	-4.4	-31.2
<b>BT 31</b>	470	5.4	58.8	1.3	687	1.0	-2.0	-3.2	-31.1
<b>BT 30</b>	2840	2.9	17.4	4.3	604	4.3	-2.9	-5.2	-32.1

<b>Sample</b>	<b>Diag. carb.</b> <i>[peak area]</i>	<b>TOC</b> <i>[%]</i>	<b>Cc<sub>eq</sub></b> <i>[%]</i>	<b>S</b> <i>[%]</i>	<b>HI</b> <i>[mg HC/g TOC]</i>	<b>Fe</b> <i>[%]</i>	<b>δ<sup>13</sup>C<sub>carb</sub></b> <i>[‰ VPDB]</i>	<b>δ<sup>18</sup>O<sub>carb</sub></b> <i>[‰ VPDB]</i>	<b>δ<sup>13</sup>C<sub>org</sub></b> <i>[‰ VPDB]</i>
<b>BT 29</b>	740	6.8	60.7	1.6	686	1.2	-1.9	-3.8	-31.6
<b>BT 28</b>	2520	3.5	29.2	7.1	588	6.0	-2.8	-4.1	-31.7
<b>BT 27</b>	3070	6.0	36.8	2.8	670	-	-2.9	-5.1	-
<b>BT 26</b>	2830	7.6	37.9	3.0	653	0.1	-3.0	-4.8	-31.5
<b>BT 25</b>	580	12.9	27.2	2.9	622	0.5	-2.6	-6.0	-32.1
<b>BT 24</b>	1830	11.7	30.7	2.8	621	0.5	-2.6	-5.9	-31.7
<b>BT 23</b>	1360	9.0	31.1	2.7	649	2.6	-2.9	-5.3	-31.8
<b>BT 22</b>	260	8.6	38.0	3.2	645	0.2	-3.0	-5.4	-32.2
<b>BT 21</b>	13460	1.8	43.6	4.2	519	3.5	-6.3	-3.7	-31.0
<b>BT 20</b>	12720	2.0	40.0	4.3	495	3.6	-6.2	-3.6	-31.1
<b>BT 19</b>	4280	3.3	31.0	5.6	612	4.0	-4.0	-4.0	-32.0
<b>BT 18</b>	2200	2.5	32.1	2.2	577	3.3	-1.8	-3.9	-31.0
<b>BT 17</b>	12060	1.8	42.2	4.3	537	4.2	-6.9	-3.6	-31.5
<b>BT 16</b>	11350	2.3	34.6	3.8	497	4.4	-6.3	-3.4	-31.6
<b>BT 15</b>	4940	1.9	30.7	5.5	427	5.2	-6.1	-3.4	-31.7
<b>BT 14</b>	11630	1.4	39.6	5.7	306	3.5	-10.0	-3.5	-31.5
<b>BT 13</b>	7750	1.1	43.4	3.6	307	9.2	-4.7	-2.3	-31.6
<b>BT 12</b>	3820	2.2	24.4	5.3	518	4.2	-3.2	-3.9	-32.0
<b>BT 11</b>	13820	1.8	34.1	3.7	441	4.8	-6.9	-3.8	-32.0
<b>BT 10</b>	13750	1.8	31.2	5.5	452	5.2	-8.7	-3.5	-31.7
<b>BT 9</b>	12200	1.6	32.9	5.4	459	4.8	-9.8	-3.6	-31.6
<b>BT 8</b>	-	1.8	0.6	0.1	37	11.7	-26.0	-24.3	-
<b>BT 7</b>	-	1.8	1.0	0.1	74	21.9	-23.5	-22.9	-28.7
<b>BT 6</b>	-	0.1	87.5	1.1	-	0.3	1.5	-1.4	-23.6
<b>BT 5</b>	-	0.1	89.8	0.1	-	0.0	0.9	-1.4	-26.9
<b>BT 4</b>	-	0.1	76.2	0.1	-	0.0	0.8	-2.3	-25.8
<b>BT 3</b>	-	0.1	84.2	0.5	-	0.0	1.0	-1.6	-27.4
<b>BT 2</b>	-	0.1	80.4	0.1	-	0.0	1.0	-1.6	-26.3
<b>BT 1</b>	-	0.1	90.2	0.0	-	-	1.4	-1.2	-

981

982

983

984

985

986

987

988

989

990

991



992 **Table 2:** Organic geochemical data for investigated bituminous marls of Bächental section.

Sample	<i>n</i> -C <sub>15-19</sub> / Σ <i>n</i> -alkanes [rel. prop.]	<i>n</i> -C <sub>27-31</sub> / Σ <i>n</i> -alkanes [rel. prop.]	Pr/Ph [conc. ratios]	C <sub>27</sub> /C <sub>29</sub> <i>ααα</i> R Steranes [conc. ratios]	C <sub>27</sub> /C <sub>29</sub> Steranes [conc. ratios]	4-Methylsteranes/ C <sub>29</sub> Steranes [conc. ratios]
BT58	0.30	0.16	1.39	0.59	0.59	0.74
BT 55	0.30	0.16	1.76	0.76	1.03	1.00
BT 50	0.33	0.15	1.73	0.62	0.88	0.92
BT 45	0.34	0.15	1.59	0.66	0.91	1.08
BT 44	0.31	0.16	0.88	0.70	0.76	2.55
BT 40	0.34	0.16	1.30	0.75	1.01	1.34
BT 39	0.22	0.20	0.92	0.81	1.10	1.68
BT 37	0.32	0.15	1.06	0.56	0.77	1.16
BT 36	0.24	0.19	0.89	0.75	0.97	1.04
BT 35	0.56	0.02	0.93	0.56	0.57	3.10
BT 33	0.30	0.16	0.73	0.73	0.95	1.81
BT 31	0.35	0.13	0.76	0.60	0.77	2.80
BT 30	0.25	0.22	0.76	0.54	0.68	1.50
BT 29	0.39	0.11	0.78	0.51	0.62	2.89
BT 28	0.34	0.15	0.70	0.56	0.77	2.14
BT 26	0.34	0.13	0.76	0.57	0.68	2.90
BT 25	0.52	0.09	1.01	0.52	0.58	3.22
BT 24	0.32	0.21	0.86	0.57	0.64	3.06
BT 23	0.23	0.32	0.82	0.50	0.57	2.39
BT 22	0.31	0.17	0.80	0.50	0.59	2.79
BT 20	0.34	0.17	1.33	0.60	0.83	1.72
BT 18	0.27	0.16	1.35	0.91	1.24	1.95
BT 15	0.33	0.16	1.80	0.74	0.97	0.89
BT 12	0.30	0.16	0.96	0.69	0.79	2.24
BT 10	0.31	0.18	1.08	0.60	0.79	1.56
BT 8	0.23	0.24	0.94	0.59	0.70	2.10

993

994

995

996

997

998

999

1000

1001

1002

1003

1004

1005 **Table 3:** Organic geochemical data for investigated bituminous marls of Bächental section.

Sample	Mono-/triaromatic Steroids [conc. ratios]	Steranes [S/(S+R)] [conc. ratios]	DBT/Phen [conc. ratios]	Gammacerane Index [conc. ratios]	Hopanes [S/(S+R)] [conc. ratios]	Aryl- Isoprenoids [ $\mu\text{g/g TOC}$ ]
BT 58	3.39	0.11	0.32	0.07	0.80	107.65
BT 55	3.41	0.10	0.23	0.05	0.73	52.76
BT 50	3.16	0.12	0.30	0.12	0.92	37.93
BT 45	2.68	0.11	0.48	0.16	0.93	25.00
BT 44	1.64	0.32	0.46	0.59	1.16	112.14
BT 40	3.15	0.12	0.48	0.17	0.80	52.61
BT 39	2.98	0.12	0.46	0.16	0.77	62.17
BT 37	2.94	0.11	0.49	0.09	0.78	5.76
BT 36	2.55	0.14	0.60	0.14	0.91	69.93
BT 35	1.48	0.23	0.75	0.80	1.33	33.65
BT 33	2.17	0.29	0.69	0.41	1.0	54.14
BT 31	1.34	0.31	0.76	0.63	1.43	15.54
BT 30	1.74	0.30	0.78	0.27	1.27	28.82
BT 29	1.29	0.32	0.83	0.77	1.72	10.92
BT 28	1.61	0.31	0.78	0.39	1.35	10.03
BT 26	1.31	0.33	0.75	0.71	1.42	9.31
BT 25	1.33	0.25	0.78	0.77	1.28	84.01
BT 24	1.41	0.32	0.72	0.72	1.25	21.20
BT 23	1.54	0.28	0.64	0.55	1.21	15.59
BT 22	1.25	0.28	0.78	0.75	1.46	9.63
BT 20	2.91	0.11	0.46	0.13	0.79	27.82
BT 18	3.81	0.18	0.23	0.15	0.81	8.01
BT 15	3.78	0.11	0.25	0.05	0.77	3.15
BT 12	2.07	0.27	0.29	0.53	1.01	22.88
BT 10	2.06	0.16	0.33	0.37	0.99	13.31
BT 8	1.68	0.23	0.38	0.58	1.11	1.26

1006

1007

1008

1009

1010

1011

1012

1013

1014

1015

1016

1017

1018 **References**

1019

1020 Algeo, T.J., Wilkinson, B.H., Lohmann, K.C., 1992. Meteoric-burial diagenesis of Pennsylvanian carbonate:  
1021 water/rock interactions and basin geothermics. *Journal of Sedimentary Petrology* 62, 652-670.

1022 Al-Suwaidi, A.H., Angelozzi, G.N., Baudin, F., Damborenea, S.E., Hesselbo, S.P., Jenkyns, H.C., Manceñido,  
1023 M.O., Riccardi, A.C., 2010. First record of the Early Toarcian Oceanic Anoxic Event from the Southern  
1024 Hemisphere, Neuquén Basin, Argentina. *Journal of the Geological Society, London* 167, 633-636.

1025 Arthur, M.A., Sageman, B.B., 1994. Marine black shales: Depositional mechanisms and environments of ancient  
1026 deposits. *Annual Review of Earth and Planetary Sciences* 2, 126-166.

1027 Auras, S., Püttmann, W., 2004. Zusammensetzung und Herkunft der 4-Methylsterioide im Messeler Ölschiefer.  
1028 *Cour. Forsch.-Inst. Senckenberg* 252, 139-149.

1029 Barakat, A.O., Rullkötter, J., 1997. A comparative study of molecular paleosalinity indicators: chromans,  
1030 tocopherols and C<sub>20</sub> isoprenoid thiophenes in Miocene lake sediments (Nördlinger Ries, Southern  
1031 Germany). *Aquatic Geochemistry* 3, 169-190.

1032 Bechtel, A., Jia, J., Strobl, S.A.I., Sachsenhofer, R.F., Liu, Z., Gratzner, R., Püttmann, W., 2012.  
1033 Palaeoenvironmental conditions during deposition of the Upper Cretaceous oil shale sequences on the  
1034 Songliao Basin (NE China): Implications from geochemical analysis. *Organic Geochemistry* 46, 76-95.

1035 Berner, R.A., 1970. Sedimentary pyrite formation. *Am. J. Sci.* 268, 1-23.

1036 Berner, R.A., 1984. Sedimentary pyrite formation: An update. *Geochimica et Cosmochimica Acta* 48, 605-615.

1037 Berner, R.A., Raiswell, R., 1983. Burial of organic carbon and pyrite sulfur in sediments over Phanerozoic time:  
1038 A new theory. *Geochimica et Cosmochimica Acta* 47, 862-885.

1039 Bernoulli, D., Jenkyns, H.C., 1974. Alpine, Mediterranean and Central Atlantic Mesozoic facies in relation to the  
1040 early evolution of the Tethys. In: Dott, R.H., Shaver, R.H. (Eds.), *Modern and Ancient Geosynclinal*  
1041 *Sedimentation, a Symposium. Special Publication of the Society of economic Paleontologists and*  
1042 *Mineralogists* 19, 129-160.

1043 Bernoulli, D., Jenkyns, H.C., 2009. Ancient oceans and continental margins of the Alpine-Mediterranean Tethys:  
1044 deciphering clues from Mesozoic pelagic sediments and ophiolites. *Sedimentology* 56, 149-190.

1045 Blumenberg, M., Krüger, M., Nauhaus, K., Talbot, H.M., Oppermann, B., Seifert, R., Pape, T., Michaelis, W.,  
1046 2006. Biosynthesis of hopanoids by sulfate-reducing bacteria (genus *Desulfovibrio*). *Environ. Microbiol.*  
1047 8, 1220-1227.

1048 Bray, E.E., Evans, E.D., 1961. Distribution of n-paraffins as a clue to recognition of source beds. *Geochimica et*  
1049 *Cosmochimica Acta* 22, 2-15.

1050 Brandner, R., 2011. In: *Geologie des Achenseegebietes. Tagungsband der Arbeitstagung der Geologischen*  
1051 *Bundesanstalt, Wien*: 220-224.

1052 Brown, S.A.E., Scott, A.C., Glasspool, I.J., Collinson, M.E., 2012. Cretaceous wildfires and their impact on the  
1053 Earth system. *Cretaceous Research* 36, 162-190.

- 1054 Calvert, S.E., Pedersen, T.F., 1996. Sedimentary Geochemistry of Manganese: Implications for the Environment  
1055 of Formation of Manganiferous Black Shales. *Economic Geology* 91, 36-47.
- 1056 Caruthers, A.H., Gröcke, D.R., Smith, P.L., 2011. The significance of an Early Jurassic (Toarcian) carbon-  
1057 isotope excursion in Haida Gwaii (Queen Charlotte Islands), British Columbia, Canada. *Earth and*  
1058 *Planetary Science Letters* 307, 19-26.
- 1059 Caruthers, A.H., Smith, P.L., Gröcke, D.R., 2013. The Pliensbachian-Toarcian (Early Jurassic) extinction, a  
1060 global multi-phased event. *Palaeogeography, Palaeoclimatology, Palaeoecology* 386, 104-118.
- 1061 Cohen, A.S., Coe, A.L., 2007. The impact of the Central Magmatic province on climate and on the Sr- and Os-  
1062 isotope evolution of seawater. *Palaeogeography, Palaeoclimatology, Palaeoecology* 244, 374-390.
- 1063 Cohen, A.S., Coe, A.L., Harding, S.M., Schwark, L., 2004. Osmium isotope evidence for the regulation of  
1064 atmospheric CO<sub>2</sub> by continental weathering. *Geology* 32, 157-160.
- 1065 Cranwell, P.A., 1977. Organic geochemistry of CamLoch (Sutherland) sediments. *Chemical Geology* 20, 205-  
1066 221.
- 1067 Dean, W.E., Arthur, M.A., 1989. Iron-sulfur-carbon relationships in organic-rich sequences. In: *Cretaceous*  
1068 *Western Interior Seaway*. *American Journal of Science* 289, 708-743.
- 1069 Decarlis, A., Dallagiovanna, G., Lualdi, A., Maino, M., Seno, S., 2013. Stratigraphic evolution in the Ligurian  
1070 Alps between Variscian heritages and the Alpine Tethys opening: A review. *Earth-Science Reviews* 125,  
1071 43-68
- 1072 Demaison, G.J., Moore, G.T., 1980. Anoxic environments and oil source bed genesis. *AAPG Bulletin* 64, 1179-  
1073 1209.
- 1074 Dera, G., Neige, P., Dommergues, J.-L., Fara, E., Laffont, R., Pellenard, P., 2010. High-resolution dynamics of  
1075 Early Jurassic marine extinctions: the case of Pliensbachian–Toarcian ammonites (Cephalopoda). *J. Geol.*  
1076 *Soc. (Lond.)* 167, 21–33.
- 1077 Didyk, B.M., Simoneit, B.R.T., Brassell, S.C., Eglinton, G., 1978. Organic geochemical indicators of  
1078 palaeoenvironmental conditions of sedimentation. *Nature* 272, 216-222.
- 1079 Ebli, O., 1991. Beiträge von Draxler, I., Klein, P., Kodina, L.A., Lobitzer, H., Schwaighofer, B. Fazies,  
1080 Paläontologie und organische Geochemie der Sachranger Schiefer (Untertoarcium) im Mittelabschnitt der  
1081 Nördlichen Kalkalpen zwischen Isar und Saalach. *Jahrbuch der Geologischen Bundesanstalt* 134/1, 5-14.
- 1082 Ebli, O., Vetö, I., Lobitzer, H., Sajgò, C., Demény, A., Hetényi, M., 1998. Primary productivity and early  
1083 diagenesis in the Toarcian Tethys on the example of the Mn rich black shales of the Sachrang Formation,  
1084 Northern Calcareous Alps. *Organic Geochemistry* 29, 1635-47.
- 1085 Encarnación, J., Fleming, T.H., Elliot, D.H., Eales, H.V., 1996. Synchronous emplacement of Ferrar and Karoo  
1086 dolerites and the early breakup of Gondwana. *Geology* 24, 535-538.
- 1087 Espitalié, J., Marquis, F., Barsoni, I., 1984. Geochemical logging. In: Voorhess, K.J. (Eds.), *Analytical Pyrolysis*.  
1088 Butterworth, Boston. pp. 53-79.

- 1089 Fabricus, F., 1966. Beckensedimentation und Riffbildung an der Wende Trias/Jura in den Bayrisch-Tiroler  
1090 Kalkalpen. *Internat. Sedim. Petrogr. Series 9*, 143 S.
- 1091 Faupl, P., Wagreich, M., 2000. Late Jurassic to eocene palaeogeography and geodynamic evolution of the  
1092 Eastern Alps. *Mitteilungen der Österreichischen Geologischen Gesellschaft 92*, 79-94.
- 1093 Frimmel, A., Oschmann, W., Schwark, L., 2004. Chemostratigraphy of the Posidonia Shale, SW Germany I.  
1094 Influence of sea-level variation on organic facies evolution. *Chemical Geology 206*, 199-230.
- 1095 Frisch, W., 1979. Tectonic Progradation on plate tectonic evolution of the Alps. *Tectonophysics 60*, 121-139.
- 1096 Frisch, W., Gawlick, H.-J., 2003. The nappe structure of the central Northern Calcareous Alps and its  
1097 disintegration during Miocene tectonic extrusion – a contribution to understanding the orogenic evolution  
1098 of the Eastern Alps. *International Journal of Earth Sciences 92*, 712-727.
- 1099 Frisch, W., Meschede, M., Blakey, R., 2011. *Plate Tectonics*. Springer, pp. 112.
- 1100 Fu, J.G., Sheng, P., Peng, S.C., Brassell, S.C., Eglinton, G., 1986. Peculiarities of salt lake sediments as  
1101 potential source rocks in China. *Organic Geochemistry 10*, 119-127.
- 1102 Gawlick, H.-J., Frisch, W., Hoxha, L., Dumitrica, P., Krystyn, L., Lein, R., Missoni, S., Schlagintweit, F., 2008.  
1103 Mirdita Zone ophiolites and associated sediments in Albania reveal Neotethys Ocean origin. *International*  
1104 *Journal of Earth Sciences 97*, 865-881. Gawlick, H.-J., Missoni, S., Schlagintweit, F., Suzuki, H., Frisch,  
1105 W., Krystyn, L., Blau, J., Lein, R., 2009. Jurassic Tectonostratigraphy of the Austroalpine Domain.  
1106 *Journal of Alpine Geology 50*: 1-152.
- 1107 Golonka, J., 2002. Plate-tectonic Maps of the Phanerozoic. In: Kiessling, W., Flügel, E., Golonka, J. (Eds.),  
1108 *Phanerozoic Reef Patterns*. SEPM Special Publication 72, 21-75.
- 1109 Goossens, H., de Leeuw, J.W., Schenck, P.A., Brassell, S.C., 1984. Tocopherols as likely precursors of pristane  
1110 in ancient sediments and crude oils. *Nature 312*, 440-442.
- 1111 Gradstein, F.M., Ogg, J.G., Schmitz, M.D., et al., 2012. *The Geologic Time Scale 2012*. Elsevier, Boston.
- 1112 Grantham, P.J., Posthuma, J., Baak, A., 1983. Triterpanes in a number Far Eastern crude oils. In: Bjoroy, M., et  
1113 al. (Eds.), *Advances in Organic Geochemistry*. Wiley, Chichester. pp. 675-683.
- 1114 Grice, K., Gibbison, R., Atkinson, J.E., Schwark, L., Eckardt, C.B.E., Maxwell, J.R., 1996. Maleimides (1H-  
1115 pyrrole-2,5-diones) as indicators of anoxygenic photo-synthesis in ancient water columns. *Geochim.*  
1116 *Cosmochim. Acta 60*, 3913-3924.
- 1117 Gröcke, D.R., Hori, R.S., Trabucho-Alexandre, J., Kemp, D.B., Schwark, L., 2011. An open ocean record of the  
1118 Toarcian oceanic anoxic event. *Solid Earth 2*, 245-57.
- 1119 Hallam, A., 1992. *Phanerozoic Sea-level Changes*. Columbia University Press, New York. pp. 266.
- 1120 Harnik, P.G., Lotze, H.K., Anderson, S.C., Finkel, Z.V., Finnegan, S., Lindberg, D.R., Liow, L.H., Lockwood,  
1121 R., McClain, C.R., McGuire, J.L., O'Dea, A., Pandolfi, J.M., Simpson, C., Tittensor, D.P., 2012.  
1122 Extinctions in ancient and modern seas. *Trends in Ecology and Evolution 27*, 608-617.

- 1123 Haq, B.U., Hardenbol, J., Vail, P.R., 1988. Mesozoic and Cenozoic chronostratigraphy and cycles of sea-level  
1124 change. In: Wilgus, C.K., Hastings, B.S., Posamentier, H., Wagoner, J.V., Ross, C.A., Kendall, C.G.S.C.  
1125 (Eds.), *Sea-Level Changes - An Integrated Approach*. SEPM Special Publications 42, 71-108.
- 1126 Hesselbo, S.P., Gröcke, D.R., Jenkyns, H.C., Bjerrum, C.J., Farrimond, P., Morgans Bell, H.S., Green, O.R.,  
1127 2000. Massive dissociation of gas hydrate during a Jurassic oceanic anoxic event. *Nature* 406, 392-395.
- 1128 Hesselbo, S.P., Jenkyns, H.C., Duarte, L.V., Oliviera, L.C.V., 2007. Carbon-isotope record of the Early Jurassic  
1129 (Toarcian) Oceanic Anoxic Event from fossil wood and marine carbonate (Lusitanian Basin, Portugal).  
1130 *Earth and Planetary Science Letters* 253, 455-470.
- 1131 Hofmann, P., Ricken, W., Schwark, L., Leythaeuser, D., 2000. Carbon–sulfur–iron relationships and  $\delta^{13}\text{C}$  of  
1132 organic matter for Late Albian sedimentary rocks from the North Atlantic Ocean: Palaeoceanographic  
1133 implications. *Palaeogeography, Palaeoclimatology, Palaeoecology* 163 (3-4), 97-113.
- 1134 Hollander, D.J., Smith, M.A., 2001. Microbially mediated carbon cycling as a control on the  $\delta^{13}\text{C}$  of  
1135 sedimentary carbon in eutrophic Lake Mendota (USA): new models for interpreting isotopic excursions in  
1136 the sedimentary record. *Geochimica et Cosmochimica Acta* 65, 4321-4337.
- 1137 Hughes, W.B., Holba, A.G., Dzou, L.I.P., 1995. The ratios of dibenzothiophene to phenanthrene and pristane to  
1138 phytane as indicators of depositional environment and lithology of petroleum source rocks. *Geochimica et*  
1139 *Cosmochimica Acta* 59, 3581-3598.
- 1140 Hutton, A.C., 1987. Petrographic classification of oil shales. *Internat. J. Coal Geol.* 8, 203-231.
- 1141 Ikeda, M., Hori, R.S., 2014. Effects of Karoo-Ferrar volcanism and astronomical cycles on the Toarcian Anoxic  
1142 Events (Early Jurassic). *Palaeogeography, Palaeoclimatology, Palaeoecology* 410, 134-142.
- 1143 Irwin, H., Curtis, C.D., Coleman, M., 1977. Isotopic evidence for source of diagenetic carbonates formed during  
1144 burial of organic-rich sediments. *Nature* 269, 209-213.
- 1145 Izumi, K., Miyaji, T., Tanabe, K., 2012. Early Toarcian (Early Jurassic) oceanic anoxic event recorded in the  
1146 shelf deposits in the northwestern Panthalassa: Evidence from the Nishinakayama Formation in the  
1147 Toyora area, west Japan. *Palaeogeography, Palaeoclimatology, Palaeoecology* 315-316, 100-108.
- 1148 Jaminski, J., Algeo, T.J., Maynard, J.B., Hower, J.C., 1998. Climatic origin of dm-scale compositional cyclicity  
1149 in the Cleveland Member of the Ohio Shale (Upper Devonian), Central Appalachian Basin, U.S.A. In:  
1150 Schieber, J., Zimmerle, W., Sethi, P.S. (Eds.), *Shales and Mudstones*. I.E. Schweizerbart'sche  
1151 Verlagsbuchhandlung, Stuttgart. pp. 217-242.
- 1152 Jenkyns H. C., 1985. The Early Toarcian and Cenomanian–Turonian anoxic events in Europe: comparisons and  
1153 contrasts. *Geologische Rundschau* 74, 505-518.
- 1154 Jenkyns, H.C., 1988. The Early Toarcian (Jurassic) anoxic event: stratigraphic, sedimentary, and geochemical  
1155 evidence. *American Journal of Science* 288, 101-151.
- 1156 Jenkyns, H.C., 2003. Evidence for rapid climate change in the Mesozoic–Palaeogene greenhouse world.  
1157 *Philosophical Transactions of the Royal Society of London* 361 A, 1885-1916.

- 1158 Jenkyns, H.C., 2010. The geochemistry of oceanic anoxic events. *Geochemistry Geophysics Geosystems* 11,  
1159 Q03004, doi: 10.1029/2009GC002788.
- 1160 Jenkyns, H.C., Clayton, C.J., 1986. Black shales and carbon isotopes in pelagic sediments from the Tethyan  
1161 Lower Jurassic. *Sedimentology* 33, 87-106.
- 1162 Jenkyns, H.C., Clayton, C.J., 1997. Lower Jurassic epicontinental carbonates and mudstones from England and  
1163 Wales: chemostratigraphic signals and the early Toarcian anoxic event. *Sedimentology* 44, 687-706.
- 1164 Jenkyns, H.C., Gröcke, D.R., Hesselbo, S.P., 2001. Nitrogen isotope evidence for water mass denitrification  
1165 during the early Toarcian (Jurassic) ocean anoxic event. *Paleoceanography* 16, 593–603.
- 1166 Jenkyns, H.C., Jones, C.E., Gröcke, D.R., Hesselbo, S.P., Parkinson, D.N., 2002. Chemostratigraphy of the  
1167 Jurassic System: applications, limitations and implications for palaeoceanography. *Journal of the*  
1168 *Geological Society of London* 159, 351-378.
- 1169 Jourdan, F., Féraud, G., Bertrand, H., Watkeys, M.K., Renne, P.R., 2008. The  $^{40}\text{Ar}/^{39}\text{Ar}$  ages of the sill complex  
1170 of the Karoo large igneous province: implications for the Pliensbachian-Toarcian climate change.  
1171 *Geochemistry, Geophysics, Geosystems* 9, 1-20.
- 1172 Kafousia, N., Karakitsios, V., Mattioli, E., Kenjo, S., Jenkyns, H.C., 2014. The Toarcian Oceanic Anoxic Event  
1173 in the Ionian Zone, Greece. *Palaeogeography, Palaeoclimatology, Palaeoecology* 393, 135-145.
- 1174 Kemp, D.B., Coe, A.L., Cohen, A.S., Schwark, L., 2005. Astronomical pacing of methane release in the early  
1175 Jurassic period. *Nature* 437, 396-399.
- 1176 Klebelsberg, R.v., 1935. *Geologie von Tirol*. Gebr. Borntraeger, Berlin.
- 1177 Kodina, L.A., Bogatecheva, M.P., Lobitzer, H., 1988. An anorganic geochemical study of Austrian bituminous  
1178 rocks. *Jb. Geol. B.-A.* 131, 291-300, Wien.
- 1179 Kohnen, M.E.L., Sinninghe Damsté, J.S., de Leeuw, J.W., 1991. Biases from natural sulphurization in  
1180 palaeoenvironmental reconstruction based on hydrocarbon biomarker distributions. *Nature* 349, 775-778.
- 1181 Koopmans, M.P., Köster, J., van Kaam-Peters, H.M.E., Kenig, F., Schouten, S., Hartgers, W.A., de Leeuw, J.W.,  
1182 Sinninghe Damsté, J.S., 1996. Diagenetic and catagenetic products of isorenieratene: molecular indicators  
1183 for photic zone anoxia. *Geochim. Cosmochim. Acta* 60, 4467-4496.
- 1184 Köster, J., Schouten, S., Sinninghe Damsté, J.S., de Leeuw, J.W., 1995. Reconstruction of the depositional  
1185 environment of Toarcian marlstones (Allgäu Formation, Tyrol/Austria) using biomarkers and compound  
1186 specific carbon isotope analysis. In: Grimalt, J.O., Dorronsoro, C. (Eds.), *Organic Geochemistry:*  
1187 *Developments and applications to energy, climate, environment and human history*. A.I.G.O.A., San  
1188 Sebastian. pp. 76-78.
- 1189 Kuehl, S.A., Fuglseth, T.J., Thunell, R.C., 1993. Sediment mixing and accumulation rates in the Sulu and South  
1190 China Seas: Implications for organic carbon preservation in deep-water environments. *Mar. Geol.* 111,  
1191 15-35.
- 1192 Küspert, W., 1982. Environmental changes during oil shale deposition as deduced from stable isotope ratios. In:  
1193 Einsele, G., Seilacher, A. (Eds.), *Cyclic and Event Stratification*. Springer, Berlin. pp. 482-501.

- 1194 Küspert, W., 1983. Faziestypen des Posidonienschiefers (Toarcium, Süddeutschland): Eine isotopen-  
1195 geologische, organisch-chemische und petrographische Studie. Ph.D. Thesis, Tübingen University.
- 1196 Langford, F.F., Blanc-Valleron, M.-M., 1990. Interpreting Rock-Eval pyrolysis data using graphs of pyrolyzable  
1197 hydrocarbons vs. total organic carbon. American Association of Petroleum Geologists Bulletin 74, 799-  
1198 804.
- 1199 Leventhal, J.S., 1983. An interpretation of carbon and sulfur relationships in Black Sea sediments as indicators  
1200 of environments of deposition. *Geochim. Cosmochim. Acta* 47, 133-137.
- 1201 Lewan, M.D., 1986. Stable carbon isotopes of amorphous kerogens from Phanerozoic sedimentary rocks.  
1202 *Geochim. Cosmochim. Acta* 50, 1583-1591.
- 1203 Littke, R., Rotzal, H., Leythaeuser, D., Baker, D.R., 1991. Organic facies and maturity of Lower Toarcian  
1204 Posidonia Shale in Southern Germany (Schwäbische Alb). *Erdöl & Kohle Erdgas*  
1205 *Petrochemie/Hydrocarbon Technology* 44, 407-414.
- 1206 Luo, G.M., Algeo, T.J., Zhou, W.F., Wang, Y.B., Yang, H., Huang, J.H., Richoz, S., Xie, S.C., 2014. Vertical  
1207  $\delta^{13}\text{C}_{\text{org}}$  gradients record changes in planktonic microbial community composition during the end-Permian  
1208 mass extinction. *Palaeogeography Palaeoclimatology Palaeoecology* 396, 119-131.
- 1209 Mackenzie, A.S., Maxwell, J.R., 1981. Assessment of thermal maturation in sedimentary rocks by molecular  
1210 measurements. In: Brooks, J. (Eds.), *Organic Maturation Studies and Fossil Fuel Exploration*. Academic  
1211 Press, London. pp. 239-254.
- 1212 Mackenzie, A.S., Brassell, S.C., Eglinton, G., Maxwell, J.R., 1982. Chemical fossils: the geological fate of  
1213 steroids. *Science* 217, 491-504.
- 1214 Mangini, A., Dominik, J., 1979. Late Quaternary sapropel on the Mediterranean ridge: U-budget and evidence  
1215 for low sedimentation rates. *Sedim. Geol.* 23, 113-125.
- 1216 Martin, E.E., Macdougall, J.D., 1995. Sr and Nd isotopes at the Permian Triassic Boundary – a record of climate  
1217 change. *Chemical Geology* 125, 73-99.
- 1218 Marzoli, A., Renne, P.R., Piccirillo, E.M., Ernesto, M., Bellieni, G., De Min, A., 1999. Extensive 200 million-  
1219 year-old continental flood basalts of the central Atlantic magmatic province. *Science* 284, 616-618.
- 1220 Mazzini, A., Svensen, H., Leanza, H.A., Corfu, F., Planke, S., 2010. Early Jurassic shale chemostratigraphy and  
1221 U–Pb ages from the Neuquén Basin (Argentina): implications for the Toarcian Oceanic Anoxic Event.  
1222 *Earth Planet. Sci. Lett.* 297, 633–645.
- 1223 McArthur, J.M., Algeo, T.J., van de Schootbrugge, B., Li, Q., Howarth, R.J., 2008. Basinal restriction, black  
1224 shales, Re–Os dating, and the Early Toarcian (Jurassic) oceanic anoxic event. *Paleoceanography* 23, 1–  
1225 22.
- 1226 McElwain, J.C., Beerling, D.J., Woodward, F.I., 1999. Fossil plants and global warming at the Triassic-Jurassic  
1227 boundary. *Science* 285, 1386-1390.
- 1228 McElwain, J.C., Murphy, J.W., Hesselbo, S.P., 2005. Changes in carbon dioxide during an oceanic anoxic event  
1229 linked to intrusion of Gondwana coals. *Nature* 435, 479-483.



- 1230 McHone, J.G., 2003. Volatile Emissions from Central Atlantic Magmatic Province Basalts: Mass Assumptions  
1231 and Environmental Consequences. In: Hames, W.E., McHone, J.G., Ruppel, C., Renne, P. (Eds.), The  
1232 Central Atlantic Magmatic Province. American Geophysical Union Monograph. pp 136: 267.
- 1233 Minor, D.R., Mukasa, S.B., 1997. Zircon U-Pb and hornblende  $^{40}\text{Ar}$ - $^{39}\text{Ar}$  ages for the Dufek layered mafic  
1234 intrusion, Antarctica: Implications for the age of the Ferrar large igneous province. *Geochimica and*  
1235 *Cosmochimica Acta* 61, 2497-2504.
- 1236 Missoni, S., Gawlick, H.-J., 2011. Evidence for Jurassic subduction from the Northern Calcareous Alps  
1237 (Berchtesgaden; Austroalpine, Germany). *International Journal of Earth Sciences* 100, 1605-1631.
- 1238 Mohn, G., Manatschal, G., Müntener, O., Beltrando, M., Masini, E., 2010. Unravelling the interaction between  
1239 tectonic and sedimentary processes during lithospheric thinning in the Alpine Tethys margins. *Int. J.*  
1240 *Earth Sci. (Geol. Rundsch.)* 99, 75-101.
- 1241 Morard, A., Guex, J., Bartolini, A., Morettini, E., De Wever, P., 2003. A new scenario for the Domerian-  
1242 Toarcian transition. *Bulletin de la Société géologique France* 174, 351-356.
- 1243 O'Neil, J.R., Clayton, R.N., Mayeda, T.K., 1969. Oxygen isotope fractionation in divalent metal carbonates. *J.*  
1244 *Chem. Phys.* 51, 5547-5558.
- 1245 Oschmann, W., 2000. Microbes and black shales. In: Riding, R.E., Awramik, S.M. (Eds.), *Microbial Sediments.*  
1246 Springer, Berlin, pp. 137-148.
- 1247 Ourrison, G, Albrecht, P, Rohmer, M., 1979. The hopanoids: palaeo-chemistry and biochemistry of a group of  
1248 natural products. *Pure and Applied Chemistry* 51: 709-729.
- 1249 Pálffy, J., Smith, P.L., 2000. Synchrony between Early Jurassic extinction, oceanic anoxic event, and the Karoo-  
1250 Ferrar flood basalt volcanism. *Geology* 28, 747-750.
- 1251 Parrish, J.T., 1993. Climate of the supercontinent Pangaea. *Journal of Geology* 101, 215-233.
- 1252 Parrish, J.T., Curtis, R.L., 1982. Atmospheric circulation, upwelling, and organic-rich rocks in the Mesozoic and  
1253 Cenozoic areas. *Palaeogeography, Palaeoclimatology, Palaeoecology* 40, 31-66.
- 1254 Pearce, C.R., Cohen, A.S., Coe, A.L., Burton, K.W., 2008. Molybdenum isotope evidence for global ocean  
1255 anoxia coupled with perturbations to the carbon cycle during the Early Jurassic. *Geology* 36, 231-234.
- 1256 Pedersen, T.F., Calvert, S.E., 1990. Anoxia vs. productivity: What controls the formation of organic-carbon-rich  
1257 sediments and sedimentary rocks? *AAPG Bulletin* 74, 454-472.
- 1258 Peters, K.E., Moldowan, J.M., Sundararaman, P., 1990. Effects of hydrous pyrolysis on biomarker thermal  
1259 maturity parameters: Monterey Phosphatic and Siliceous Members. *Organic Geochemistry* 15, 249-265.
- 1260 Peters, K.E., Walters, C.C., Moldowan, J.M., 2005. *The Biomarker Guide, Biomarkers and Isotopes in*  
1261 *Petroleum Exploration and Earth History, Vol. 1 & 2.* Cambridge University Press, New York, NY.
- 1262 Praus, M., Riegel, W., 1989. Evidence from phytoplanktonic associations for causes of black shale formation in  
1263 epicontinental seas. *N. Jb. Geol. Paläontol. Mh.* 11, 671-682.
- 1264 Price, G.D., 1999. The evidence and implications of polar ice during the Mesozoic. *Earth Science Reviews* 48,  
1265 183-210.

- 1266 Radke, M., Willsch, H., Welte, D.H., 1980. Preparative hydrocarbon group type determination by automated  
1267 medium pressure liquid chromatography. *Analytical Chemistry* 52, 406-411.
- 1268 Raiswell, R., Berner, R.A., 1985. Pyrite formation in euxinic and semi-euxinic sediments. *Am. J. Sci.* 285, 710-  
1269 724.
- 1270 Raiswell, R., Canfield, D.E., Berner, R.A., 1994. A comparison of iron extraction methods for the determination  
1271 of degree of pyritisation and the recognition of iron-limited pyrite formation. *Chem. Geol.* 111, 101-110.
- 1272 Ratschbacher, L., Dingeldey, C., Miller, C., Hacker, B.R., McWilliams, M.O., 2004. Formation, subduction, and  
1273 exhumation of Penninic oceanic crust in the Eastern Alps: time constraints from  $^{40}\text{Ar}/^{39}\text{Ar}$  geochronology.  
1274 *Tectonophysics* 394, 155-170.
- 1275 Riegraf, W., Werner, G., Lörcher, F., 1984. Der Posidonienschiefer: Biostratigraphie, Fauna und Fazies des  
1276 südwestdeutschen Untertoarciums (Lias  $\epsilon$ ). Enke. pp. 195.
- 1277 Riegraf, W., 1985. Mikrofauna, Biostratigraphie und Fazies im Unteren Toarcium Südwestdeutschlands und  
1278 Vergleiche mit benachbarten Gebieten. *Tübinger Mikropaläontologische Mitteilungen* 3, pp. 232.
- 1279 Rimmer, S.M., Thompson, J.A., Goodnight, S.A., Robl, T.L., 2004. Multiple controls on the preservation of  
1280 organic matter in Devonian-Mississippian marine black shales: geochemical and petrographic evidence.  
1281 *Palaeogeography, Palaeoclimatology, Palaeoecology* 215, 125-154.
- 1282 Robinson, N., Eglinton, G., Brassell, S.C., Cranwell, P.A., 1984. Dinoflagellate origin for sedimentary 4 $\alpha$ -  
1283 methylsteroids and 5 $\alpha$ (H)-stanols. *Nature* 308, 439-442.
- 1284 Röhl, H.J., Schmid-Röhl, A., Oschmann, W., Frimmel, A., Schwark, L., 2001. The Posidonia Shale (Lower  
1285 Toarcian) of SW-Germany: an oxygen-depleted ecosystem controlled by sea level and palaeoclimate.  
1286 *Palaeogeography, Palaeoclimatology, Palaeoecology* 165, 27-52.
- 1287 Rohmer, M., Bissere, P., Neunlist, S., 1992. The hopanoids, prokaryotic triterpenoids and precursors of  
1288 ubiquitous molecular fossils. In: Moldowan, J.M., Albrecht, P., Philp, R.P. (Eds.), *Biological Markers in*  
1289 *Sediments and Petroleum*. Prentice Hall, Englewood Cliffs, N.J. pp. 1-17.
- 1290 Rullkötter, J., Wendisch, D., 1982. Microbial alteration of 17 $\alpha$ (H) hopanes in Madagascar asphalts: removal of  
1291 C-10 methyl group and ring opening. *Geochim. Cosmochim. Acta* 41, 1341-1353.
- 1292 Sabatino, N., Neri, R., Bellanca, A., Jenkyns, H.C., Baudin, F., Parisi, G., Masetti, D., 2009. Carbon-isotope  
1293 records of the Early Jurassic (Toarcian) Oceanic Anoxic Event from the Valdorbia (Umbria-Marche  
1294 Apennines) and Monte Mangart (Julian Alps) sections: palaeoceanographic and stratigraphic  
1295 implications. *Sedimentology* 56, 1307-1328.
- 1296 Sabatino, N., Vlahović, I., Jenkyns, H.C., Scopelliti, G., Neri, R., Prtoljan, B., Velić, I., 2013. Carbon-isotope  
1297 record and palaeoenvironmental changes during the early Toarcian oceanic anoxic event in shallow-  
1298 marine carbonates of the Adriatic Carbonate Platform in Croatia. *Geological Magazine* 150, Issue 6,  
1299 1085-1102.
- 1300 Sælen, G., Doyle, P., Talbot, M.R., 1996. Stable-isotope analysis of belemnite rostra from the Whitby Mudstone  
1301 Fm., England: Surface water conditions during deposition of a marine black shale. *Palaios* 11, 97-117.

- 1302 Schlager, W., Schöllnberger, W., 1973. Das Prinzip stratigraphischer Wenden in der Schichtfolge der Nördlichen  
1303 Kalkalpen. Mitt. Geol. Ges. Wien 66, 166-193.
- 1304 Schmid-Röhl, A., Röhl, H.-J., Oschmann, W., Frimmel, A., Schwark, L., 2002. Palaeoenvironmental  
1305 reconstruction of Lower Toarcian epicontinental black shales (Posidonia Shale, SW Germany): global  
1306 versus regional control. *Geobios* 35, 13-20.
- 1307 Schwark L., Vliex, M., Schaeffer, P., 1998. Geochemical characterization of Malm Zeta laminated carbonates  
1308 from the Franconian Alb, SW Germany (II). *Organic geochemistry* 29, No. 8, 1921-1952.
- 1309 Schwark, L., Frimmel, A., 2004. Chemostratigraphy of the Posidonia Black Shale, SW Germany II. Assessment  
1310 of extent and persistence of photic-zone anoxia using aryl isoprenoids distributions. *Chem. Geol.* 206,  
1311 231-248.
- 1312 Sell, B., Ovtcharova, M., Guex, J., Bartolini, A., Jourdan, F., Spangenberg, J.E., Vicente, J.-C., Schaltegger, U.,  
1313 2014. Evaluating the temporal link between the Karoo LIP and climatic-biologic events of the Toarcian  
1314 Stage with high-precision U-Pb geochronology. *Earth and Planetary Science Letters* 408, 48-56.
- 1315 Sinninghe Damsté, J.S., Kock-Van Dalen, A.C., de Leeuw, J.W., Schenk, P.A., Guoying, S., Brassell, S.C.,  
1316 1987. The identification of mono-, di-, and trimethyl 2-methyl-2-(4,8,12-trimethyltridecyl)chromans and  
1317 their occurrence in geosphere. *Geochimica et Cosmochimica Acta* 51, 2393-2400.
- 1318 Sinninghe Damsté, J.S., van Duin, A.C.T., Hollander, D., Kohnen, M.E.L., de Leeuw, J.W., 1995. Early  
1319 diagenesis of bacteriohopanepolyol derivatives: Formation of fossil homohopanooids. *Geochimica et*  
1320 *Cosmochimica Acta* 59, 5141-5156.
- 1321 Spieler, A., Brandner, R., 1989. Vom jurassischen Pull-Apart Becken zur Westüberschiebung der Achantaler  
1322 Schubmasse (Tirol, Österreich). *Geol. Paläont. Mitt. Innsbruck* 16, 191-194.
- 1323 Suan, G., Pittet, B., Bour, I., Mattioli, E., Duarte, L.V., Mailliot, S., 2008. Duration of the Early Toarcian carbon  
1324 isotope excursion deduced from spectral analysis: consequence for its possible causes. *Earth Planet. Sci.*  
1325 *Lett.* 267, 666-679.
- 1326 Summons, R.E., Powell, T.G., 1986. Chlorobiaceae in Palaeozoic seas revealed by biological markers, isotopes  
1327 and geology. *Nature* 319, 763-765.
- 1328 Svensen, H., Planke, S., Chevalier, L., Malthe-Sørensen, A., Corfu, F., Jamveit, B., 2007. Hydrothermal venting  
1329 of greenhouse gases triggering Early Jurassic global warming. *Earth and Planetary Science Letters* 256,  
1330 554-566.
- 1331 Svensen, H., Corfu, F., Polteau, S., Hammer, Ø., Planke, S., 2012. Rapid magma emplacement in the Karoo  
1332 Large Igneous Province. *Earth Planet. Sci. Lett.* 325–326, 1–9.
- 1333 Taylor, G.H., Teichmüller, M., Davis, A., Diessel, C.F.K., Littke, R., Robert, P., 1998. *Organic Petrology*, Gebr.  
1334 Borntraeger, Berlin & Stuttgart, 704 p.
- 1335 ten Haven, H.L., de Leeuw, J.W., Peakman, T.M., Maxwell, J.R., 1986. Anomalies in steroid and hopanoid  
1336 maturity indices. *Geochimica et Chosmochimica Acta* 50, 853-855.

- 1337 ten Haven, H.L., de Leeuw, J.W., Rullkötter, J., Sinninghe Damsté, J.S., 1987. Restricted utility of the pristane /  
1338 phytane ratio as a palaeoenvironmental indicator. *Nature* 330, 641-643.
- 1339 ten Haven, H.L., de Leeuw, J.W., Schenk, P.A., 1985. Organic geochemical studies of a Messinian evaporitic  
1340 basin, northern Appenines (Italy): Hydrocarbon biological markers for a hypersaline environment.  
1341 *Geochim. Cosmochim. Acta* 49, 2181-2191.
- 1342 Thomas, H., Schiettecatte, L.-S., Suykens, K., Kone, Y.J.M., Shadwick, E.H., Prowe, A.E.F., Bozec, Y., de Baar,  
1343 H.J.W., Borges, A.V., 2008. Enhanced ocean carbon storage from anaerobic alkalinity generation in  
1344 coastal sediments. *Biogeosciences Discuss.* 5, 3575-3591.
- 1345 Tissot, B.T., Welte, D.H., 1984. *Petroleum Formation and Occurrences*, Second Ed. Springer-Verlag, Berlin. pp.  
1346 699.
- 1347 Tollmann, A., 1976. *Analyse des klassischen nordalpinen Mesozoikums. Stratigraphie, Fauna und Fazies der*  
1348 *Nördlichen Kalkalpen*. Deuticke, Wien, pp. 580.
- 1349 Tollmann, A., 1985. *Geologie von Österreich, Band 2*. Deuticke, Wien, pp. 718.
- 1350 Tsikos, H., Jenkyns, H.C., Walsworth-Bell, B., Petrizzo, M.R., Forster, A., Kolonic, S., Erba, E., Premoli Silva,  
1351 I., Baas, M., Wagner, T., Sinninghe Damsté, J.S., 2004. Carbon-isotope stratigraphy recorded by the  
1352 Cenomanian–Turonian Oceanic Anoxic Event: correlation and implications based on three key localities.  
1353 *J. Geol. Soc. Lond.* 161, 711-719
- 1354 Tyson, R.V., 1995. *Sedimentary Organic Matter - Organic Facies and Palynofacies*. Chapman and Hall, London.
- 1355 van de Schootbrugge, B., McArthur, J.M., Bailey, T.R., Rosenthal, Y., Wright, J.D., Miller, K.G., 2005.  
1356 Toarcian anoxic event: An assessment of global using belemnite C isotope records. *Paleoceanography* 20,  
1357 PA3008, doi:10.1029/2004PA001102.
- 1358 Volkman, J.K., Maxwell, J.R., 1986. Acyclic isoprenoids as biological markers. In: Johns, R.B. (Eds.),  
1359 *Biological Markers in the Sedimentary Record*. Elsevier, Amsterdam. pp. 1-42.
- 1360 Volkman, J.K., Kearney, P., Jeffrey, S.W., 1990. A new source of 4-methyl steroids and 5 $\alpha$ (H)-stanols in  
1361 sediments: prymnesiophyte microalgae of the genus *Pavlova*. *Organic Geochemistry* 15, 489-497.
- 1362 Volkman, J.K., Barrett, S.M., Blackburn, S.I., 1999. Eustigmatophyte microalgae are potential sources of C<sub>29</sub>  
1363 sterols, C<sub>22</sub>-C<sub>28</sub> n-alcohols and C<sub>28</sub>-C<sub>32</sub> n-alkyl diols in freshwater environments. *Organic Geochemistry*  
1364 30, 307-318.
- 1365 Vortisch, W., 1982. Clay mineralogical studies of some tills in northern Germany. *Geologica et Palaeontologica*  
1366 15, 167-192.
- 1367 Watson, J.S., Jolley, D.W., Kelly, S.P., 2009. High concentration of 28,30-bisnorhopane and 25,28,30-  
1368 trisnorhopane at the PETM in the Faroe-Shetland basin. In: 24<sup>th</sup> International Meeting on Organic  
1369 Geochemistry, 6-11 September 2009. Bremen, Germany.
- 1370 Weissert, H., 2000. Deciphering methane's fingerprint. *Nature* 406, 356-357.
- 1371 Weissert, H., 2013. C-isotope geochemistry – tool for chemostratigraphy and carbon cycle history. *Ciencias da*  
1372 *terra* 18.

1373 Whiteside, J.H., Olsen, P.E., Kent, D.V., Fowell, S.J., Et-Touhami, M., 2007. Synchrony between the Central  
1374 Atlantic magmatic province and the Triassic-Jurassic mass extinction event? *Palaeogeography,*  
1375 *Palaeoclimatology, Palaeoecology* 244, 345-367.

1376 Wignall, P.B., Newton, R.J., Little, C.T.S., 2005. The timing of paleoenvironmental change and cause-and-effect  
1377 relationships during the Early Jurassic mass extinction. *Europ. American Journal of Science* 305, 1014-  
1378 1032.

1379

## 1380 **Figure captions**

1381

1382 Fig. 1: (A) Schematic tectonic map of the Eastern Alps after Frisch and Gawlick  
1383 (2003). The position of the studied section in the Bächental valley is indicated.  
1384 (B) Palaeogeographic position of the study section as part of the Northern  
1385 Calcareous Alps within the Austroalpine domain in late Early Jurassic time  
1386 (after Frisch, 1979; Golonka, 2002; Vlahović et al., 2005; Gawlick et al., 2008;  
1387 Bernoulli and Jenkyns, 2009; Missoni and Gawlick, 2011). The Northern  
1388 Calcareous Alps are part of a continent between the Alpine Atlantic Ocean to  
1389 the northwest and the Neotethys Ocean to the east/southeast. Formation of  
1390 oceanic crust started in the late Early Jurassic (Ratschbacher et al., 2004). (C)  
1391 Schematic cross section (for position, see line a-b in Fig. 1.B) showing the  
1392 passive continental margin of the Lower Austroalpine domain (e.g., Frisch,  
1393 1979; Tollmann, 1985, Faupl & Wagreich, 2000; Gawlick et al., 2009; Frisch  
1394 et al., 2011). Rifting and spreading of the Alpine Atlantic commencing in the  
1395 late Early Jurassic affected the Austroalpine domain by the formation of  
1396 extensional basins (horst-and-graben structure, asymmetric basins; cf.  
1397 Bernoulli and Jenkyns, 1974). (D) Paleogeography of the depositional area of  
1398 Bächental bituminous marl in the Lower Jurassic (Spieler and Brandner, 1989;  
1399 Brandner, 2011). The accumulation of organic-rich rocks was restricted to the  
1400 deepest parts of a basin with half-graben geometry. (E) Photograph of the  
1401 outcropping Bächental bituminous marl in the open pit.

1402

1403 Fig. 2: Left: Lithological profile of the investigated Bächental section containing rocks  
1404 of the *Scheibelberg Fm.*, the *Sachrang Member (Middle Allgäu Fm.)* and the  
1405 *Upper Allgäu Fm.* Stratigraphy follows the new data gained within this study  
1406 premised on the occurrence of *Cleviceras exaratum* and the comparison of

1407  $C_{27}/C_{29}$  steranes ratios. Positions of the 68 investigated samples and the  
1408 differentiated units are indicated (see text for explanations). Right: Photographs  
1409 of thin sections: (A) Greyish wackestone with mainly radiolarians and  
1410 subordinated *Bositra*, sponge spicules, ostracods and some foraminifera;  
1411 secondary carbonates are abundant (Unit 1; 5.05 m). (B) Finely laminated  
1412 mudstone containing some low-energy carbonatic turbidites (Subunit 2a; 13.39  
1413 m). (C) Radiolarian wackestone (Subunit 2a; 19.15 m). (D) Mudstone with  
1414 frequent carbonate turbidites directly below the debrite (Subunit 2b; 21.55 m).  
1415 (E) Wackestone (Unit 3; 29.45 m) with similar features as (A). Positions of the  
1416 samples are displayed next to the lithological profile.

1417

1418 Fig. 3: Vertical variation of (A) protodolomite (peak area), (B) total organic carbon  
1419 (TOC, %), (C) calcite equivalent (C<sub>ceq</sub>, %), (D) sulphur content (S, %), (E)  
1420 hydrogen index (HI, mg HC/g TOC) for samples of the study section. The  
1421 distinguished units within the Bächental bituminous marl are highlighted. See  
1422 text for explanations.

1423

1424 Fig. 4: Vertical variation of (A) iron concentration (Fe, %), (B) inorganic carbon  
1425 isotope composition ( $\delta^{13}C_{carb}$ , ‰ VPDB), (C) oxygen isotope composition of  
1426 carbonate ( $\delta^{18}O_{carb}$ , ‰ VPDB), (D) organic carbon isotope composition  
1427 ( $\delta^{13}C_{org}$ , ‰ VPDB) for samples of the study section. The distinguished units  
1428 within the Bächental bituminous marl are highlighted. See text for  
1429 explanations.

1430

1431 Fig. 5: Microphotographs of Bächental bituminous marls (A) Sample BT 15 (Unit 1,  
1432 7.65 m), (B) sample BT 25 (Subunit 2a, 13.39 m), (C) BT 44 (Unit 3, 22.60 m),  
1433 and (D) BT 58 (Unit 3, 29.45 m). All photos under UV light.

1434

1435 Fig. 6: Total ion current gas chromatograms of saturated hydrocarbon fractions: (A)  
1436 sample BT 15 (Unit 1; 7.65 m), (B) sample BT 25 (Subunit 2a; 13.39 m), (C)  
1437 sample BT 30 (Subunit 2a; 16.55 m), (D) sample BT 50 (Unit 3; 25.55 m). *n*-  
1438 alkanes are labelled according to carbon number [Std., standard (deuterated *n*-  
1439 tetracosane)].

1440

- 1441 Fig. 7: Vertical variation of (A) *n*-alkane proportions of low (*n*-C<sub>15-19</sub>) and high (*n*-C<sub>27-</sub>  
1442 31) molecular weight relative to the concentration of total *n*-alkanes ( $\Sigma n$ -  
1443 alkanes), (B) concentration ratio of pristane vs. phytane, (C) concentration  
1444 ratios of C<sub>27</sub>/C<sub>29</sub>  $\alpha\alpha\alpha$ R steranes and C<sub>27</sub>/C<sub>29</sub> steranes, (D) concentration ratios  
1445 of 4-methylsteranes/ $\Sigma$ C<sub>29</sub> steranes and mono- vs. triaromatic steroids, (E)  
1446 concentration ratios of [20S/(20S + 20R)] C<sub>29</sub> steranes and dibenzothiophene  
1447 vs. phenantrene (DBT/Phen), (F) concentration ratios of gammacerane index  
1448 and [22S/(22S + 22R)] isomers of C<sub>31</sub> hopane for bituminous marl samples.  
1449 The distinguished units within the Bächental bituminous marl are highlighted.  
1450 See text for explanations.  
1451
- 1452 Fig. 8: Partial mass chromatograms of steranes (m/z 217) and 4-methylsteranes (m/z  
1453 231) in saturated hydrocarbon fractions of (A) sample BT 15 (Unit 1; 7.65 m),  
1454 (B) sample BT 25 (Subunit 2a; 13.39 m), (C) sample BT 30 (Subunit 2a; 16.55  
1455 m), (D) sample BT 50 (Unit 3; 25.55 m).  
1456
- 1457 Fig. 9: Partial mass chromatograms of hopanes (m/z 191) in saturated hydrocarbon  
1458 fractions of (A) sample BT 15 (Unit 1; 7.65 m), (B) sample BT 25 (Subunit 2a;  
1459 13.39 m), (C) sample BT 30 (Subunit 2a; 16.55 m), (D) sample BT 50 (Unit 3;  
1460 25.55 m). Variations of gammacerane and hopane isomerization are  
1461 remarkable.  
1462
- 1463 Fig. 10: The plot of pristane/phytane vs. dibenzothiophene/phenantrene (Pr/Ph vs.  
1464 DBT/Phen) suggests the predominance of anoxic conditions during deposition  
1465 of Subunit 2a and a shift to less reducing conditions in Subunit 2b. In contrast,  
1466 suboxic conditions prevailed during deposition of Units 1 and 3. Modified after  
1467 Didyk et al. (1978) and Hughes et al. (1995).  
1468
- 1469 Fig. 11: Ternary diagram (Fe-TOC-S) after Dean and Arthur (1989). Samples of Units  
1470 1 and 3 plot along the pyrite line and in the field of excess Fe availability  
1471 suggesting suboxic to anoxic conditions during deposition. In contrast, the plot  
1472 indicates Fe limitation and persistent anoxia in Unit 2.  
1473

1474 Fig. 12: The plot of gammacerane indices vs. 4-methylsteranes/ $\Sigma C_{29}$  steranes (GI vs. 4-  
1475 methylsteranes/ $\Sigma C_{29}$  steranes) indicates enhanced salinity of bottom waters and  
1476 a stratified water column during deposition of samples from Subunit 2a  
1477 whereas normal-marine salinity was prevailing during deposition of the  
1478 remaining parts of the section. The well-defined positive correlation between  
1479 GI and 4-methylsteranes suggest a flourishing of halophilic organisms during  
1480 phases of enhanced salinity. Modified after Schwark et al. (1998) and Bechtel  
1481 et al. (2012).  
1482

1483 Fig. 13: Influence of sea-level changes on depositional environment and correlation of  
1484 Pliensbachian to Toarcian OM-rich sediments of Alpine (Bächental) and  
1485 epicontinental (Dotternhausen; Frimmel et al., 2004) settings with global sea-  
1486 level curve (Haq et al., 1988) using sterane ratios. See text for explanations.  
1487

1488 Fig. 14: Sketches showing factors controlling the depositional environment of the  
1489 Bächental bituminous marl. Paleogeographical setting modified after Brandner  
1490 (2011). (A) Units 1 and 3, (B) Subunit 2a, (C) Subunit 2b. See text for  
1491 explanations.



Figure 1  
[Click here to download high resolution image](#)

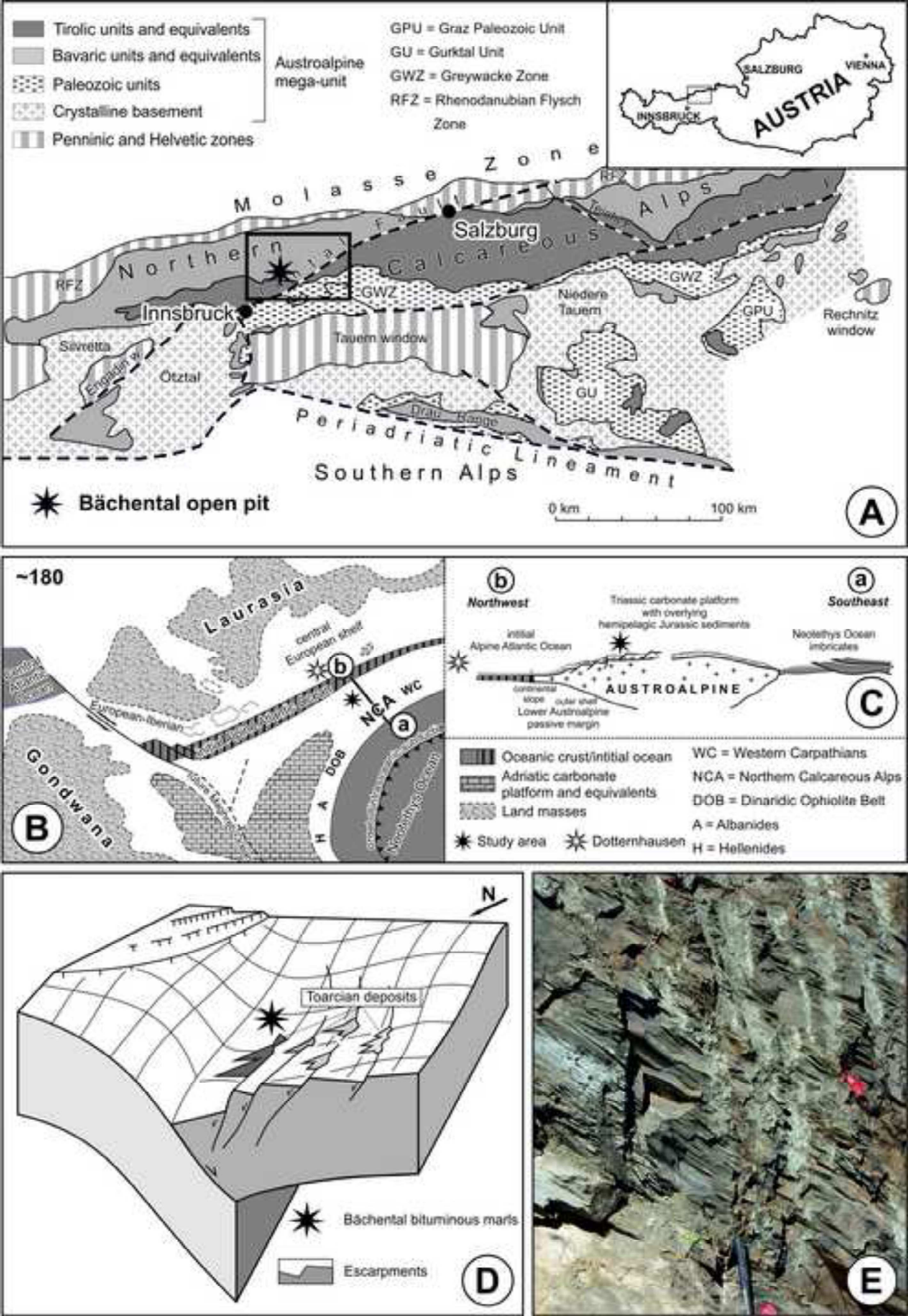


Figure 2

[Click here to download high resolution image](#)

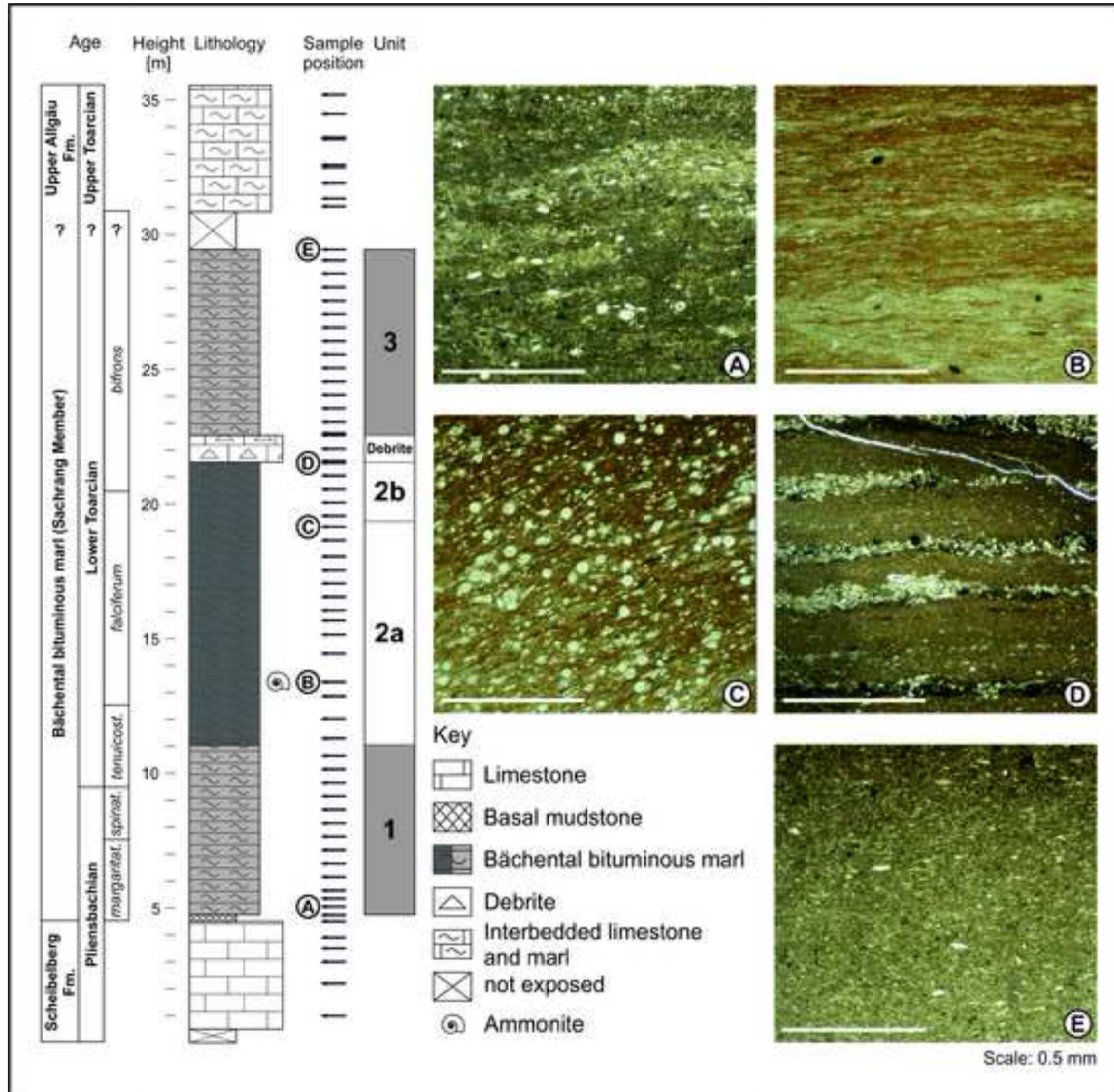


Figure 3  
[Click here to download high resolution image](#)

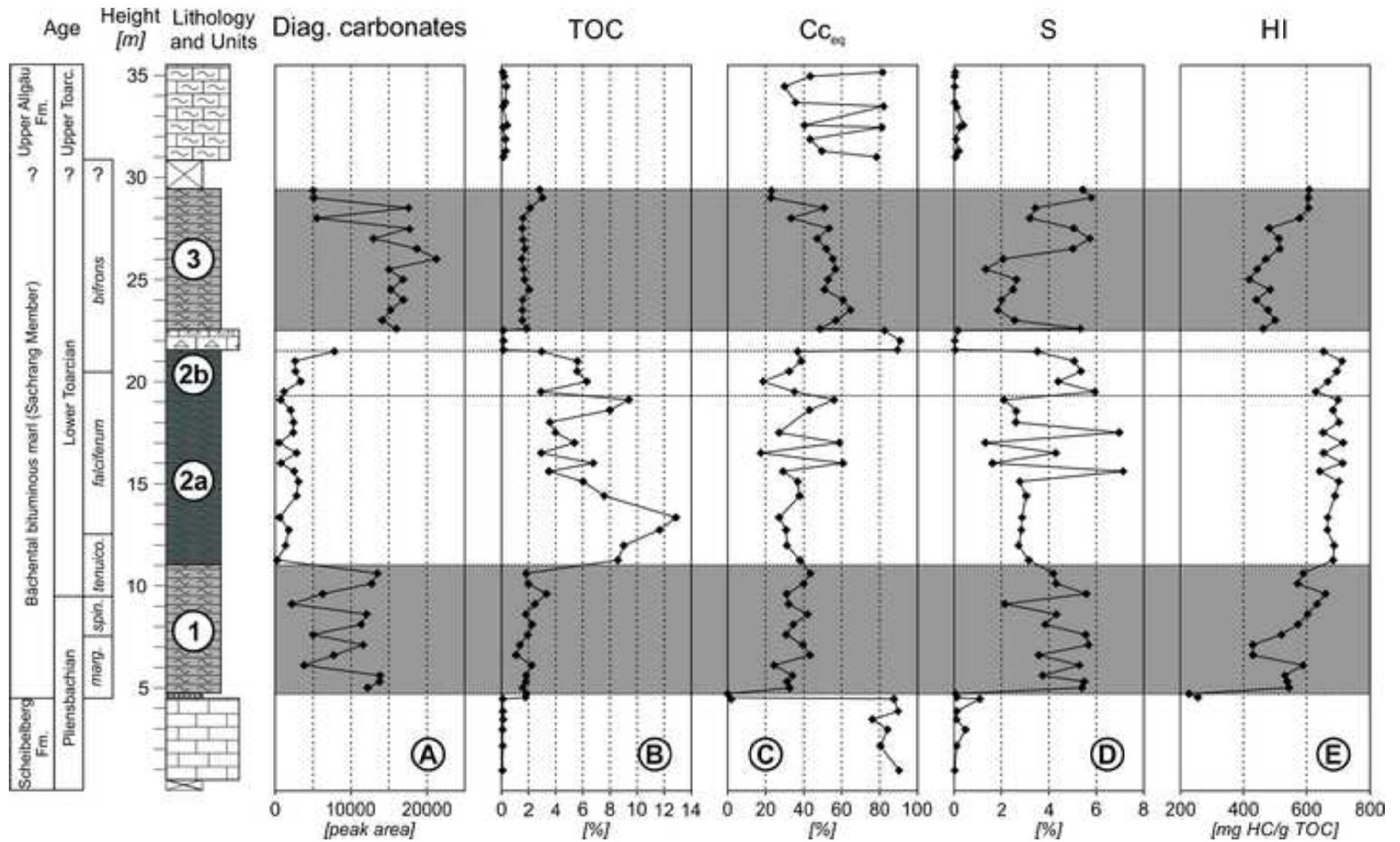


Figure 4  
[Click here to download high resolution image](#)

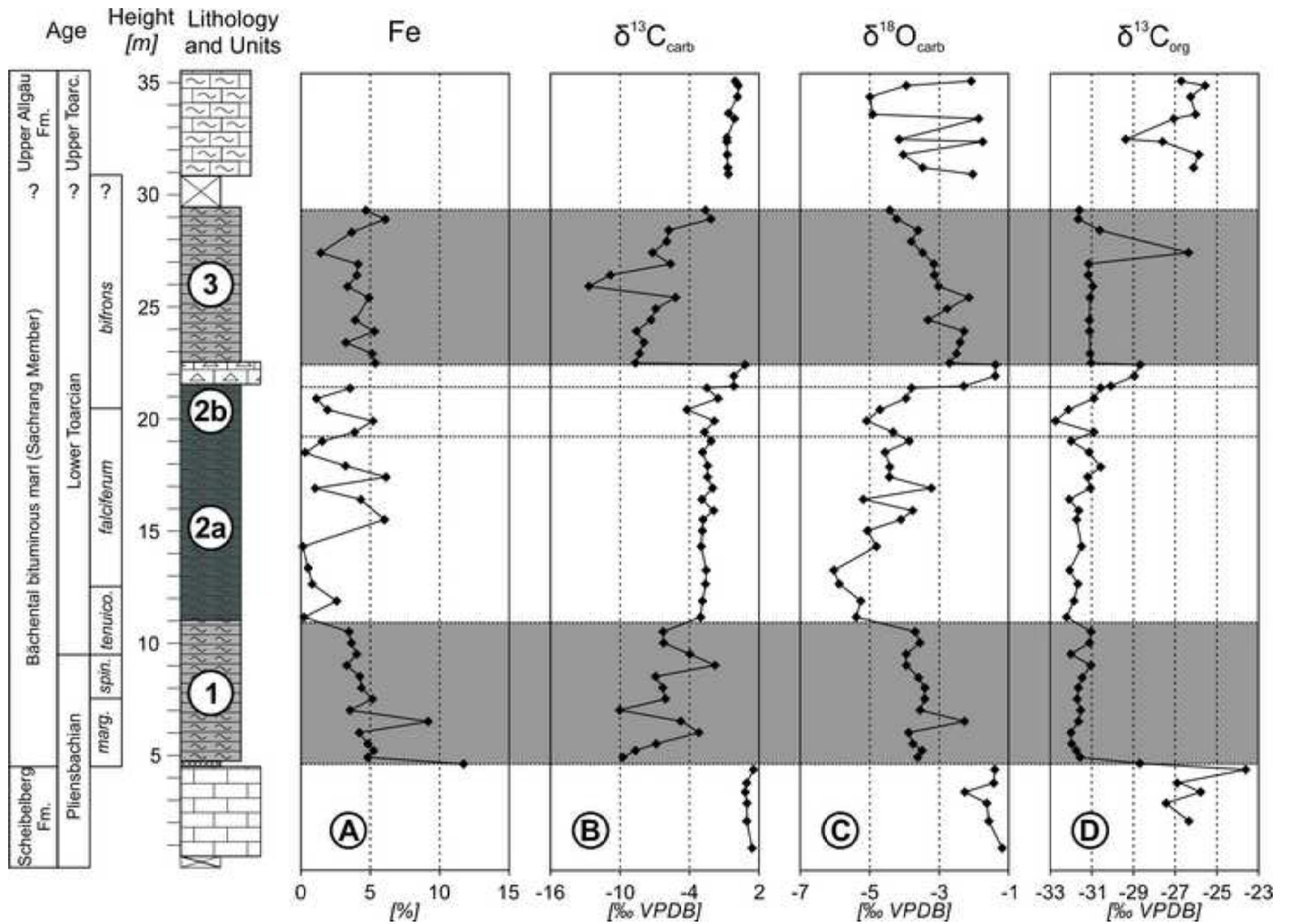


Figure 5  
[Click here to download high resolution image](#)

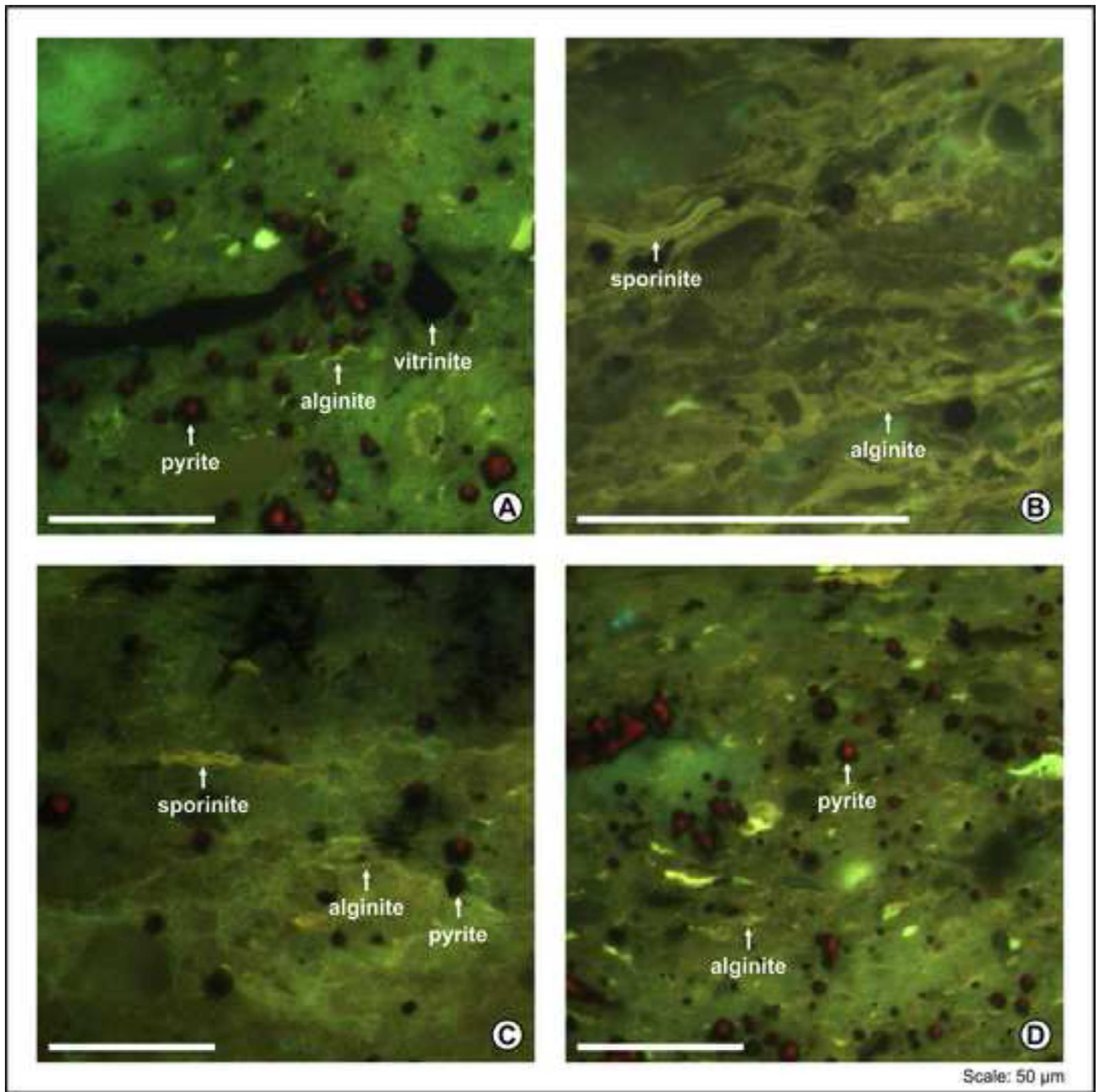


Figure 6

[Click here to download high resolution image](#)

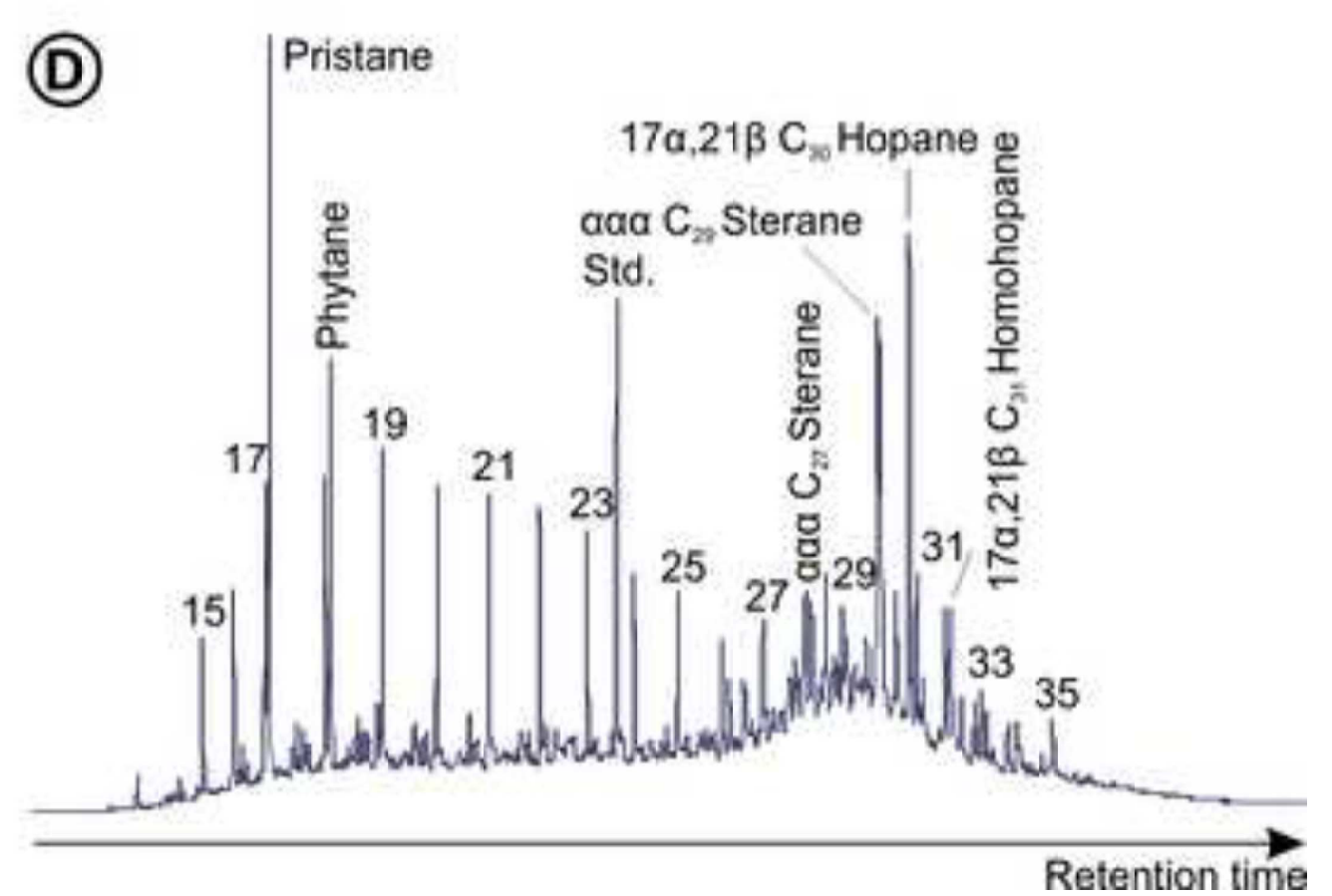
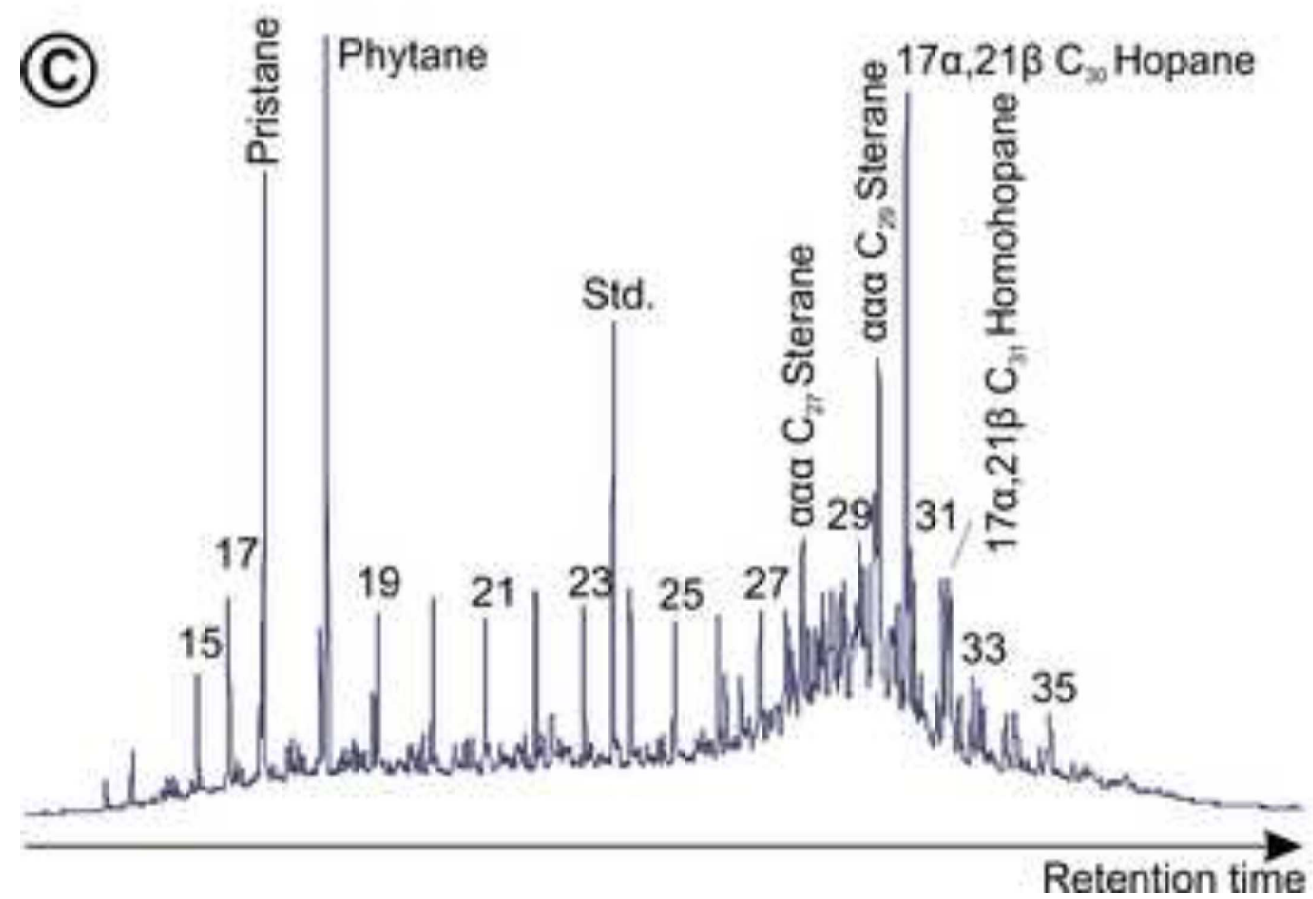
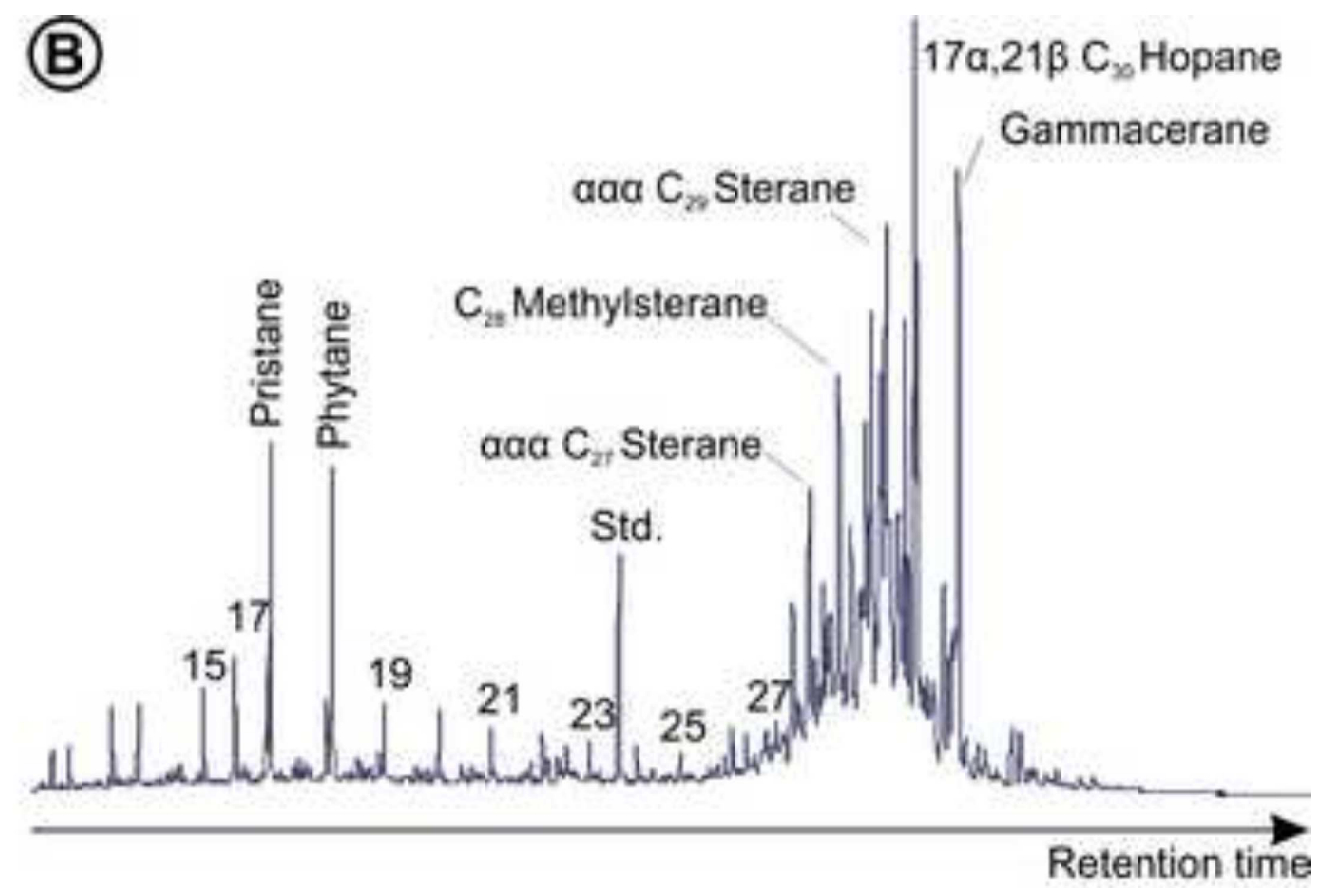
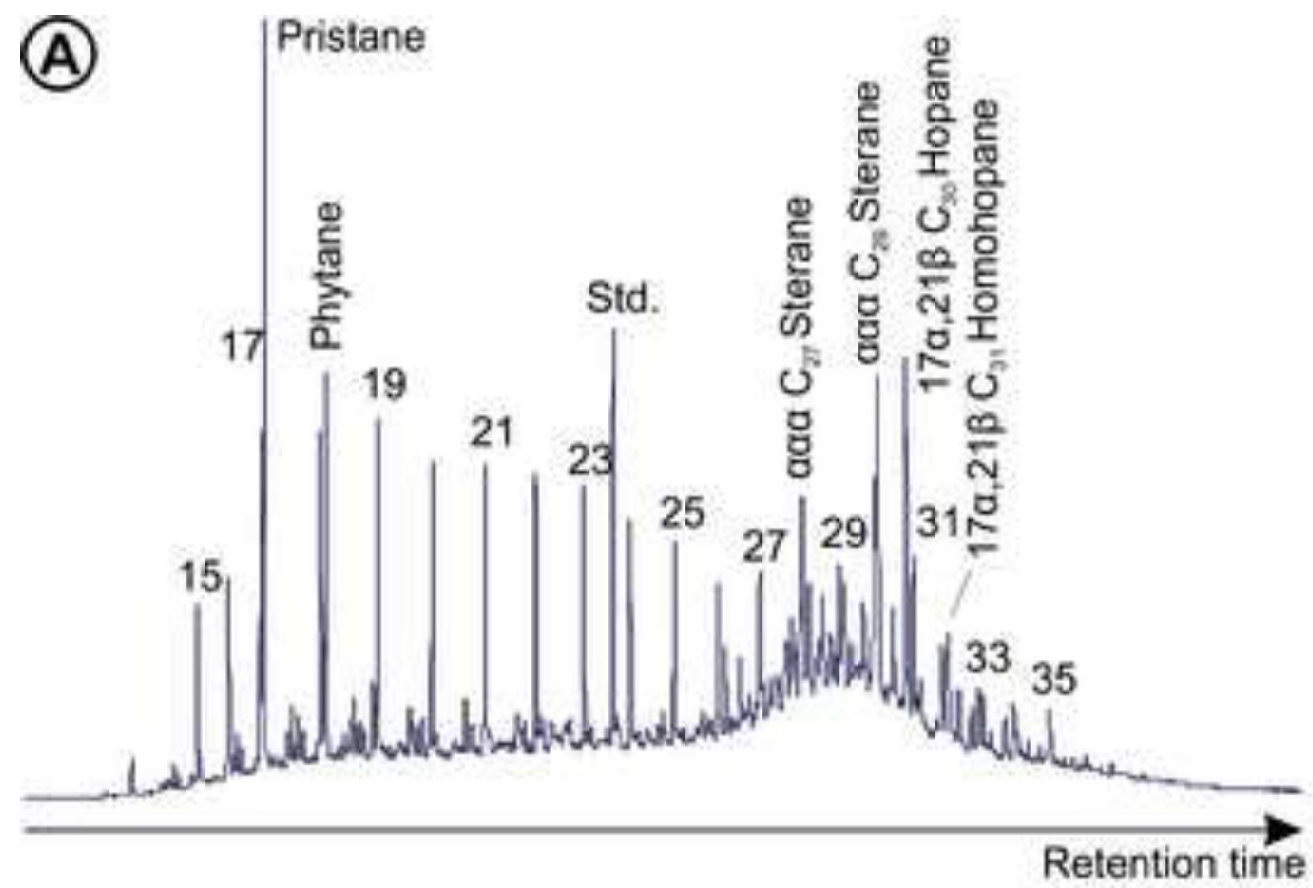


Figure 7

[Click here to download high resolution image](#)

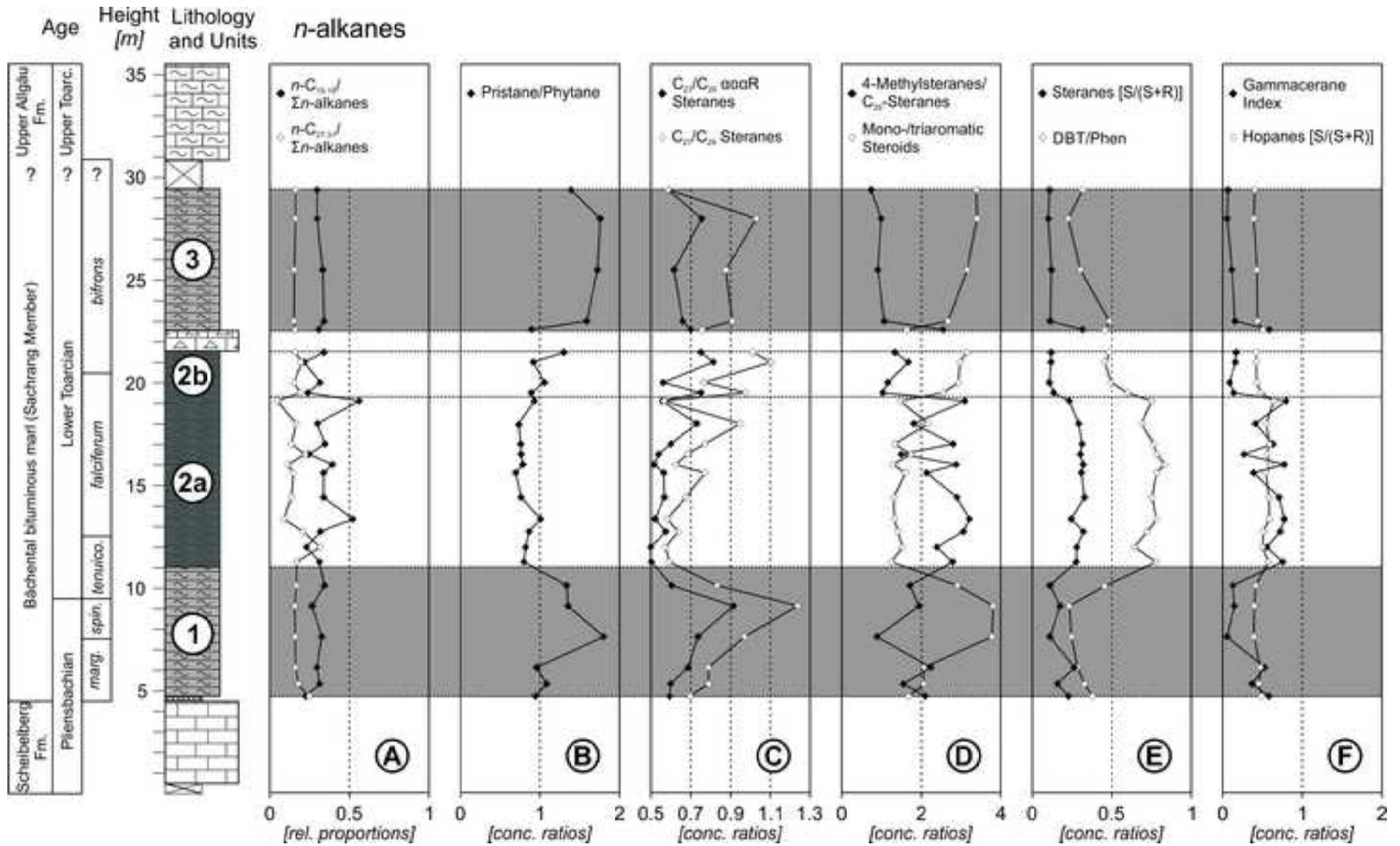


Figure 8

[Click here to download high resolution image](#)

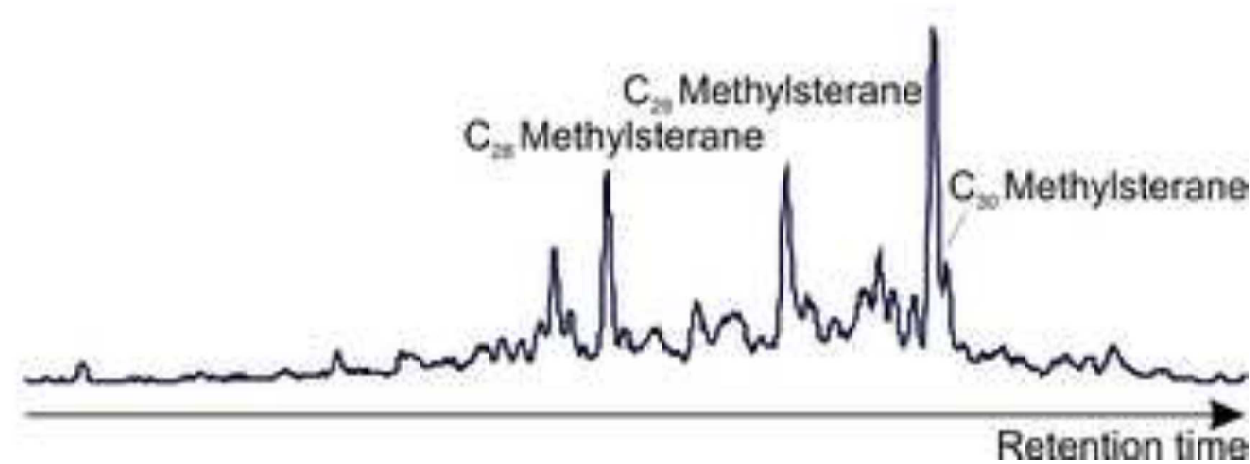
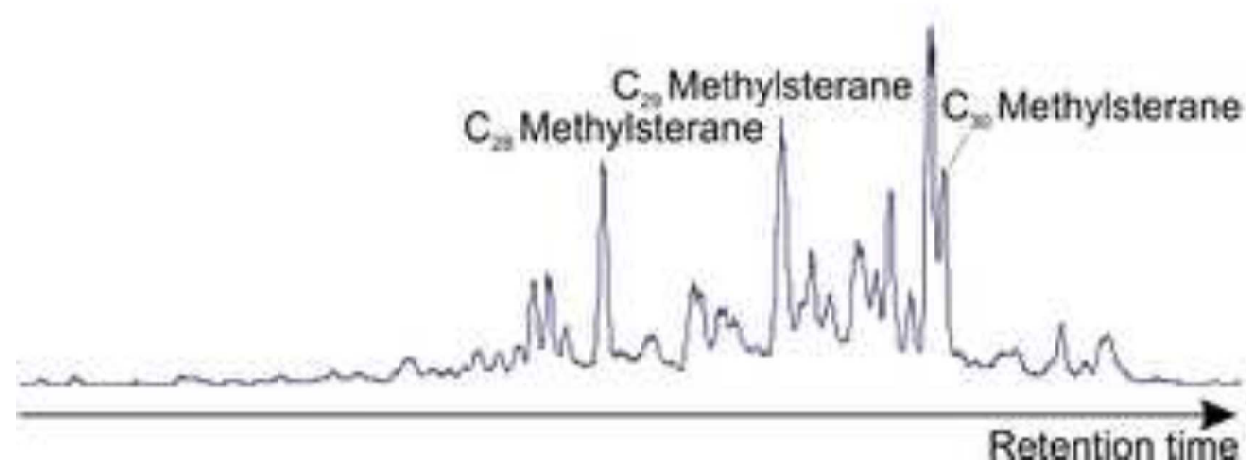
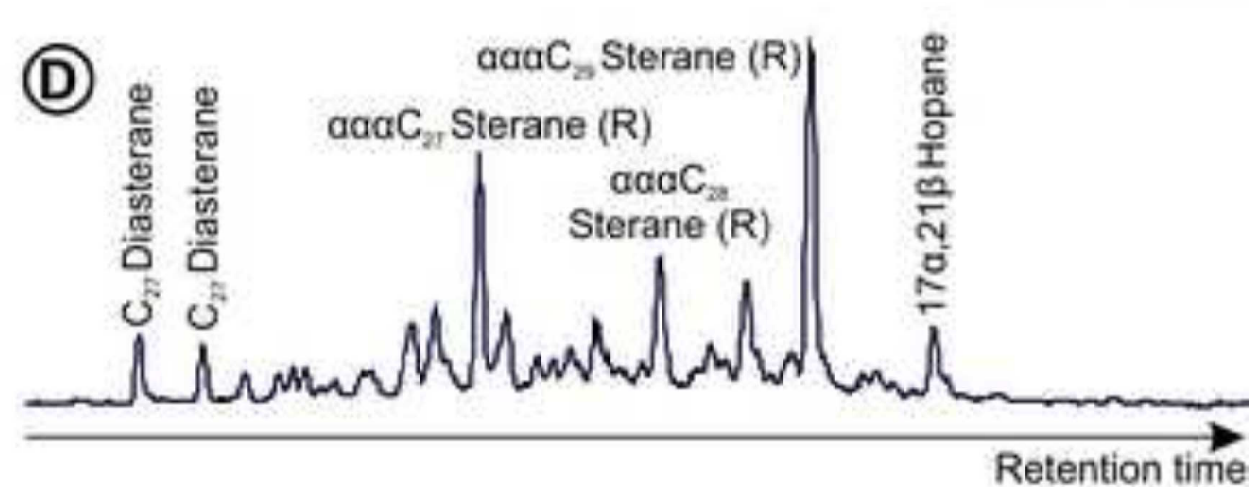
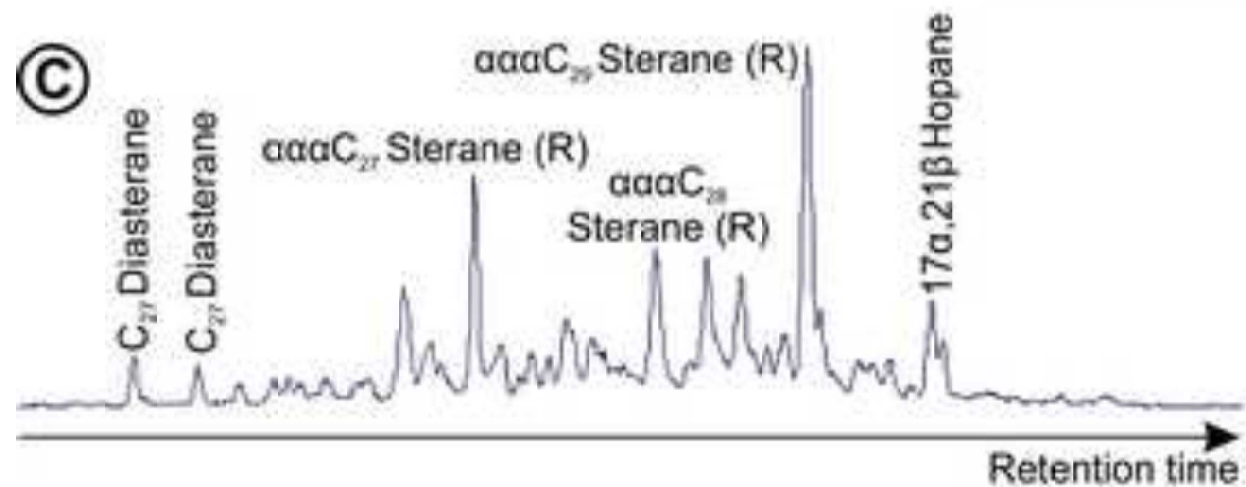
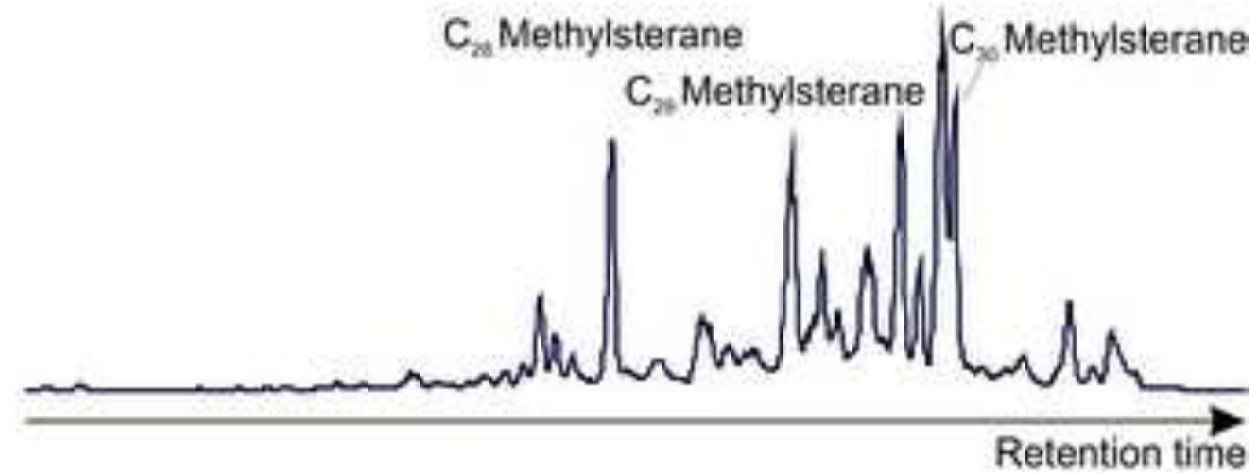
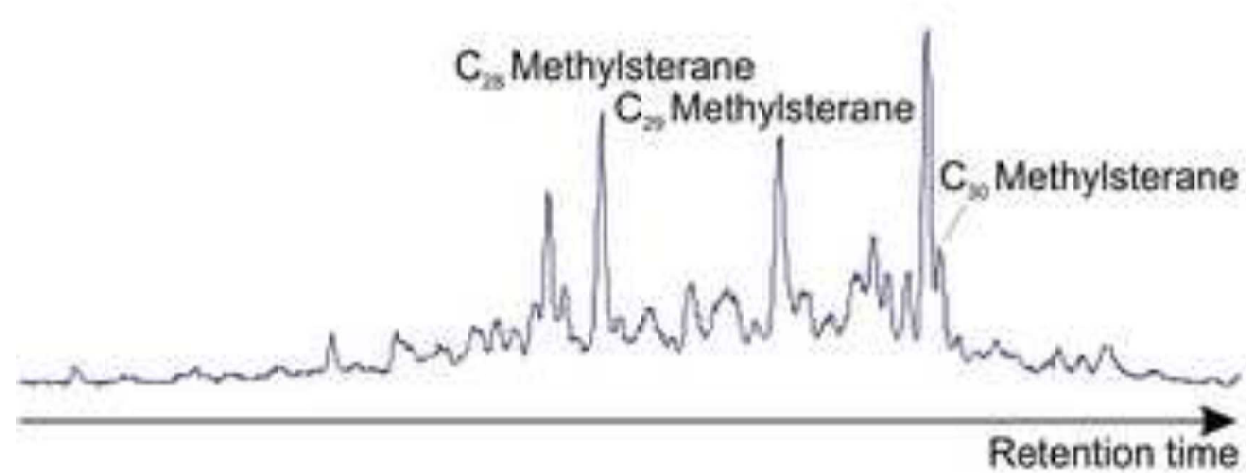
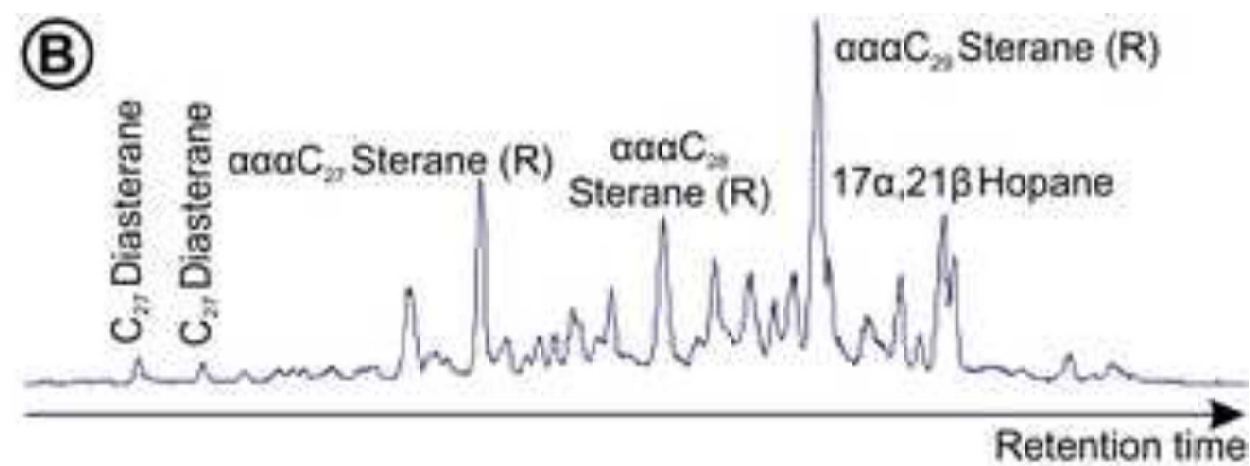
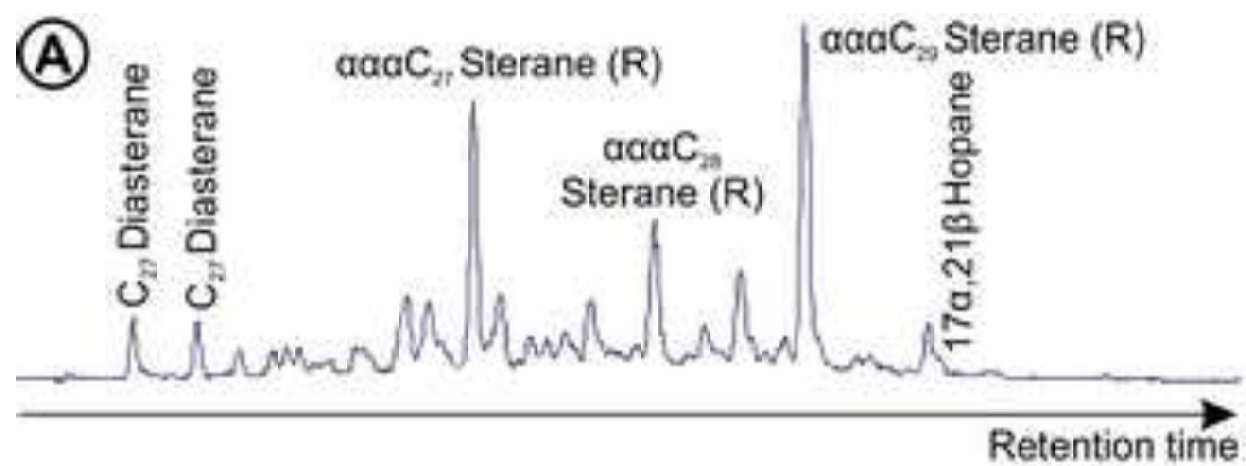




Figure 9

[Click here to download high resolution image](#)

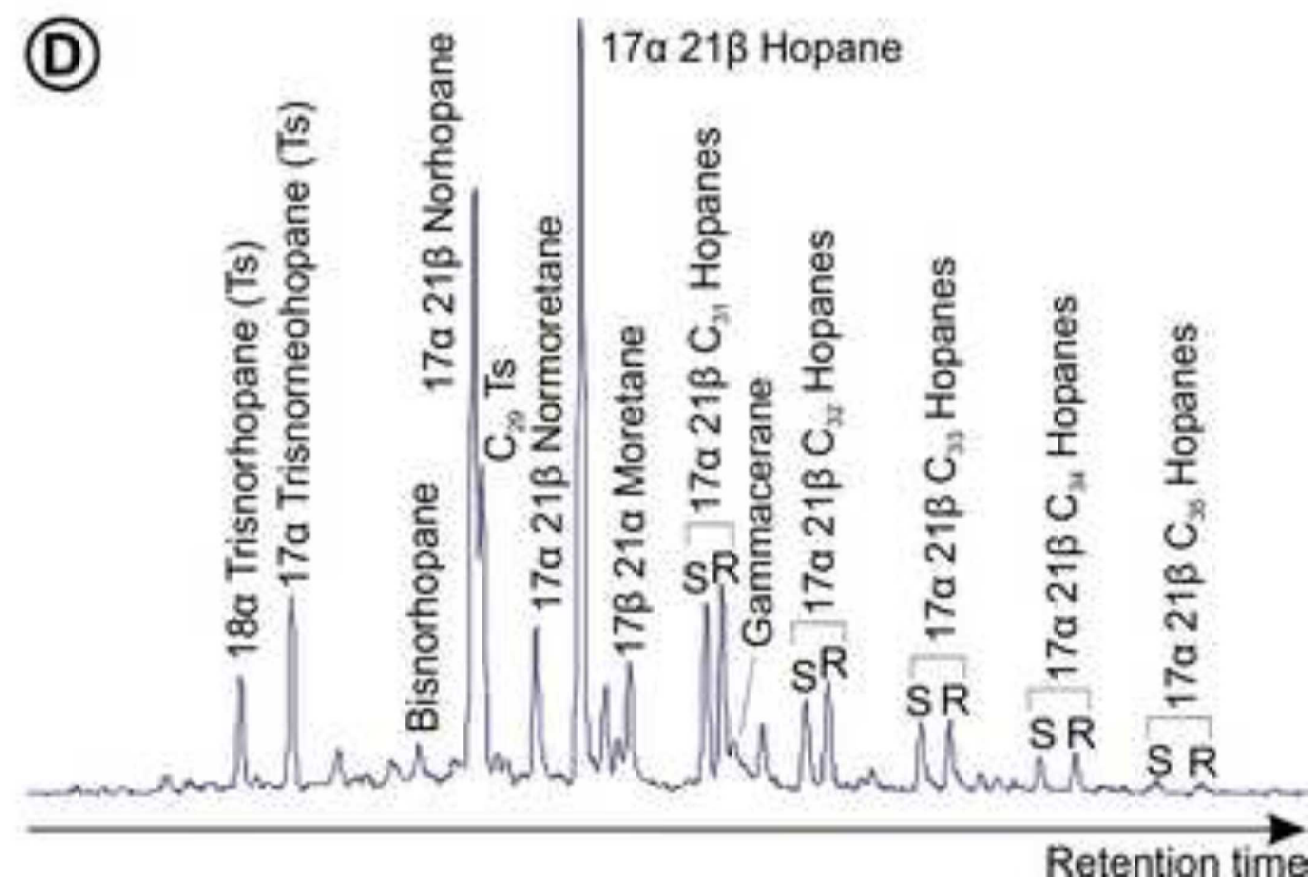
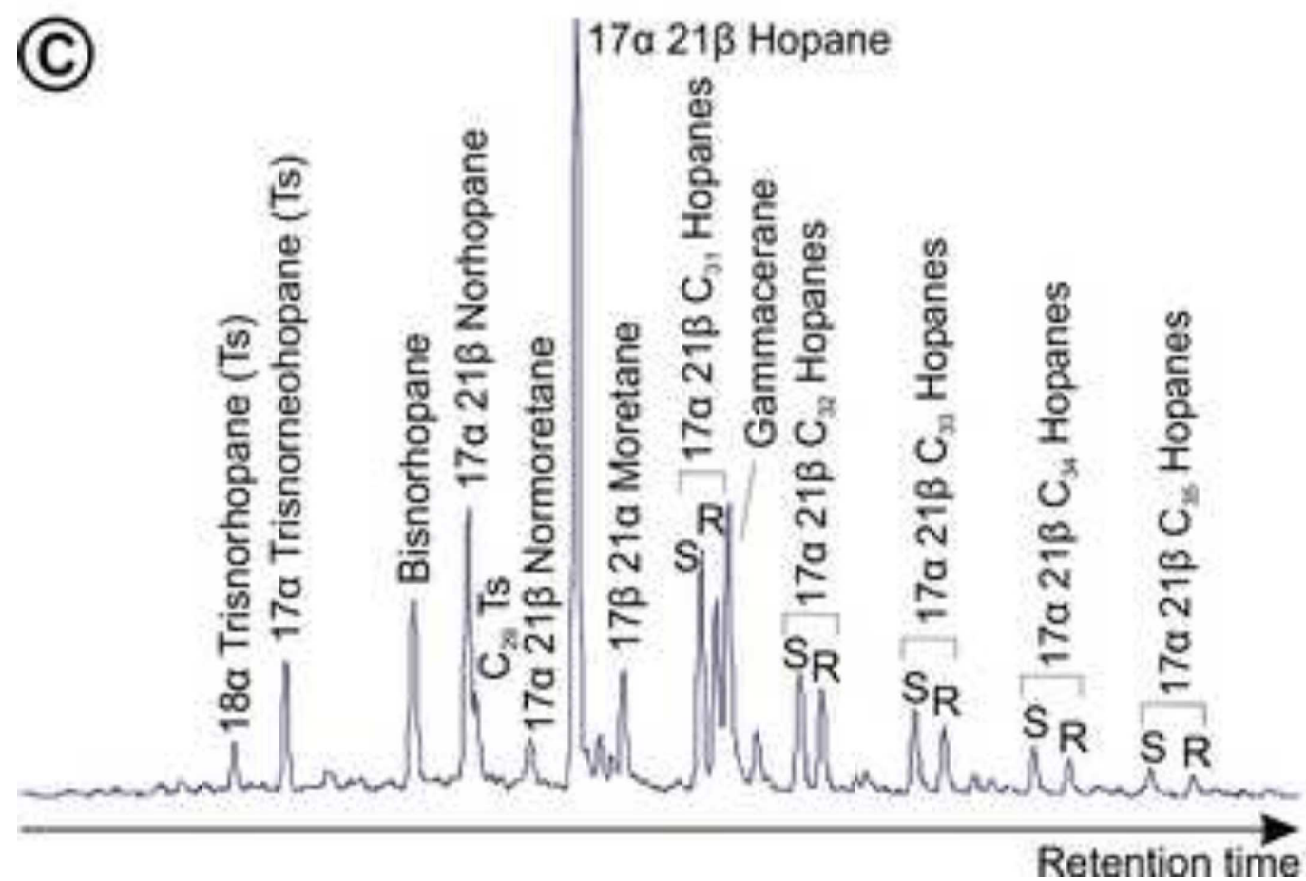
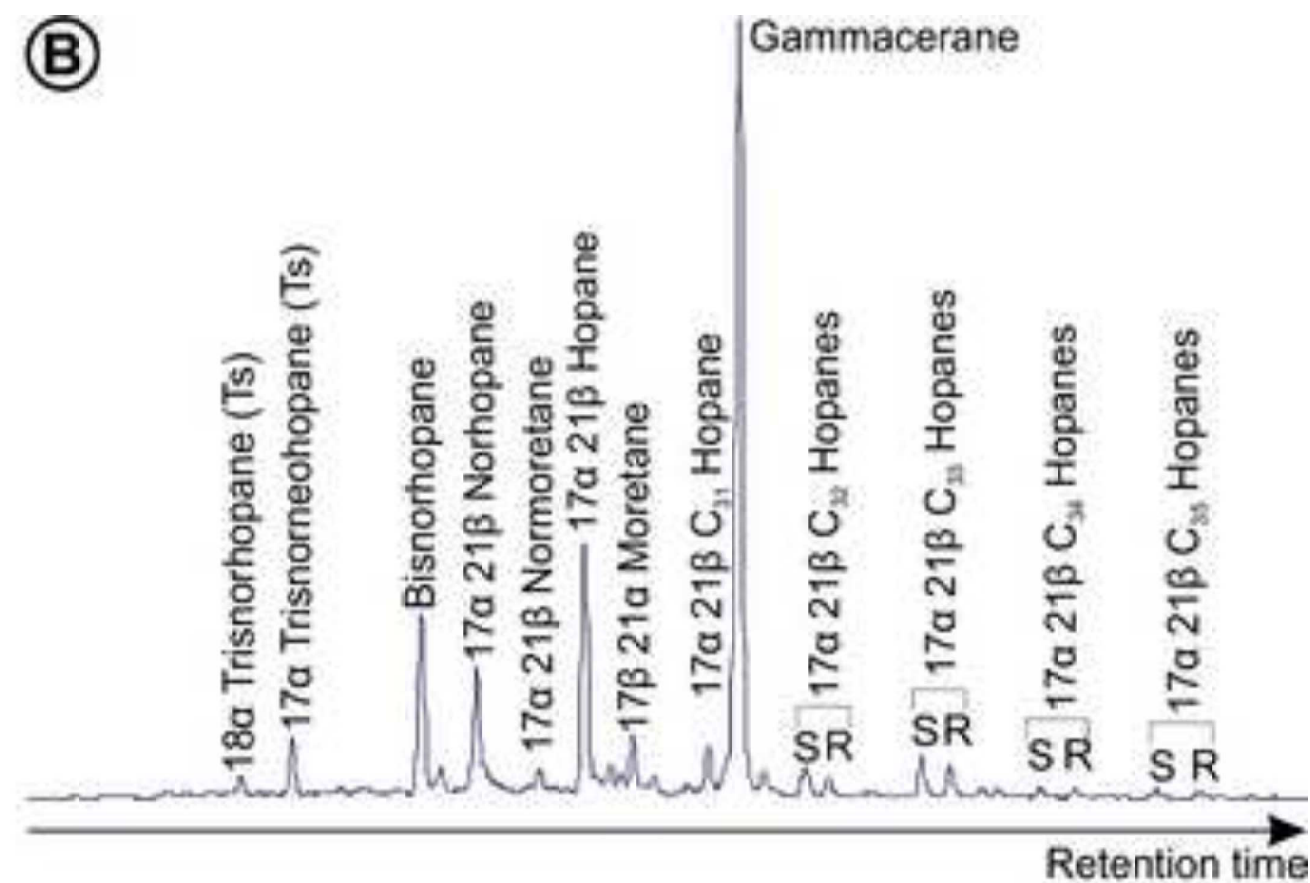
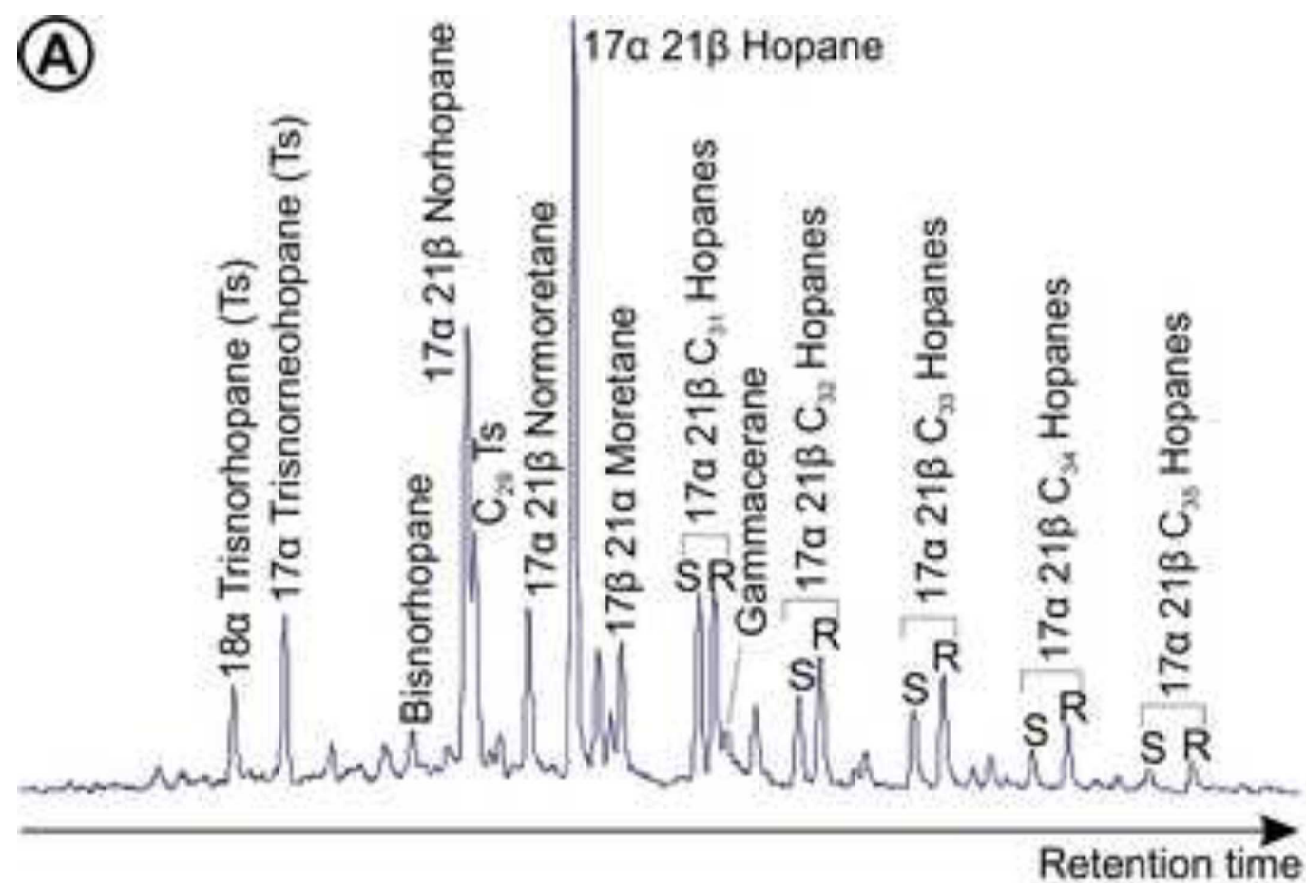


Figure 10

[Click here to download high resolution image](#)

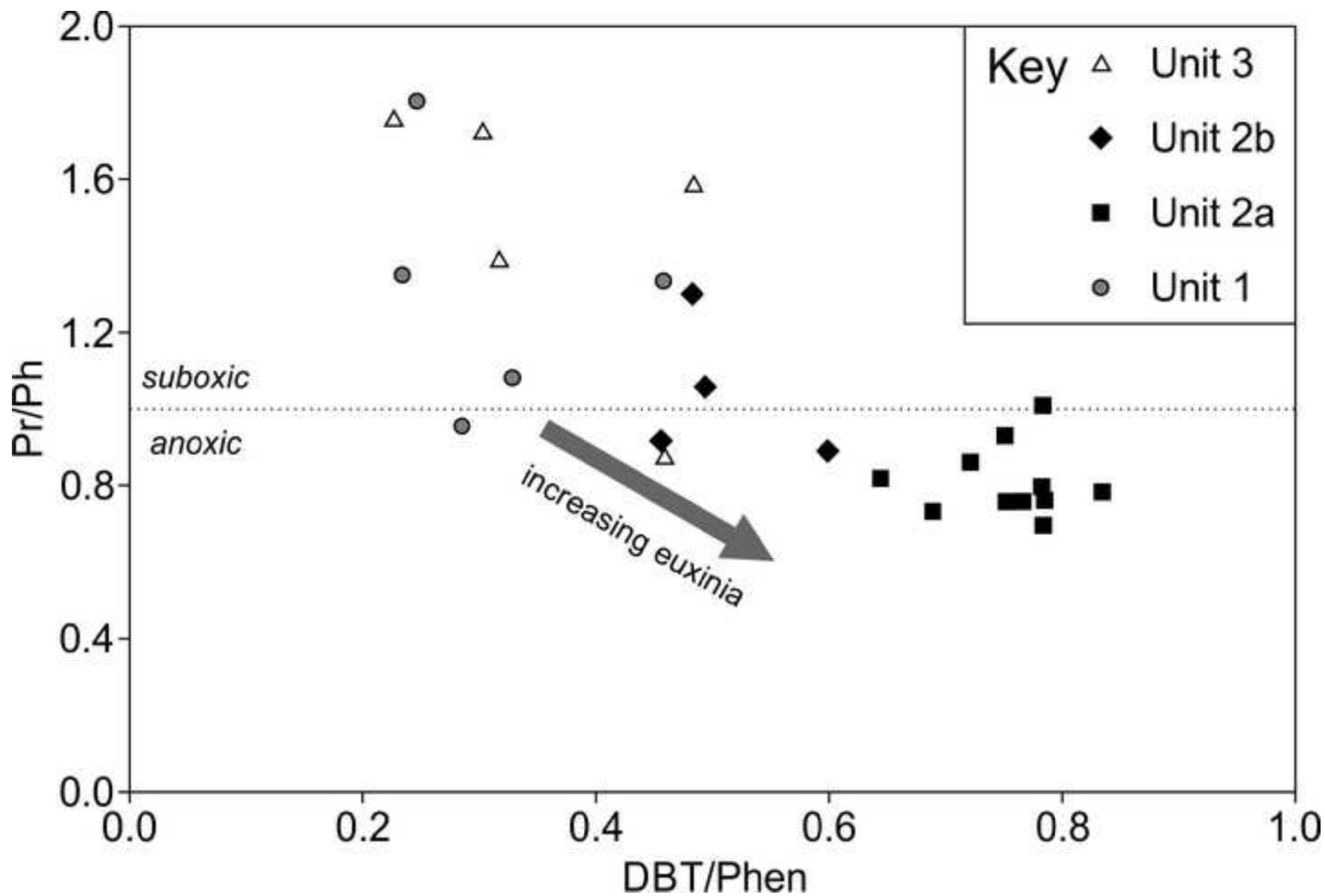


Figure 11

[Click here to download high resolution image](#)

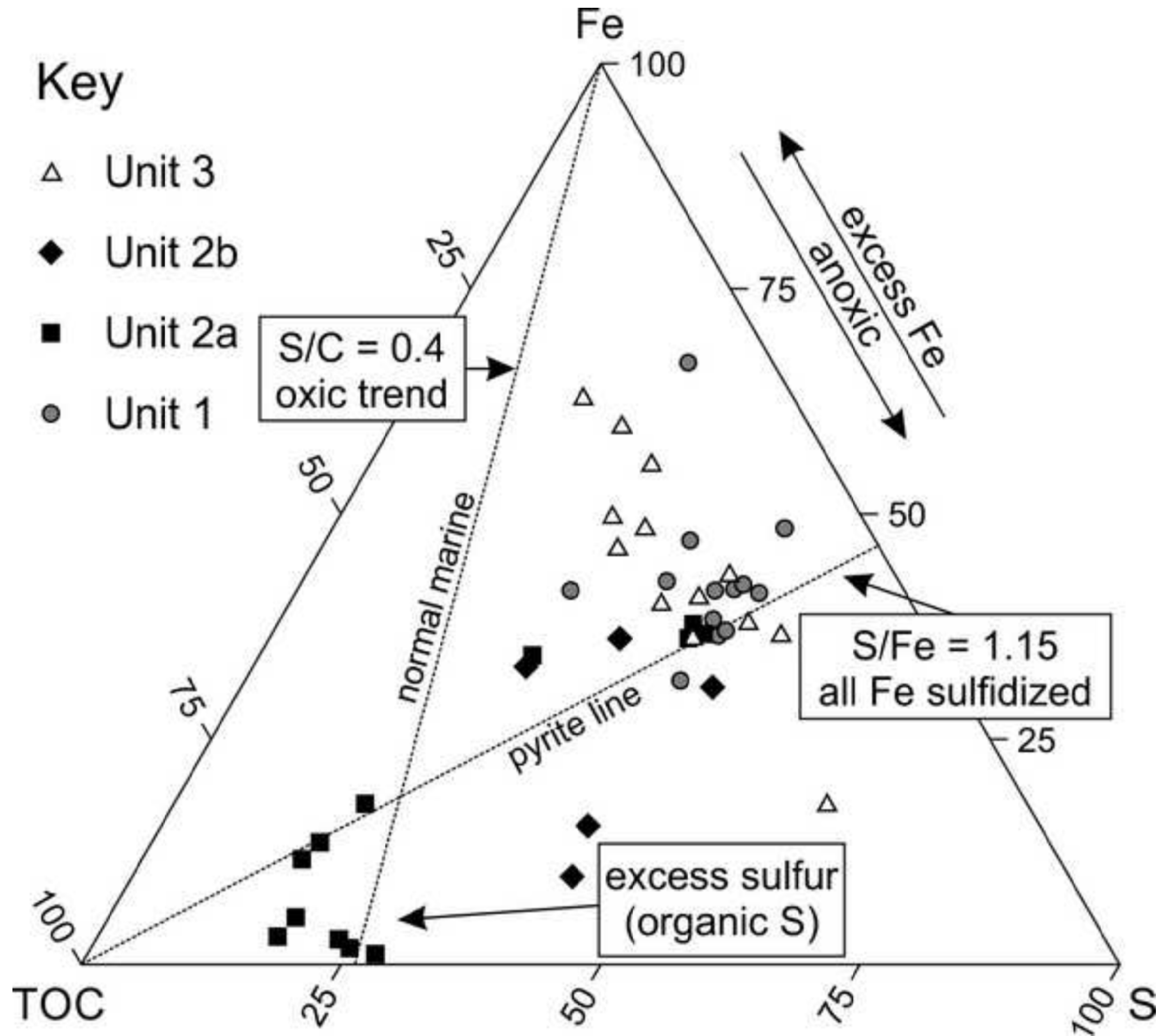


Figure 12

[Click here to download high resolution image](#)

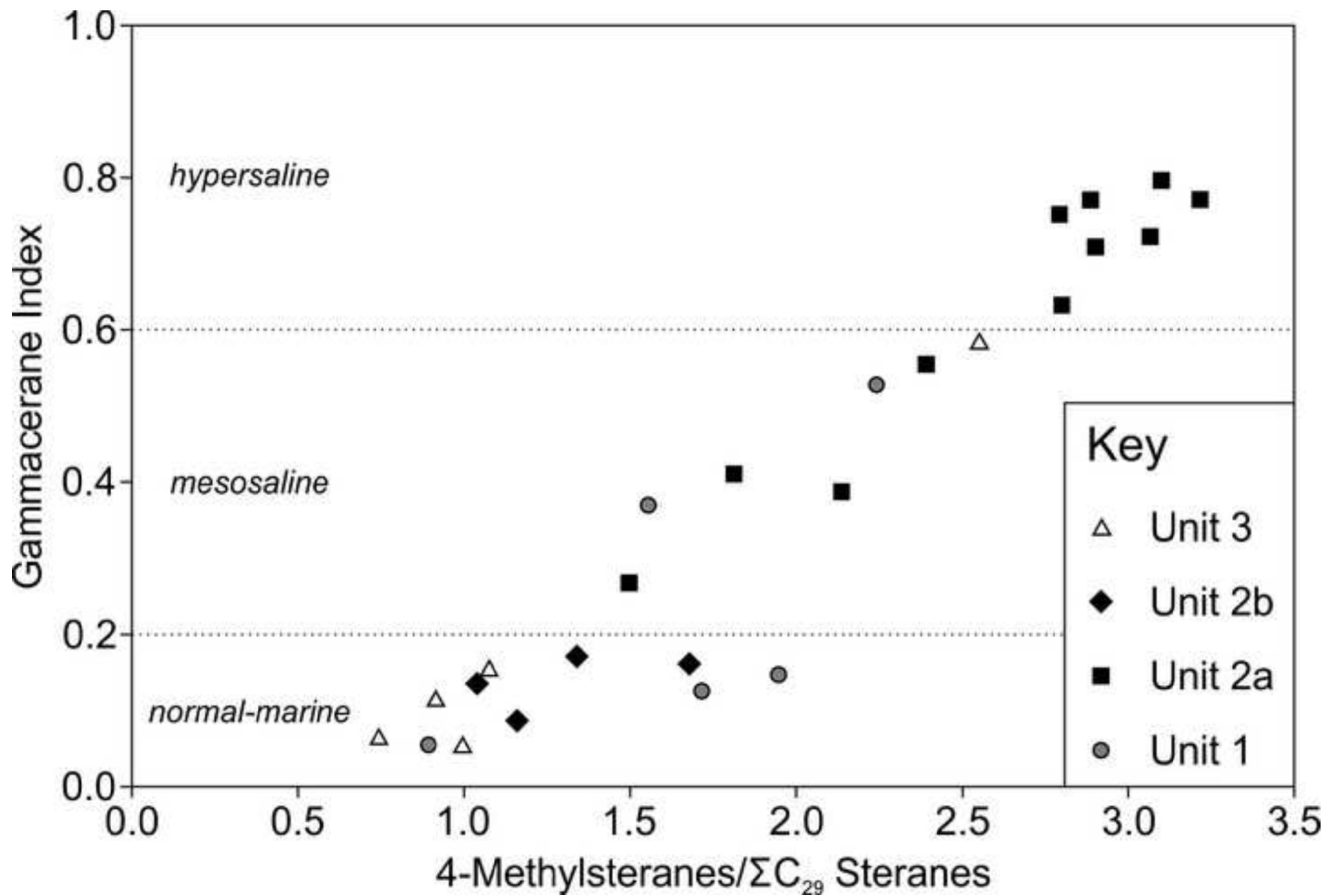


Figure 13  
[Click here to download high resolution image](#)

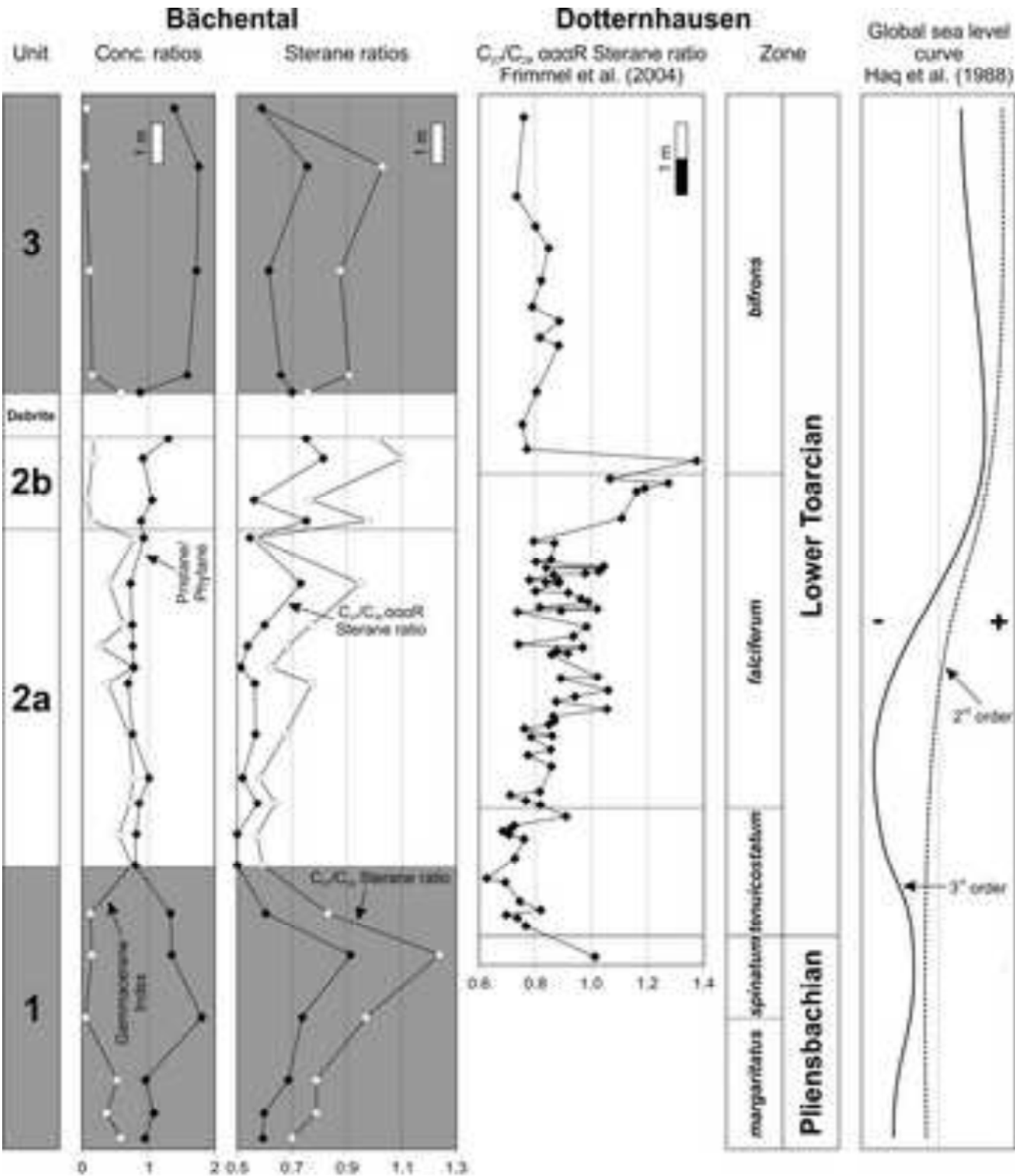
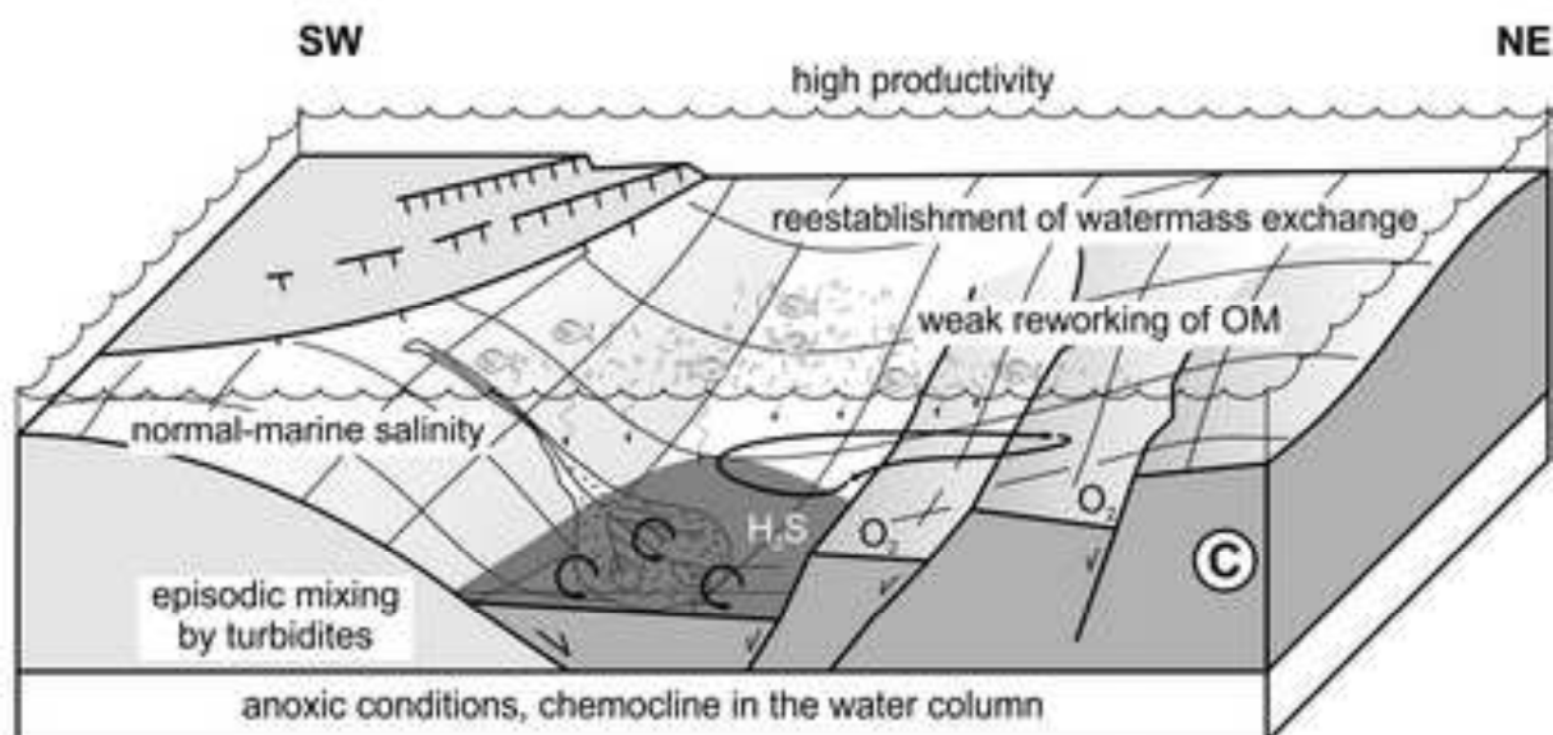
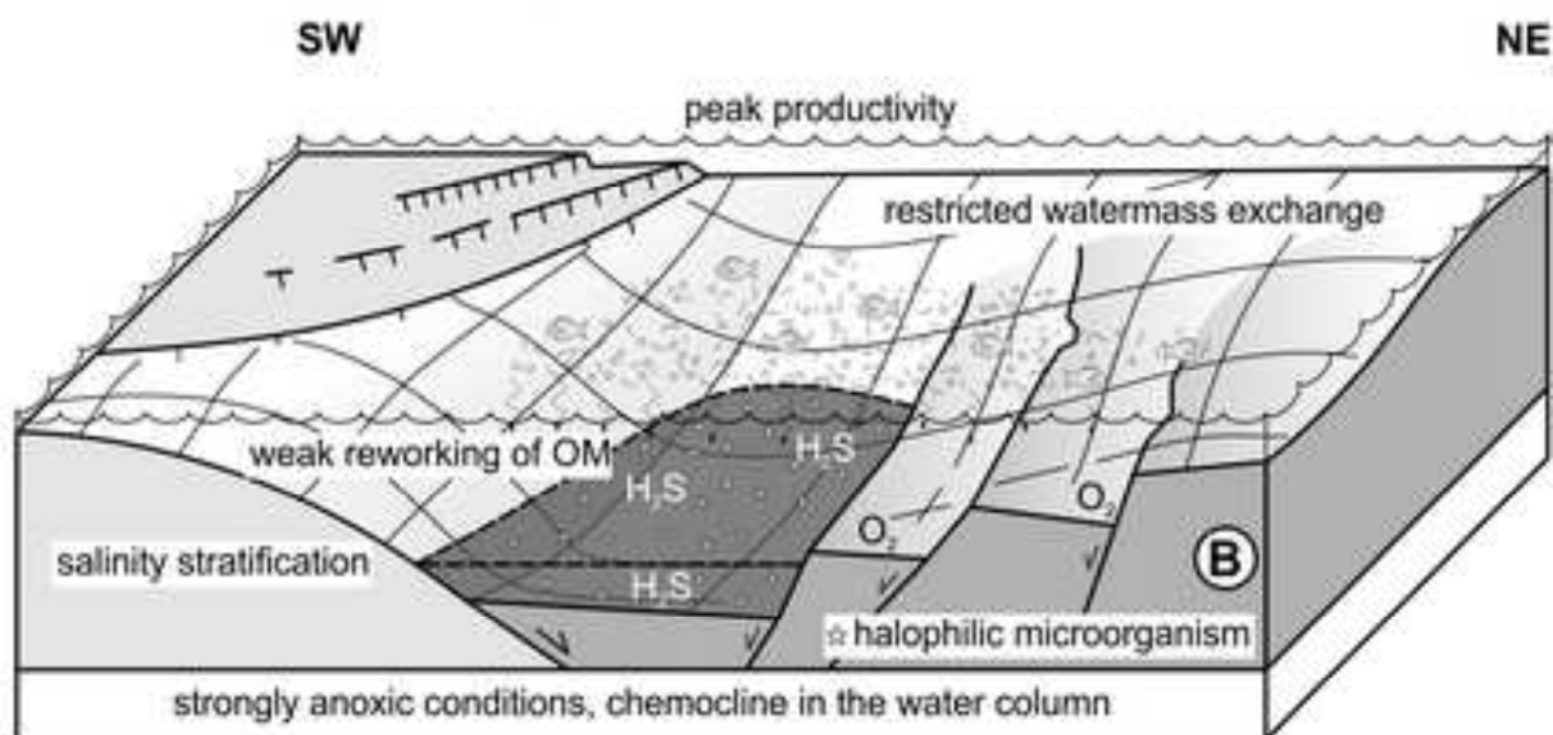


Figure 14  
[Click here to download high resolution image](#)

### Intermediate sea-level: Subunit 2b



### Sea-level lowstand/minor transgression: Subunit 2a



### Sea-level highstand: Units 1 and 3

